



The  
University  
Of  
Sheffield.

# Local Active Control of Reflected Sound

Michail T. Pelegrinis

Department of Automatic Control and Systems Engineering

University of Sheffield

A thesis submitted for the degree of

*Doctor of Philosophy*

September, 2014

*God made water, but man made wine*

*Victor Hugo*

*To my family*

# Abstract

The growth of high-density housing increases the exposure to pollution of noise from a variety of sources. Furthermore, the use of lighter materials for buildings and transportation equipment is now being deployed and this kind of actions can result in a significant increase in environmental and enclosure noise due to vibroacoustic emissions. It is therefore important to develop a solution that will reduce the undesired acoustic pollution. Because the primary disturbance will always be present, an intuitive approach to reduce acoustic pollution is to cancel the reflecting sound that occurs when the incident disturbance interacts with a boundary. By cancelling the reflected wave it is possible to avoid negative acoustic resonances. The project undertaken, deals with active cancelation of reflected sound with a control design that will be low in implementation complexity and resource cost. Specifically, a novel application of a PID Frequency Loop Shaping feedback design, which uses local measurements of the controlled element, was developed. In order to appreciate the resource efficiency and performance of the application, a comparison with the popular Filtered-x Least Mean Square algorithm (FxLMS), which requires intrusive remote microphone measurements, was conducted. A pulse tube setup was used as an experimental validation rig. Due to the complex dynamics of the control device used to implement the FLS PID design, the proposed solution was not able to perform successfully on the test rig. In order to bypass this problem, three additional feedback designs were considered, while retaining the local nature of the initially proposed design. Specifically, a  $H_2$ , a Remote Geometric and a Selective Resonance Geometric feedback control design are successfully implemented experimentally on the rig and compared with the FxLMS feedforward design. The implementation complexity and resource efficiency of the feedback approaches are superior to the feedforward one. Finally, an investigation of the benefits and trade offs of applying local feedback control designs on thin flat panels is considered. Interest is focused on the reduction of reflecting sound waves with the use of a  $H_2$  and a Remote Geometric feedback controller. The suggested designs made use of a theoretical model developed for the purpose of simulations. In addition the modelling included actuator dynamics, making the proposed solution more viable for future experimental validation.

# Acknowledgment

I would like to acknowledge support from BAE Systems, EPSRC and the Onassis foundation during the course of this work.

I would like to sincerely thank Professor Stephen Daley for giving me the opportunity to pursue this PhD. I benefitted immensely from the discussions during the time spent working with him. I am also very indebted to him for all the provisions of the experimental work that he arranged.

I would like to thank Dr. Simon Pope for his guidance and constructive feedback of my work, which has been very useful to further improve it. His support and supervision has made the PhD experience a pleasant and smooth one.

I would like thank Dr. Ilias Zazas for assisting me with setting up and running the experiments in the laboratory. Besides his valuable help given to me to complete the experiments, his relaxed mentality made this PhD much more pleasant.

I would like to thank Dr. Ubaid for helping me understand and implement the remote geometric design he has developed and for the long and funny conversations.

I would like to give special thanks to my family and to my girlfriend whose love and encouragement enabled me to finish this work.

Finally, I would like to thank all my friends here in Sheffield who filled these years with wonderful memories.

# Contents

<b>1</b>	<b>Introduction</b>	<b>1</b>
1.1	Motivation and Problem Definition . . . . .	1
1.2	Introduction to Active Noise Control Methods . . . . .	4
1.2.1	Feedforward Designs . . . . .	5
1.2.2	Feedback Designs . . . . .	6
1.3	Contribution to Knowledge . . . . .	8
1.4	Thesis Overview . . . . .	10
<b>2</b>	<b>Active Impedance Matching an Approach to Control Reflecting Sound</b>	<b>13</b>
2.1	Introduction . . . . .	13
2.2	Passive Noise Control . . . . .	15
2.2.1	Helmholtz Resonators . . . . .	16
2.3	Previous Work In Active Noise Control . . . . .	18
2.3.1	Filtered x Least Mean Square . . . . .	18
2.3.2	Direct Velocity Feedback Control . . . . .	25
2.3.3	Electroacoustic Absorbers Via Lead Lag Control . . . . .	26
2.4	Candidate Controller for Cancelling Reflecting Sound Waves . . . . .	29
2.5	PID Control Designs . . . . .	30
2.5.1	Ziegler - Nichols PID Tuning Methodology . . . . .	30
2.5.2	Pole Placement Method . . . . .	32
2.5.3	Frequency Loop Shaping . . . . .	33
2.5.4	Stability Analysis . . . . .	35
2.5.5	Robust Analysis . . . . .	35

2.6	Conclusions . . . . .	37
<b>3</b>	<b>Reduction of Reflected Sound Via Local Frequency Loop Shaping Control</b>	<b>38</b>
3.1	Introduction . . . . .	38
3.2	Development Of a System Model . . . . .	40
3.2.1	Acoustic Duct Model . . . . .	40
3.2.2	Disturbance Boundary . . . . .	43
3.2.3	Reflecting Boundary for FxLMS . . . . .	44
3.2.4	Reflecting Boundary for FLS . . . . .	45
3.3	Impedance Matching . . . . .	46
3.3.1	Feedback Control Arrangement . . . . .	47
3.3.2	FLS Minimisation for Impedance Matching . . . . .	48
3.4	Calculation of Reflecting Sound Wave for the Coupled System . . . . .	49
3.5	Implementation of Control Designs . . . . .	51
3.5.1	Implementation of FxLMS Control Design . . . . .	52
3.5.2	Implementation of FLS Control Design . . . . .	54
3.6	Performance and Implementation Analysis . . . . .	58
3.7	Conclusions . . . . .	59
<b>4</b>	<b>Reflected Noise suppression using local acceleration feedback control</b>	<b>61</b>
4.1	Introduction . . . . .	61
4.2	Modelling of Experimental Test Rig . . . . .	62
4.2.1	Matching of Acoustic Pressure Microphones . . . . .	65
4.2.2	Separation Technique . . . . .	67
4.2.3	Experimental Model . . . . .	68
4.3	Problem Implementing FLS Design . . . . .	71
4.4	Suggested Control Design . . . . .	73
4.4.1	Output Feedback Control Design Method . . . . .	74
4.4.2	Offline Calculation of Output Feedback Controller . . . . .	76
4.4.3	FxLMS Control Design for Experimental Implementation . . . . .	79
4.5	Results and Analysis . . . . .	80

4.5.1	Experimental Implementation of $H_2$ Design . . . . .	81
4.5.2	Experimental Implementation of FxLMS Design . . . . .	84
4.5.3	Comparison . . . . .	85
4.6	Conclusions . . . . .	86
<b>5</b>	<b>Remote Geometric Control Design for Suppression of Reflected Noise</b>	<b>89</b>
5.1	Introduction . . . . .	89
5.2	Control Design . . . . .	90
5.2.1	Remote Geometric Feedback Control . . . . .	92
5.2.1.1	Nevanlinna - Pick Interpolation Method . . . . .	95
5.2.2	Stability Analysis . . . . .	98
5.2.3	Implementation of the Geometric Design . . . . .	100
5.3	Results and analysis . . . . .	102
5.3.1	Experimental Implementation of $H_2$ Design . . . . .	104
5.3.2	Experimental Implementation of Geometric Design . . . . .	105
5.3.3	Comparison . . . . .	107
5.4	Conclusions . . . . .	111
<b>6</b>	<b>Selective Resonance Geometric Control Design for Suppression of Reflected Noise</b>	<b>113</b>
6.1	Introduction . . . . .	113
6.2	Control Design . . . . .	114
6.2.1	Parallel Feedback Control Arrangement . . . . .	115
6.2.2	Stability Assurance . . . . .	116
6.2.3	Implementation of Selective Resonance Geometric Design . . . . .	116
6.3	Results and Analysis . . . . .	118
6.3.1	Experimental Implementation of Remote Geometric Control . . . . .	119
6.3.2	Experimental Implementation of Selective Resonance Control . . . . .	120
6.3.3	Comparison . . . . .	121
6.4	Conclusions . . . . .	123

<b>7</b>	<b>Reflecting panel work</b>	<b>125</b>
7.1	Introduction . . . . .	125
7.2	Development of a System Model . . . . .	126
7.2.1	Model Assumptions . . . . .	126
7.2.2	Duct Model . . . . .	128
7.2.3	Control Boundary Model . . . . .	130
7.2.4	Disturbance Boundary Model . . . . .	132
7.2.5	Coupled MIMO Model . . . . .	133
7.3	Control Design . . . . .	134
7.3.1	Continuous Time Domain $H_2$ Control . . . . .	134
7.3.2	Implementation of $H_2$ Design . . . . .	136
7.3.3	Remote Geometric Control . . . . .	139
7.3.4	Implementation of Remote Geometric Design . . . . .	139
7.4	Results and Analysis . . . . .	141
7.4.1	$H_2$ Control Design . . . . .	141
7.4.2	Remote Geometric Design . . . . .	143
7.4.3	Comparison . . . . .	145
7.5	Conclusions . . . . .	146
<b>8</b>	<b>Summary and Future Work</b>	<b>148</b>
8.1	Summary of Achievements . . . . .	148
8.2	Future Work . . . . .	151
	<b>References</b>	<b>152</b>
	<b>Appendix A</b>	<b>161</b>
A.1	Boundary Value Problem for Coupled Loudspeakers Acoustic Duct . . . . .	161
A.2	Plate Formulas . . . . .	165
A.3	Boundary Value Problem for Coupled Rectangular Thin Plate Acoustic Duct . . . . .	168
A.4	Panel Velocity for Coupled Acoustic Duct Plant . . . . .	169

**Appendix B**

**171**

# List of Figures

1.1	Acoustic duct with a disturbance source placed inside it. . . . .	4
1.2	Proposed feedback control architecture to solve the acoustic resonance problem. $G$ is the plants dynamics and $K$ is the feedback controller. . . . .	4
2.1	Acoustic cylinder shaped duct of constant diameter $a$ and fixed length $L$ with disturbance source placed at one end (D) and at the other end is a controlled boundary surface. . . . .	15
2.2	Acoustic cylinder shaped duct of constant diameter $a$ and semi-infinitely long with disturbance source placed at one end (D). . . . .	15
2.3	(a) Schematic illustration of a Helmholtz resonator that consists of a cavity of total volume equal to $V$ and a neck of length $L$ connected to it. (b) The mechanical analogous description of a Helmholtz resonator could be described as a mass concentrated in the narrow end of the tube (M) and the fluid in the cavity mimics the characteristics of a spring with a stiffness coefficient (K), this is because of the difference in pressure. . . . .	16
2.4	Block diagram of feedforward LMS algorithm. With $x(n)$ is the input signal vector, $w(n)$ is the adaptive filter's coefficients, $K$ is the forward path of the process, $y_K(n)$ is the output control signal $T(n)$ is the desired output signal and $e(n)$ is the error between output and desired signal. . . . .	19

2.5	Block diagram of a plant with an active controller tuned with the FxLMS algorithm. With $x(n)$ is the input signal vector, $w(n)$ is the adaptive filter's coefficients, $K$ is the forward path of the process, $y_K(n)$ is the output control signal $T(n)$ is the desired output signal, $e(n)$ is the error between output and desired signal $K^*$ is a model of the feedforward path of the plant and $x_{K^*}(n)$ is the filtered output of the plant's input $x(n)$ signal by the model of the feedforward path. . . . .	22
2.6	Direct velocity feedback control block diagram. $Y_{cp}$ is the control path transfer function and $Y_{dp}$ is the disturbance path transfer function. . . . .	26
2.7	Electroacoustic absorber illustration describing the controller-sensor-loudspeaker setup [Lissek et al., 2011]. . . . .	28
2.8	Block diagram layout for electroacoustic absorbers. $C_{lead}(s)$ is a lead controller, $C_{lag}(s)$ is a lag controller, $C_{gain}(s)$ is a gain controller, $Z_1(s)$ is the transfer function describing the path between the disturbance pressure wave ( $P$ ) and the velocity of the transducer's diaphragm and $Z_2(s)$ is the transfer function describing the path between the control signal ( $E$ ) and the velocity of the transducer's diaphragm. . . . .	29
2.9	Feedback system with multiplicative uncertainty. With $C$ being the controller block, $W_I$ is the frequency dependent magnitude uncertainty, $\Delta_I$ is any stable transfer function such that $\ \Delta_I\ _\infty < 1$ and $G$ is the plant to be controlled. . . . .	36
3.1	Schematic layout of acoustic duct. The acoustic duct is of length $L$ and diameter $r$ . A Disturbance source at one end of the duct (D) and control source at distance $x_c$ (C). Two pressure microphones placed near the control source at distance $\Delta x_1$ from each other and $\Delta x_2$ from the control loudspeaker. . . . .	43
3.2	Mass-spring-damper element used to model the reflecting surface of the acoustic duct. $M$ is the mass of the reflecting surface, $K$ is the stiffness, $C$ is the absolute damping, $f_{acoustic}$ is the external force due to the acoustic wave. . . . .	45
3.3	Acoustic duct for implementing the FLS design. The reflecting boundary end considered is a mass-spring-damper element (figure 3.2). . . . .	46

3.4	Mass-spring-damper element used to model the reflecting surface of the acoustic duct with addition of the PID feedback controller $C_{cont}(s)$ . $M$ is the mass of the reflecting surface, $K$ is the stiffness, $C$ is the absolute damping, $f_{acoustic}$ is the external force due to the acoustic wave, $f_c$ is the control force applied on the mass by the local velocity feedback control loop. . . . .	48
3.5	Block diagram of control loop of reflecting surface with a control force related to the velocity of the reflecting surface. The force due to the incident acoustic wave is $f_{acoustic}$ , $G(s)$ is the transfer function relating the external force to the velocity of the mass of the reflecting surface ( $G(s) = \frac{s}{Ms^2 + Cs + K}$ ), $C_{cont}(s)$ is the PID controller, equation (2.28). . . . .	48
3.6	Block diagram describing the dynamics of a coupled duct system (figure 3.1). The transfer function blocks ( $T_{11}$ , $T_{21}$ , $T_{12}$ and $T_{22}$ ) are based on equations found in table 3.2. The blocks labeled as delays are based on the separation formula described in section §3.4. . . . .	52
3.7	Block diagram for implementing FxLMS design. $P$ is the <i>MIMO</i> transfer function that models the plant's dynamics. The block with label filter is a transfer function that replicates the path between control to reflecting wave. Finally the updating rule block is formulated based on the theory described in the previous chapter (section 2.3.1). . . . .	53
3.8	Simulated response of reflecting sound wave in an acoustic duct with an actively controlled reflecting surface as the boundary surface (green), Simulated response of reflecting sound wave in the same acoustic duct with the same reflecting surface without the active control applied (blue). . . . .	54
3.9	Simulated specific acoustic impedance of an actively controlled element composed of a mass-spring-damper element (blue), theoretical specific acoustic impedance of the mass-spring-damper element without control (red) and the characteristic acoustic impedance, i.e. the desired response, of air (green). For these simulations the mass of the reflecting surface is $M = 0.02(kg)$ , $C = 0.05(Ns/m)$ and $K = 10(N/m)$ . . . . .	56

3.10	Simulated response of reflecting sound wave in an acoustic duct with an actively controlled reflecting surface as the boundary surface (blue), Simulated response of reflecting sound wave in the same acoustic duct with the same reflecting surface without the active control applied (green). . . . .	57
3.11	Nyquist plot open loop . . . . .	58
4.1	Duct setup for local feedback designs with sensor actuator dynamics embedded on one structure. . . . .	61
4.2	Illustration of the experimental acoustic duct of length $L = 2.054m$ and diameter $d = 0.099m$ . A Disturbance source at one end of the duct (D) and control source at the other end (C). Two pressure microphones (green) placed near the control source at distance $\Delta x_1 = 0.0428m$ from each other and $\Delta x_2 = 0.2m$ from the control loudspeaker. Accelerometer is connected to the cone of the control loudspeaker (green). . . . .	63
4.3	Picture of the experimental acoustic tube consisting of the disturbance source (near end), control source (far end) and the three sensors (two microphones and the accelerometer). . . . .	64
4.4	dSPACE PPC Controller Board, Power Amplifiers and Pre-amplifiers required to implement the proposed control strategy. . . . .	64
4.5	Control loudspeaker with embedded accelerometer and two non matched pressure microphones. . . . .	65
4.6	Reading from pressure microphone 1 (blue), non calibrated reading from pressure microphone 2 (green) . . . . .	66
4.7	Reading from pressure microphone 1 (blue), calibrated reading from pressure microphone 2 (green dashed) . . . . .	67
4.8	(a) Block diagram of disturbance path for the experimental pulse tube setup relating disturbance voltage (disturbance loudspeaker) with reflecting sound wave (pressure microphones) (b) Block diagram of disturbance path for the experimental pulse tube setup relating disturbance voltage (disturbance loudspeaker) with acceleration of control loudspeaker's cone (accelerometer). . . .	68

4.9	(a) Block diagram of control path for the experimental pulse tube setup relating disturbance voltage (control loudspeaker) with reflecting sound wave (pressure microphones) (b) Block diagram of control path for the experimental pulse tube setup relating disturbance voltage (control loudspeaker) with acceleration of control loudspeaker's cone (accelerometer). . . . .	69
4.10	Bode plot of the raw experimental data for the disturbance paths (blue) and bode plot of the high order FIR filter fitted to the experimental data (green).	70
4.11	Bode plot of the raw experimental data for the control paths (blue) and bode plot of the high order FIR filter fitted to the experimental data (green). . .	71
4.12	Control loudspeaker's acceleration response to random input signal. . . . .	73
4.13	LFT control architecture described by a MIMO generalised process ( $P$ ) and a output feedback controller ( $K$ ). Inputs of the generalised process are the voltage of the disturbance loudspeaker ( $E_{dis}$ ) and the voltage of the control loudspeaker ( $E_{con}$ ), furthermore the outputs are the undesired reflecting sound wave signal ( $P_{ref}$ ) to be minimised and the acceleration signal of the control loudspeaker's baffle ( $w_{loud}$ ). . . . .	74
4.14	Disturbance path (disturbance to reflecting sound wave). Bode plot of the raw experimental data (blue), bode plot of the high order FIR filter fitted to the experimental data (green) and bode plot of the reduced order FIR filter fitted to the experimental data (red). . . . .	77
4.15	Disturbance path (disturbance to acceleration). Bode plot of the raw experimental data (blue), bode plot of the high order FIR filter fitted to the experimental data (green) and bode plot of the reduced order FIR filter fitted to the experimental data (red). . . . .	77
4.16	Control path (control to reflecting sound wave). Bode plot of the raw experimental data (blue), bode plot of the high order FIR filter fitted to the experimental data (green) and bode plot of the reduced order FIR filter fitted to the experimental data (red). . . . .	78

4.17	Control path (control to acceleration). Bode plot of the raw experimental data (blue), bode plot of the high order FIR filter fitted to the experimental data (green) and bode plot of the reduced order FIR filter fitted to the experimental data (red). . . . .	78
4.18	Offline $H_2$ control design for reduction of reflecting noise inside an experimental acoustic duct. . . . .	79
4.19	Offline $H_2$ control design for reduction of reflecting noise inside an experimental acoustic duct. . . . .	80
4.20	Block diagram for implementing FxLMS design. $P$ is the <i>MIMO</i> plant's dynamics. The block with label filter is a transfer function that replicates the path between control to reflecting wave. Finally the updating rule block is formulated based on the theory developed in the previous chapter (section 2.3.1). . . . .	80
4.21	Nyquist plot of open loop with $H_2$ feedback control for simulated response .	82
4.22	Nyquist plot of open loop system with $H_2$ output feedback control for experimental response . . . . .	83
4.23	Magnitude of the power spectral density of the reflecting sound wave without and with $H_2$ output feedback control for experimental data (green, blue). In the legend ex control stands for experimental response with controller and ex no control stands for experimental response without control. . . . .	83
4.24	Magnitude of the power spectral density of the reflecting sound wave without control and with $H_2$ output feedback control for simulated response (green, blue). In the legend box sim control stands for simulated response with controller and sim no control stands for simulated response without control. . .	84
4.25	Time domain response of the reflecting sound wave. The FxLMS controller is tuned online. . . . .	84
4.26	Magnitude of the power spectral density of the reflecting sound wave without control and with FxLMS feedforward control for experimental response (blue, green) . . . . .	85

5.1	$\gamma - plane$ with remote and local output reduction circles for single frequency. In this illustration the distance between the two centres is greater than the sum of the radius of the two locus (red line). . . . .	94
5.2	$\gamma - plane$ with remote and local output reduction circles for single frequency. In this illustration the distance between the two centres is smaller than the sum of the radius of the two locus (red line). . . . .	94
5.3	Minimum phase reflecting technique . . . . .	95
5.4	Bode plot of the raw experimental data for the control paths (blue) and bode plot of the high order FIR filter fitted to the experimental data (green). . .	101
5.5	Bode plot of the raw experimental data for the disturbance paths (blue) and bode plot of the high order FIR filter fitted to the experimental data (green). . .	102
5.6	Remote geometric feedback control design procedure . . . . .	102
5.7	Nyquist plot of open loop system with $H_2$ output feedback control for experimental response . . . . .	104
5.8	Magnitude of the power spectral density of the reflecting sound wave without and with $H_2$ output feedback control for experimental data (blue, green). . .	105
5.9	Nyquist plot of open loop system with remote geometric feedback control for experimental response . . . . .	106
5.10	Magnitude of the power spectral density of the reflecting sound wave without and with remote geometric feedback control for experimental data (blue green). . .	107
5.11	Magnitude of the power spectral density of the reflecting sound wave with remote geometric feedback control and with $H_2$ output feedback control for experimental data (green, blue). . . . .	108
5.12	Remote measurement reduction loci (green circles). Local measurement reduction loci (blue circles). $\gamma - values$ for $H_2$ controller (red squares). $\gamma - values$ for Remote geometric controller (red crosses). . . . .	109
5.13	Remote measurement reduction loci (green circles). $\gamma - points$ for optimal remote reductio (blue squares). $\gamma - values$ for $H_2$ controller (red squares). $\gamma - values$ for Remote geometric controller (red crosses). . . . .	110

5.14	Distance (Euclidian norm) of the optimal remote reduction points and the $\gamma$ - values for the $H_2$ and Geometric designs . . . . .	111
6.1	LFT control architecture described by a MIMO generalised process ( $P$ ) and two output feedback controller ( $K_1$ and $K_2$ ) connected in parallel. Inputs of the generalised process are the voltage of the disturbance loudspeaker ( $E_{dis}$ ) and the voltage of the control loudspeaker ( $E_{con}$ ), furthermore the outputs are the undesired reflecting sound wave ( $P_{ref}$ ) to be minimised and the velocity of the control loudspeaker's baffle ( $w_{loud}$ ). . . . .	115
6.2	Bode plot of the raw experimental data for the control paths (blue) and bode plot of the high order FIR filter fitted to the experimental data (green). . .	117
6.3	Magnitude response of the raw experimental data for the disturbance path (disturbance voltage to reflecting sound wave). . . . .	117
6.4	Selective resonance geometric feedback control design procedure. . . . .	118
6.5	Nyquist plot of open loop system with $H_2$ output feedback control for experimental response. . . . .	119
6.6	Magnitude of the power spectral density of the reflecting sound wave without and with standard remote Geometric output feedback control for experimental data (blue,green). . . . .	120
6.7	Nyquist plot of open loop system with remote geometric feedback control for experimental response. . . . .	120
6.8	Magnitude of the power spectral density of the reflecting sound wave without and with selective resonance geometric feedback control for experimental data (blue,green). . . . .	121
6.9	Magnitude of the power spectral density of the reflecting sound wave with standard geometric feedback control and with selective geometric control for experimental data (green, blue). . . . .	122

6.10	Remote measurement reduction loci (green circles). Local measurement reduction loci (blue circles). $\gamma$ - values for selective Geometric controller (blue squares). $\gamma$ - values for Remote geometric controller (green squares). Optimal reduction points (red crosses). . . . .	123
6.11	Distance (Euclidian norm) of the optimal remote reduction points and the $\gamma$ - values for the Selective Geometric and Standard Geometric designs. . .	123
7.1	Rectangular acoustic duct with a disturbance loudspeaker source at position $z = 0$ (red) and a simply supported boundary reflecting panel at position $z = L$ (red). To ideal microphones are positioned at point $z_1 = L - 0.1$ and $z_2 = L - 0.1 - \Delta z$ . . . . .	127
7.2	Primary mode shape of thin acoustic panel . . . . .	128
7.3	Simply supported thin rectangular panel with dimensions $L_x, L_y$ , thickness $h_p$ . The excitation of the panel is due to the incident sound wave and the control force (inertia actuator illustrated with yellow) positioned in the centre of the panel. . . . .	132
7.4	Inputs of the generalised process are the disturbance pressure wave and the control force, furthermore the outputs are the undesired reflecting sound wave to be minimised and the velocity of the reflecting panel. . . . .	134
7.5	Original model for the disturbance path of coupled acoustic duct-loudspeaker-panel setup (blue) Low order ( $8 - th$ ) transfer function model fitted to the original model (green) . . . . .	137
7.6	Original model for the control path of coupled acoustic duct-loudspeaker-panel setup (blue) Low order ( $8 - th$ ) transfer function model fitted to the original model (green) . . . . .	138
7.7	Offline $H_2$ control design for reduction of reflecting noise inside simulated coupled acoustic duct-loudspeaker-panel setup. . . . .	139
7.8	Bode plot of the simulated data for the control path to velocity (blue) and bode plot of low order ( $8 - th$ ) transfer function fitted to the simulated data (green). . . . .	140

7.9	Remote geometric control design for reduction of reflecting noise inside simulated coupled acoustic duct-loudspeaker-panel setup. . . . .	141
7.10	Nyquist plot of open-loop system with $H_2$ controller . . . . .	142
7.11	Bode plot of reflecting sound wave without control (blue), Bode plot of reflecting sound wave with $H_2$ velocity feedback control applied (green). . . . .	143
7.12	Nyquist plot of open-loop system with geometric controller. . . . .	144
7.13	Bode plot of reflecting sound wave without control (blue), Bode plot of reflecting sound wave with Remote Geometric feedback control applied (green). . . . .	145
7.14	Bode plot of reflecting sound wave with $H_2$ velocity feedback control applied (blue), Bode plot of reflecting sound wave with Remote Geometric feedback control applied (green). . . . .	146
8.1	Rectangular panel with incident acoustic wave labelled with red. The angles $\vartheta_i$ and $\varphi_i$ represent the incident wave's direction. . . . .	168

# List of Tables

2.1	Tuning parameters based on the ZN step response methodology [Cominos and Munro, 2002] . . . . .	31
2.2	Tuning parameters based on the ZN frequency methodology [Cominos and Munro, 2002] . . . . .	32
3.1	Values of coefficients used for the simulated acoustic duct loudspeaker system	43
3.2	Equations used to simulate conduct the FxLMS design . . . . .	52
3.3	Equations used to simulate the reflecting sound wave for the controlled case	57
5.1	Predicted resonant frequencies for an acoustic duct of length 2.054m . . . . .	104
7.1	Values of coefficients used for the simulated rectangular acoustic duct . . . . .	130
7.2	Reflecting panel specifications . . . . .	132
7.3	Values of coefficients used for the simulated loudspeaker . . . . .	133

# Chapter 1

## Introduction

### 1.1 Motivation and Problem Definition

As an increased number of large industrial equipment such as engines, blowers, fans, transformers and compressors are in use, acoustic noise problems become more and more evident. In addition, the growth of high-density housing increases the exposure of the pollution of noise from a variety of sources [Kuo and Morgan, 1995]. Furthermore, because of cost constraints a tendency to use lighter materials for buildings and transportation equipment is now being deployed and this kind of actions can result in environmental noise. Acoustic noise need not be limited to air; underwater or hydro acoustic noise is a problem in certain marine settings and applications but for reasons of simplicity the focus of this research is only on airborne problems. The combination of light material and the presence of large number of sources emitting noise create a problematic environment. This could lead to hearing loss, disturb verbal communications or cause nuisance. Furthermore, noise can result in a large number of non-auditory effects on health []. Noise pollution extends beyond just the simple discomfort we feel and can have a negative impact on sensitive sensor readings in laboratories. It is therefore necessary to develop methods of reducing the unwanted noise waves.

The problem of the undesired noise pollution is that in most cases the source of emission is not accessible for applying control directly to it. Traditionally, the use of passive techniques has been the favoured method of attenuating the undesired acoustic sound waves such as enclosures, barriers and silencers. The main problem that occurs when using pass-

ive control techniques is the limited efficiency at low frequencies [Kuo and Morgan, 1995]. Passive, damping techniques provide good isolation at frequencies above 1000 Hz; however, the majority of the problems related with acoustic noise are met in systems which operate at frequencies between 20 - 1000 Hz [Fuller and Von Flotow, 1995].

In an effort to overcome this problem, Active Noise Control (ANC), in which additional secondary sources are used to cancel noise from the original primary source, has received considerable interest and has shown significant promise. ANC involves an electroacoustic or electromechanical system that cancels the primary (unwanted) noise based on the principal of superposition; specifically, an anti-noise of equal amplitude and opposite phase is generated and combined with the primary noise, thus resulting in the cancelation of both noises [Nelson et al., 1993]. The amount of primary noise cancelation depends on the accuracy of the amplitude and phase of the generated anti-noise. The ANC system efficiently attenuates low-frequency noise where passive methods either are ineffective or tend to be very expensive or bulky. Thus, application of the ANC technique is a modern supplement to conventional passive systems. Acoustic ANC is developing rapidly because it permits improvements in noise control, often with potential benefits in size, weight and volume. Its performance at higher frequencies is limited by several factors, including the need for an increased sampling rate and the existence of higher-order modes that result in a much more complicated noise field [Nelson et al., 1993]. Fortunately, passive techniques tend to be very effective at higher frequencies and offer a good approach to most noise problems. At low frequencies, where lower sampling rates are adequate and wavelengths are long, active attenuation may offer significant advantages. In addition, cost and physical size often limit the noise reduction that can be practically achieved at low frequencies with a passive silencer.

Specific applications for ANC that are now under development include attenuation of unavoidable noise sources in the following end equipment [Kuo and Morgan, 1995]:

*Automotive.* Including cars, vans, trucks, ground moving machines, military vehicles, etc.

*Industrial.* Fans, air ducts, chimneys, transformers, blowers, compressors, pumps, chain saws, wind tunnels, noisy plants, public phone booths, office cubicle partitions, ear protectors, headphones, etc.

*Transportation.* Airplanes, ships, boats, pleasure motor boats, helicopters, snowmobiles, motorcycles, diesel locomotives, etc.

The study topic to be explored is closely related with the vast research field of ANC. Specifically, the main objective of this PhD project is to investigate the undesired acoustic resonances that build inside closed cavities due to the presence of a disturbance source and to develop a control design that can reduce them, figure 1.1. The reason these acoustic resonances occur inside the closed environment is due to the standing waves that occur when the primary disturbance source and reflected sound wave superimpose with each other. An intuitive approach in order to reduce the interior noise pollution (acoustic resonances) is to develop a control design that will cancel the reflected sound wave and hence no standing waves will be present to create the undesired acoustic resonances. The control architecture considered throughout the project is an ANC Feedback controller that makes use solely of local measurements such as the velocity or the acceleration of the controlled boundary, figure 1.2. This choice of design, in contrast to popular methods that rely on remote measurements (pressure microphones), is cost more efficient and the implementation requires far less intrusion into the acoustic environment. Through the completion of this project advances in attenuating reflecting sound waves initially in one-dimensional simulated situations such as acoustic ducts and validated in experimental situations is achieved. Furthermore, the affect of the coupling of the structural dynamics of the reflecting surfaces used to cancel the reflecting sound waves is examined. This investigation is of critical importance, because in the presence of a complex structure many resonant frequencies will emerge making the solution of the problem to be solved more complicated. These added resonances have to be dealt with thorough analysis, as they might lead to destabilisation of the control system or even worse uncontrollability of the system.

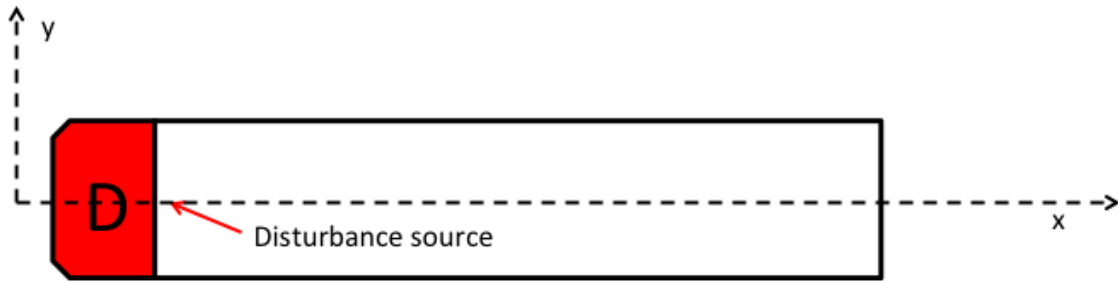


Figure 1.1: Acoustic duct with a disturbance source placed inside it.

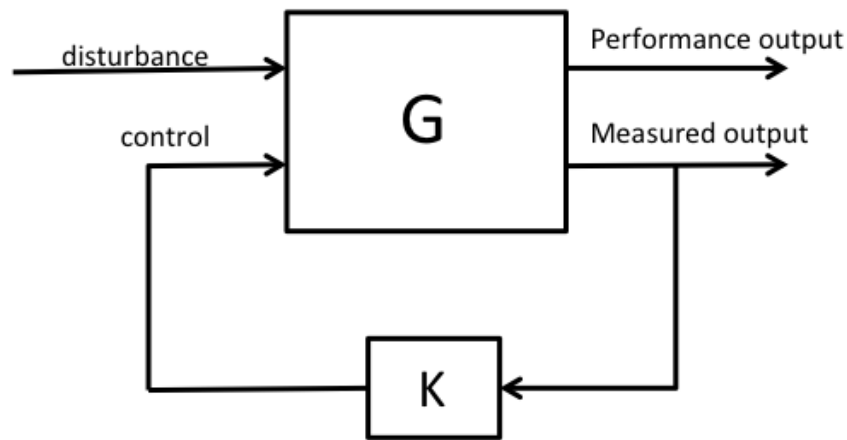


Figure 1.2: Proposed feedback control architecture to solve the acoustic resonance problem.  $G$  is the plants dynamics and  $K$  is the feedback controller.

## 1.2 Introduction to Active Noise Control Methods

The majority of ANC methods can be broadly grouped into two major classes, feedback control strategies and feedforward control strategies [Alkhatib and Golnaraghi, 2003]. In the following subsections a brief description of the two ANC methods (feedforward and feedback) is carried out.

### 1.2.1 Feedforward Designs

Feedforward control designs are rather appealing as they exhibit good performance in terms of reducing the undesired noise. This type of control requires prior knowledge of the excitation due to the primary source.

There are two cases in which such knowledge can be acquired. The first case is when the disturbance is due to a deterministic in nature action (examples of such are harmonic and tonal excitations). In principle the future behaviour of such a disturbance can be perfectly predicted from its previous behaviour. In practice, a reference signal is usually derived from the primary source of the disturbance and used to maintain the synchronisation of the secondary excitation (control source). The second example of where prior knowledge of the primary disturbance is available is when the disturbance is propagating through a media (air, fluid etc.) and a sensor can be used to detect the incident disturbance. It must be made clear that this detection sensor does not generate a measurement of the output of the plant to be controlled. Specifically, the output from these sensors are utilised to mimic the inverse of the primary source when it reaches the location of the secondary control source. Additionally, error sensors that measure the overall output of the controlled plant can be used in the feedforward control design in order to monitor the controller's performance and lead to an updating feedforward design.

It is common to utilise the adaptive tuning control methods in ANC when selecting feedforward designs and this is done in order to track any changes to the spatial distribution and frequency of the primary disturbance. Adaptive feedforward control algorithms for ANC and Active Vibration Control (AVC) are a popular method and have been extensively investigated in the literature, see for e.g. [Daley and Zazas, 2012; Elliott et al., 1987]. It has been utilised for practical applications, for example, the suppression of airplane interior noise [Borchers et al., 1992; Elliot et al., 1990; Johansson et al., 1999]. Probably one of the most popular adaptive feedforward control designs is the Filtered-x Least Mean Square (FxLMS) algorithm introduced in the early 80s [Burgess, 1981; Widrow and Stearns, 1985]. In order to achieve noise mitigation the FxLMS algorithm updates the coefficients of an FIR filter at every sampling instant by an amount dictated by a least mean squares (LMS) algorithm. The predicted (anti-noise) in this case can therefor be considered as the output signal from a dy-

dynamic system, i.e. a feedforward path. It must be emphasised that the LMS rule in order to guarantee stability, requires this filtered forward signal. Which is the reason why the method is called FxLMS. In order to avoid any confusion and assume that this type of control is a feedback controller it must be highlighted that the controller that is responsible for actively attenuating the primary disturbance is not driven by any output feedback signal of the plant. The algorithm makes use of the feedforward path's signal in order for the compensator to converge at the ideal solution. A similar algorithm causing adjustments to the coefficients of an IIR filter is termed as filtered-u LMS algorithm [Eriksson et al., 1987]. However, the convergence rate of FxLMS and FuLMS algorithm is slow for broadband disturbances, such as those encountered during changes in engine speed [Inoue et al., 2004]. For more academic research works on ANC based on feedforward control algorithms, the reader is referred to [Kuo and Morgan, 1995; Nelson et al., 1993].

### 1.2.2 Feedback Designs

Feedback control, on the other hand, is more suited when prior knowledge of the excitation is not readily available. Feedback control involves sensing the vibration output and feeding it back to a controller which then drives an actuator to cancel or minimise the effect of the primary excitation. Unlike feedforward techniques, many feedback control methods can be employed to reduce random excitation perturbations. It has also been used in conjunction with feedforward control for active vibration control [Meurers and Veres, 2000]. The stability and performance analysis tools are well developed for feedback techniques and can be implemented using a fixed parameter filter [Elliott, 2000; Hansen, 1996]. However, the controllers are mostly designed off-line for a pre-determined model of a plant. Hence, there is less possibility for adaptation to dynamical variations in the plant. In [Meurers et al., 2002], a feedback control design method for mitigation of discrete frequency excitations with a high degree of adaptability to dynamic changes in the plant is presented. Although it does not require a reference signal, vibration is attenuated only for discrete predetermined frequencies. Also, an initial model of the plant comprised of complex gains at those frequencies is required prior to implementation. Finally, the real time computation involves updating the control input instead of updating any filter coefficients for the controller.

The varied vibroacoustic attenuation requirements for many applications can be considered using different cost functions as parameters to be minimised [Anthony and Elliott, 2000; Bardou et al., 1997; Nelson et al., 1993]. This performance is evaluated based on the magnitude of vibration output at the location of one or more error sensors. A typical example is the application of modern control theory tools such as Linear Quadratic Gaussian design for vibration suppression [Bhattacharya et al., 2002].

However, the control of local outputs alone does not take into account the response of the whole structure for AVC. Active control of lightly damped structures in a narrow spatial region may lead to increased response away from the error sensor positions. Therefore, this requires a wide distribution of sensors which may not be sufficient to quantify global attenuation due to the response at the unmeasured locations. New lightweight structures have recently become widespread in the construction of cars and airplanes due to their improved strength and stiffness. This can cause discomfort to passengers due to an increase in sound transmission and radiation in the low to middle audio frequency spectrum [Gardonio, 2002].

Distributed sensors and actuators for decentralised control is another promising approach to tackle the global vibration response [Jiang and Li, 2009]. An interesting control design that has recently been introduced by researchers in the Institute of Sound and Vibration (ISVR) named Direct Velocity Feedback Control (DVFC) for decentralised control usually finds favour due to its simplicity of implementation [Lee et al., 2002] as the controller consists of a simple feedback gain which is fed the velocity measurement of the controlled structure, acquired from the distributed sensors. The objective is often to reduce the radiation of noise from vibrating structures, such as flat panels. It so happens that particular modes contribute more effectively than others towards the overall sound radiation [Baumann et al., 1992]. This leads to another consideration instead of merely mitigating the global vibration response of the structure [Zilletti et al., 2012]. Active control of vibration with an aim of reducing the sound power radiated by the structure is termed as Active Structural Acoustic Control (ASAC).

## 1.3 Contribution to Knowledge

In this section, a brief summary of the overall contributions achieved for the completion of the PhD project is listed.

- An experimental pulse tube setup, was reconfigured and used to approximate a theoretical one-dimensional duct in order to have a apparatus to validate experimentally all simulated results. Having the test rig allowed experimental validation of a feedback control architecture of a Remote Geometric design that has never before been applied in the field of ANC. This Geometric design was first introduced for AVC problems [Ubaid et al., 2011]. In terms of performance (reduction of reflecting sound wave) the Geometric controller reduces broader frequency ranges when compared to traditional feedback designs such as the  $H_2$  optimal feedback controller. For implementing the Geometric design only local measurements of the controlled active device are required, hence in provides a more compact solution when compared to feedforward designs such as the FxLMS. Additionally, the Geometric approach allows the designer to inspect the maximum feasible reduction any feedback controller can achieve regardless the controller utilised. This insight is important as it provides the designer a tool to compare any feedback controller to the optimal achievable performance allowed by the physical setup of the test rig.
- The Remote Geometric design requires a restrictive interpolation procedure in order to form the stable feedback controller. This step has a result to limit the number of the controlled acoustic resonances. Therefore an alteration of the original design was proposed. Hence in an attempt to simplify the interpolation step the novel design constructs two Remote Geometric feedback controllers that operate in parallel connection, Selective Resonance Geometric Control (SRGC). This approach, was successfully implemented on the apparatus. The Selective Geometric Resonance design has the same performance of the original Geometric design (reduction of reflecting sound) but doesn't enhance to the same level the uncontrolled acoustic resonances.
- A  $H_2$  optimal controller was designed and successfully implemented on the apparatus.

Furthermore a FxLMS controller was also successfully implemented and compared to the suggested local feedback controller. In terms of performance (reduction of the reflecting sound wave), the FxLMS design was able to reduce the reflecting sound wave more and in broader frequency ranges. Nevertheless, the intent of the proposed feedback design is focused on how an active control setup for acoustic problems can be implemented in a simpler manner. With respect to the complexity (required plant models) and cost efficiency (actuators, sensors) the feedback approach is by far superior. Emphasis was given also on the practical issues required to implement the designs on the test rig [Pelegrinis et al., 2013]. Furthermore, the critical importance of this work is the local nature of the proposed feedback design. Specifically, only the acceleration of the controlled loudspeaker's cone is required to implement the  $H_2$  controller.

- A novel application of a PID Frequency Loop Shaping (FLS) local velocity feedback control design was developed to cancel the undesired reflecting sound wave in a one-dimensional setup. An analytical model of the adopted setup was derived and utilised for simulations. In order to appreciate the novelty of the application an in depth investigation of the feedback and feedforward control designs applied in solving ANC problems was included with emphasis on the popular FxLMS. Furthermore, a numerical example of the FLS PID and the FxLMS designs was carried out. Through the investigation of the example it was possible to assess the performance of the proposed novel solution [Pelegrinis et al., 2012]. The novelty of the FLS PID controller lies in the local nature of the design in combination with the automatic tuning procedure utilised to form the feedback controller.
- The local feedback designs that were validated experimentally made use of a loudspeaker in order to deliver the control. A loudspeaker is a rather restrictive electroacoustic device for real life applications, as its dimensions are predetermined and therefore limit the range of applications. Hence, an investigation of the benefits and trade offs of applying local feedback control designs on thin flat panels is considered. This work considers flat panels with an embedded collocated actuator/sensor pair. This electroacoustic device in contrast to the loudspeaker can be fitted to the desired

problem regardless the dimension restrictions. Interest is focused on the reduction of reflecting sound waves for of plane wave propagation problem with use of these actively controlled panels. A one-dimensional acoustic duct was considered. Specifically, in order to deal with the complex dynamics of the reflecting panel the proposed feedback controllers were the  $H_2$  and Remote Geometric design and made use of a theoretical model developed for the purpose of simulations. The two proposed feedback designs ( $H_2$  and Remote Geometric) where successfully implemented and simulated. With regards to performance (reduction of the reflecting sound wave) the Geometric design was able to achieve greater reductions when compared to the  $H_2$  design. In addition the modelling included actuator dynamics, making the proposed solution more viable for future experimental validation.

## 1.4 Thesis Overview

In this section the layout of this PhD thesis is presented with a brief description of each chapter.

- Chapter 2 In order to appreciate the novelty of the application an in depth investigation of the feedback and feedforward control designs applied in solving ANC problems is included with emphasis on the popular FxLMS algorithm. Furthermore, emphasis is given to PID control and popular tuning methods, this is review is carried out because the proposed solution requires a feedback PID controller. Finally the chapter ends with a section of concluding remarks concerning the benefits of applying the proposed feedback design.
- Chapter 3 presents a novel application of a PID frequency loop shaping velocity feedback control design developed to cancel the undesired reflecting sound ways in a one dimensional setup. The chapter includes analytical modelling of the adopted setup utilised for simulations and presents the achievable performance. Furthermore there is a thorough description of the implementation of the PID tuning strategy (Frequency Loop Shape method). Additionally, a model of a coupled acoustic duct system is developed. The simulated environment is used for testing how the PID controller performs

(how much reduction of the reflecting sound wave is achieved). In order to evaluate the performance of the proposed feedback design a FxLMS controller is implemented and presented for the same simulated example. Finally the chapter ends with a section of concluding remarks concerning the benefits of applying the proposed feedback design.

- Chapter 4 presents experimental results. In this chapter, initially, a thorough description of the experimental pulse tube which is used to approximate the theoretical one dimensional setup modelled in the previous section is presented. Furthermore, a technique employed to retrieve the reflecting sound wave from two non matched microphones is described. In contrast with Chapter 2 an experimental model is developed for the purpose of designing the controller. It is reasoned and backed up with simulated responses of the plant why the FLS feedback design described in Chapter 2 is not applicable to this experiment. In order to bypass this problem, two control designs are considered, one feedback and one feedforward. Specifically, a  $H_2$  feedback control design is presented along with the FxLMS design. The proposed methods are implemented on the apparatus. The designs are compared in terms of performance, how much of the undesired reflecting sound wave is reduced. Emphasis is given also on the practical issues required to implement the designs on the test rig. Finally, the chapter ends with a section of concluding remarks concerning the benefits of the feedback designs and the importance of the successful modelling of the test rig with the use of experimental data.
- Chapter 5 presents experimental results. In this chapter, two feedback control designs are considered. Specifically, the  $H_2$  feedback control design along with a Remote Geometric feedback design. The proposed methods are implemented on the same apparatus previously described in Chapter 4. The designs are compared in terms of performance, how much of the undesired reflecting sound wave is reduced. Finally, the chapter ends with a section of concluding remarks concerning the benefits of the geometric feedback design in contrast to the  $H_2$  feedback design.
- Chapter 6 presents experimental results. In this chapter, two feedback control designs are considered. Specifically, a novel alteration of the geometric design named selective

resonance geometric feedback control design along with the standard Remote Geometric feedback design previously described in Chapter 5. The proposed methods are implemented on the same apparatus as with the other two experimental Chapters 4 and 5. The designs are compared in terms of performance, how much of the undesired reflecting sound wave is reduced. Finally, the chapter ends with a section of concluding remarks concerning the benefits of the altered geometric feedback design in contrast to the original geometric feedback design.

- Chapter 7 investigates the benefits and trade offs of applying local feedback control designs on thin flat panels in order to reduce the reflecting sound waves for a problem of plane wave propagation for a one dimensional acoustic duct. Specifically, in order to deal with the complex dynamics of the reflecting panel the proposed solutions are the  $H_2$  and the Remote geometric control designs. These controllers, make use of a theoretical model developed in similar manner as designed in Chapter 3. In addition the modelling includes actuator and sensor dynamics that makes the solution more viable for future experimental validation. Finally, the chapter ends with a section of concluding remarks concerning the benefits of the proposed feedback design and the importance of the successful modelling of the dynamics of the panel, actuator and sensor dynamics.
- Chapter 8 summarises the main results obtained and presented in this PhD thesis and the future research that can improve the performance of the suggested control schemes.

The thesis contains a list of references used to write and support this PhD thesis.

Appendix A contains the mathematical procedure (solution of the boundary value problem) required to develop a model of the plant's dynamics used in Chapter 3 and Chapter 7.

Appendix B contains up to date publication and conference papers in which the author of this thesis has been involved.

# Chapter 2

## Active Impedance Matching an Approach to Control Reflecting Sound

### 2.1 Introduction

As mentioned in section §1.1 the main goal of this project is to develop a ANC design that will be able to reduce the reflections of sound waves inside closed environments. The aim is to develop an active control strategy for an acoustic duct system as illustrated in figure 2.1, that will effectively reduce the undesired reflecting sound wave that occurs due to the presence of a reflecting boundary element placed at the opposite end of the disturbance source. Theory suggests that, when the specific acoustic impedance of the boundary surface perfectly matches the characteristic impedance of the surrounding fluid no reflection will occur and sound propagates as if contained within an infinitely long acoustic duct (figure 2.2), such a method can be referred to as impedance matching [Kinsler et al. [1999]; Beranek et al., 1954]. Therefore, the sound wave due to the disturbance source will in theory appear to propagate into infinity and not reflect at any point inside the duct. An example of a control strategy that makes use of impedance matching is found in published work such as [Lee et al., 2012], where an active acoustic coating is inserted parallel to the direction of wave propagation of a cylinder waveguide and a dynamic match of the acoustic impedance of the incoming wave is achieved. The proposed solution to the problem, in contrast to the impedance matching technique implemented by [Lee et al., 2012] is to match the specific

acoustic impedance of the controlled boundary end with the characteristic impedance of the fluid inside the acoustic duct and therefore avoiding the need of covering the entire waveguide with an intrusive active coating.

In order to achieve this matching the use of a novel output feedback design is developed. The selection of a feedback control is primarily due to the fact that in contrast to feedforward control, it does not require the use of a reference signal. Such a requirement in many acoustic problems is a rather difficult task and furthermore increases the physical size and complexity of the controller significantly.

The type of controller selected to solve the described problem is the popular PID controller. This choice is done for two reasons. Firstly, PID control has been investigated thoroughly and a large number of stable and robust tuning methods have been developed for many problems [Cominos and Munro, 2002]. The second reason for choosing PID has to do with the fact that the three controller coefficients can be related to physical values of the plant (velocity, acoustic impedance etc.) and therefore the beneficial results of applying the controller can be related to the physics of the setup. The final step is to select the tuning method of the control coefficients. The desired target frequency response of the controlled surface is well defined (acoustic impedance of ambient fluid), hence the problem of impedance matching can and will be solved with the use of a Frequency Loop Shaping (FLS) design procedure [Grassi et al. 2001]. This tuning method is developed to minimise the difference between the specific acoustic impedance of the controlled boundary end and the characteristic impedance of the fluid inside the duct, which is air (in this thesis all problems considered are airborne).

This chapter is organised in the following manner. Initially for reasons of completeness and awareness section §2.2 contains a brief description of Passive control and how it can be used for noise control. In section §2.3, a brief description and analysis of previous work related to the ANC problem that is investigated is presented. In section §2.5, a review of some popular PID tuning methods is presented, furthermore emphasis is given to the FLS tuning method and why it is ideal for solving the acoustic problem. Finally, section §2.6 provides some concluding remarks with regards to the suggested design and what benefits are achieved in comparison to other proposed designs.

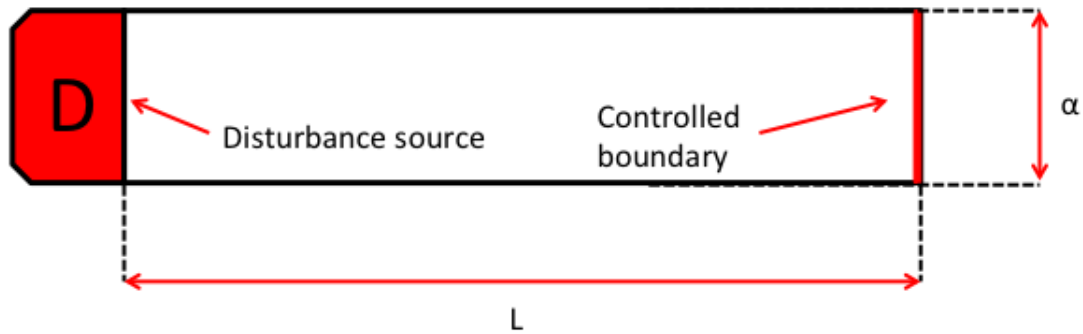


Figure 2.1: Acoustic cylinder shaped duct of constant diameter  $a$  and fixed length  $L$  with disturbance source placed at one end (D) and at the other end is a controlled boundary surface.

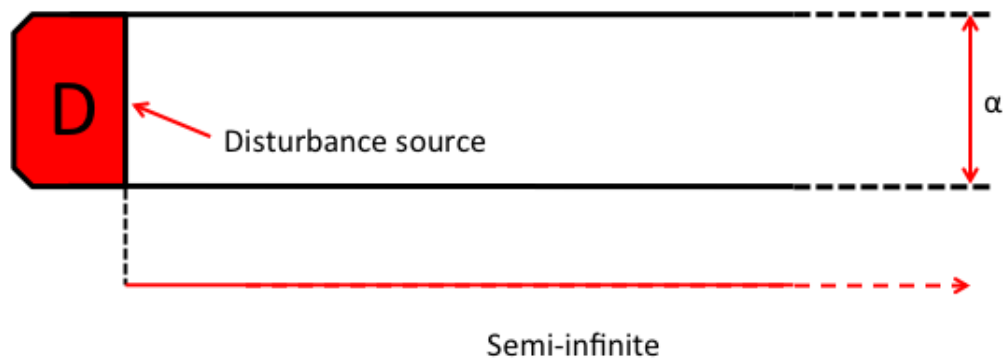


Figure 2.2: Acoustic cylinder shaped duct of constant diameter  $a$  and semi-infinitely long with disturbance source placed at one end (D).

## 2.2 Passive Noise Control

The term passive control refers to a range of approaches where no additional energy is input to the system. By definition such systems cannot be unstable. The primary reason passive approaches are selected for noise control are the low cost, the relative simplicity in implementation and the inherent guaranteed stability. Two major setbacks passive control exhibit

are the increment in physical size and the lack of good performance at the low frequency range [Nelson et al., 1993].

### 2.2.1 Helmholtz Resonators

Helmholtz resonators are commonly defined by making use of a mass-spring element model. They are commonly utilised for the absorption of acoustic sound waves. Figure 2.3 illustrates the Helmholtz resonator along with the mechanical model of the acoustic device. The actual physical device consists of a cavity of total volume equal to  $V$  with a neck of length  $L$  connected to it, figure 2.3 (a). Due to the incident sound wave, the air located in the neck of the Helmholtz device will act like a lumped mass while vibrating, furthermore the air in the in resonator will operate as a spring because of its stiffness to the pressure difference. Due to the described phenomena, the ideal lumped parameter system for describing the Helmholtz resonator is the simple mass spring element.

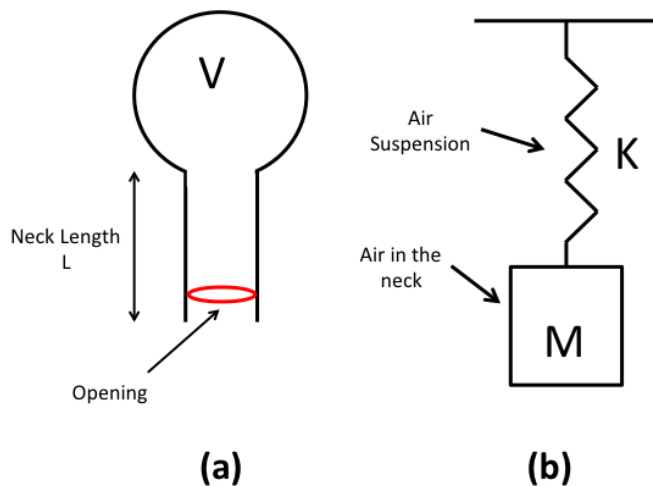


Figure 2.3: (a) Schematic illustration of a Helmholtz resonator that consists of a cavity of total volume equal to  $V$  and a neck of length  $L$  connected to it. (b) The mechanical analogous description of a Helmholtz resonator could be described as a mass concentrated in the narrow end of the tube ( $M$ ) and the fluid in the cavity mimics the characteristics of a spring with a stiffness coefficient ( $K$ ), this is because of the difference in pressure.

Because of the Helmholtz resonator can be modelled as a mass-spring element, the mechanical model will have one resonant frequency. Furthermore, it is possible to tune this resonance's characteristics (location and magnitude) by simply altering the physical parameters of the resonator (neck length, opening and volume of the cavity). Therefore, in order to increase noise attenuation the frequency at which the device resonates, is shifted as near as possible to the frequency at which the controlled plant will resonate due to its dominating frequency external input noise disturbance.

These devices have been applied in a wide range of problems, this due to the fact they are able to compensate individual resonances very effectively by interfering directly to the ambient sound field. One of the pioneers in investigating the use of Helmholtz resonators for broadband control is found in [Fahy and Schofield, 1980]. Specifically Fahy and Schofield investigated the impact of the device with the modes of enclosures. There have also been studies of the impact of the Helmholtz resonator's physical dimensions have on the signal resonance [Alster, 1972; Howe, 1976; Panton and Miller, 1975]. An intuitive approach in reducing the affect of lower resonant modes inside small rooms was derived by Doria. Specifically, he used an array of Helmholtz devices to split resonants peaks into multiple ones of smaller amplitude [Doria, 1995]. A more general investigation on the impact of Helmholtz resonators on reducing sound inside small enclosures was given by Cummings [Cummings, 1992].

It is common to consider the device rigid and this is because the materials that construct it are usually too thick to be affected by any forces generated by the vibrating air (due to the acoustic sound wave). The rigid assumption is not valid in the case when lighter materials are used to manufacture them. In order to remodel the Helmholtz resonator to include the impact the new material has to the device Photiadis introduced a theory that included an effective stiffness element in the model [Photiadis, 1991]. In addition to this modelling attempt Norris and Wickham extended Photiadis work by including a thin shell to model the cavity of the resonator [Norris and Wickham, 1993]. It must be highlighted that although the new generation of Helmholtz resonators because of their lighter frames have a smaller resonance.

## 2.3 Previous Work In Active Noise Control

As mentioned in the previous chapter the scientific field in which this project's impact lies is that of ANC. Before going into detailed analysis of the proposed feedback control strategy, a brief description and analysis of previous work involving the cancelation of reflected sound waves with the aid of active means is provided.

### 2.3.1 Filtered x Least Mean Square

Over the past few decades active noise control has been implemented efficiently with the use of a wide range of control algorithms. Probably, the most well known algorithm is the Filtered-x Least Mean Squares (FxLMS). The origin of which can be found 'Adaptive Signal Processing' [Widrow and Stearns, 1985]. Specifically, the method implements a gradient descent adaptation rule, Least Mean Square (LMS), for a filtered version of a reference signal. It is important to emphasise the use of the filtered reference signal rather than feeding the raw error signal to the adaptation rule and by doing so, possible instability is avoided [Morgan, 1980; Nelson et al., 1993]. The FxLMS algorithm is popular due to the fact that it is easy to implement and robust. It can achieve convergence even if there is a  $90^\circ$  phase error in the forward path estimate [Nelson et al., 1993]. One downfall of the FxLMS is its slow convergence rate. This is due to the small convergence coefficient. Alternatively if a larger convergence rate is selected we risk making the system unusable.

One would consider using an adaptive filter in noise reduction or cancelation problems. This because in such problems the filtered output is an estimate of the desired signal. It must be emphasised that because there are complex dynamics involved among the filter output and the estimated output, the algorithm chosen to implement the adaptation rule has to be done with caution in order to avoid an unstable design.

In order to implement the FxLMS methodology it is probably wise to start with the examining the LMS method. Once the LMS algorithm is fully explained the FxLMS algorithm will be extended by adding the filter. In figure 2.4 we illustrate a system that includes a compensator which is tuned with the LMS approach. The FIR filter output,  $y(n)$ , is expressed by the vector inner product (for each sample instant  $n$ ):

$$y(n) = w^T(n)x(n) \quad (2.1)$$

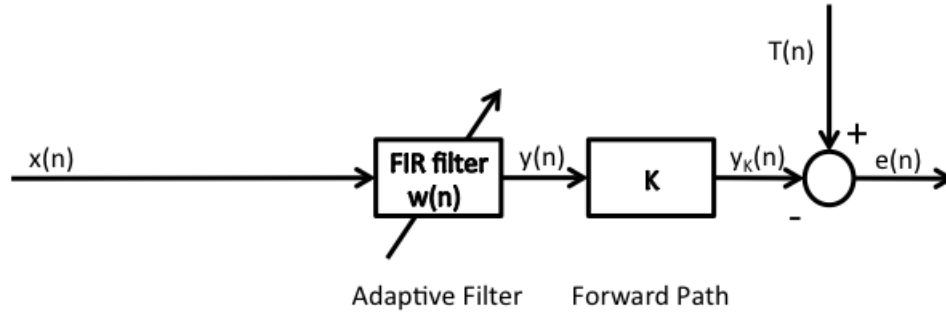


Figure 2.4: Block diagram of feedforward LMS algorithm. With  $x(n)$  is the input signal vector,  $w(n)$  is the adaptive filter's coefficients,  $K$  is the forward path of the process,  $y_K(n)$  is the output control signal  $T(n)$  is the desired output signal and  $e(n)$  is the error between output and desired signal.

Where  $x(n)$  is the signal fed to the plant and also to the adaptive filter and is expressed as:

$$x(n) = [x(n), x(n-1), \dots, x(n-M+1)]^T \quad (2.2)$$

Furthermore  $w(n)$ , is given by the following mathematical expression:

$$w(n) = [w_1(n), w_2(n), \dots, w_K(n)]^T \quad (2.3)$$

It is common in applications where controller are developed to define the estimation error. Specifically, this error is the the difference between the forward path,  $y_K(n)$  (figure 2.4), and the desired output of the plant,  $T(n)$ . The mathematical formula is given by:

$$e(n) = T(n) - y_K(n) \quad (2.4)$$

The following mathematical description is valid if it is possible to represent the control path as a FIR of  $J - th$  order:

$$D_K(n) = \begin{cases} c_n & \text{when } n \in \{0, \dots, J-1\} \\ 0 & \text{otherwise} \end{cases} \quad (2.5)$$

With this, the error can be represented by:

$$e(n) = T(n) - \sum_{i=0}^{J-1} c_i \sum_{m=0}^{M-1} w_m(n-i)x(n-i-m) \quad (2.6)$$

The Wiener (Mean Square Error) solution of the coefficient vector is acquired when we minimise the following quadratic function [Nelson et al., 1993; Widrow and Stearns, 1985]:

$$J_f(n) = E[e^2(n)] \quad (2.7)$$

For this calculation to occur, it is necessary to apply the gradient operator to the the mean square error  $J_f(n)$  which will give us:

$$\nabla_{w(n)} J_f(n) = 2E[e(n)\nabla_{w(n)}e(n)] \quad (2.8)$$

Hence if we recall that the target output of the plant,  $T(n)$ , must be independent to the filter,  $w(n)$ , and also accept that all the terms of the filter are time invariant, then the gradient for  $e(n)$  will be given by the following mathematical expression:

$$\nabla_{w(n)} e(n) = \begin{bmatrix} -\sum_{i=0}^{J-1} c_i x(n-i) \\ -\sum_{i=0}^{J-1} c_i x(n-i-1) \\ \vdots \\ -\sum_{i=0}^{J-1} c_i x(n-i-M+1) \end{bmatrix} \quad (2.9)$$

By inserting equation (2.9) in equation (2.8) we get a equation that links the gradient with the mean square error:

$$\nabla_{w(n)} J_f(n) = -2E[e(n)x_K(n)] \quad (2.10)$$

Where  $E[\cdot]$  is the expected value operator and  $x_K(n)$  is given by the following vector:

$$x_K(n) = \begin{bmatrix} -\sum_{i=0}^{I-1} c_i x(n-i) \\ -\sum_{i=0}^{I-1} c_i x(n-i-1) \\ \vdots \\ -\sum_{i=0}^{I-1} c_i x(n-i-M+1) \end{bmatrix} \quad (2.11)$$

The LMS with a gradient estimate is then given by:

$$\nabla_{w(n)} J_f^*(n) = -2e(n)x_K(n) \quad (2.12)$$

and would be able to provide a solution to the problem estimating with use of a dynamic system [Nelson et al., 1993; Morgan, 1980]. From this expression it leads us to the realisation that the original LMS algorithm is most probable to become unstable when considered for solving control problems. However it is proven that in some situations the conventional LMS algorithm will lead to a poor solution when eventually when it converges [Elliott et al., 1987; Nelson et al., 1993; Morgan, 1980]. The reason the LMS algorithm fails to achieve a stable control solution is primarily because the method utilises a estimate of the gradient which is not correct in the mean [Elliott et al., 1987].

Hence in order to bypass this inherent problem a compensated algorithm is obtained applying a filter to the reference signal. The ANC plant with the addition of a adaptive compensator that is tuned by the FxLMS approach is illustrated in 2.5 [Hakansson, 2004].

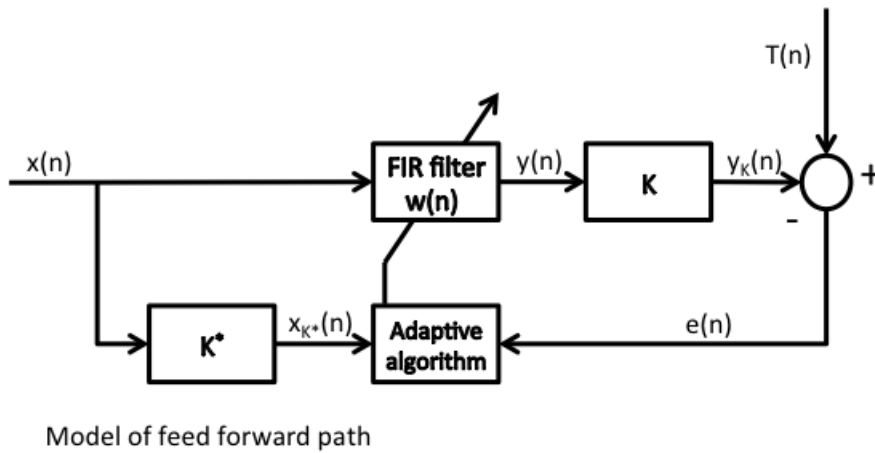


Figure 2.5: Block diagram of a plant with an active controller tuned with the FxLMS algorithm. With  $x(n)$  is the input signal vector,  $w(n)$  is the adaptive filter's coefficients,  $K$  is the forward path of the process,  $y_K(n)$  is the output control signal  $T(n)$  is the desired output signal,  $e(n)$  is the error between output and desired signal  $K^*$  is a model of the feedforward path of the plant and  $x_{K^*}(n)$  is the filtered output of the plant's input  $x(n)$  signal by the model of the feedforward path.

The FxLMS algorithm is given by the following equations:

$$y(n) = w^T(n)x(n) \quad (2.13)$$

$$e(n) = T(n) - y_K(n) \quad (2.14)$$

$$x_{K^*}(n) = \begin{bmatrix} -\sum_{i=0}^{J-1} k_i^* x(n-i) \\ -\sum_{i=0}^{J-1} k_i^* x(n-i-1) \\ \vdots \\ -\sum_{i=0}^{J-1} k_i^* x(n-i-M+1) \end{bmatrix} \quad (2.15)$$

Finally, the weights,  $w(n)$ , found in the filter are updated by the following rule:

$$w(n+1) = w(n) + \mu x_{K^*}(n)e(n) \quad (2.16)$$

With  $\mu$  we define the convergence coefficient. Additionally because the plant's forward path is again modelled with a FIR filter, its coefficients are defined with  $k_i^*$ , hence we have the following expression:

$$h_{K^*}(n) = \begin{cases} k_n^* & \text{when } n \in \{0, \dots, J-1\} \\ 0 & \text{otherwise} \end{cases} \quad (2.17)$$

It is a common choice to use an estimate of the impulse response for the forward path. Because of this,  $x_K^*(n)$  will be an approximation and not the actual reference signal, and magnitude of the differences between the estimation and actual forward path can and will affect the stability of the control algorithm and the rate with which the method converges to its solution [Elliott et al., 1987; Nelson et al., 1993; Morgan, 1980]. Having said that, it must be noted that the FxLMS method had good robust characteristics when dealing with errors in the estimation of the forward path [Elliott et al., 1987; Nelson et al., 1993; Morgan, 1980]. The literature suggests that the model used for the forward path must include a delay that is equal to the one found in the forward path of the plant [Elliott et al., 1987; Morgan, 1980]. When considering narrow-band problems the FxLMS method will eventually converge even when the phase errors in the estimate of the forward path reach values close to  $90^\circ$ . This characteristic is achieved when the convergence coefficient's ( $\mu$ ) magnitude is adequately low [Boucher et al., 1991; Nelson et al., 1993]. Finally, in the case which phase errors of the estimation are smaller than  $45^\circ$  will have insignificant influence on how fast the FxLMS algorithm converges [Boucher et al., 1991].

Having detailed all this it is necessary to establish some kind of boundaries to the convergence coefficient that will ensure that any action due to the FxLMS method will keep the system stable. Hence it is proven that a maximum value for the coefficient should be given by [Elliott and Nelson, 1989]:

$$\mu_{max} \approx \frac{2}{E[x^2 K^*(n)](M + \tau)} \quad (2.18)$$

where  $\tau$  is the total time lag found in the forward path (this is measured in discrete samples).

One of the most recently proposed solutions in the field of ANC has been focused on designing actuator setups that will enable active structural acoustic control (ASAC) of low

frequency noise radiated by vibrating structures [Zhu et al., 2003; Yu et al., 2007]. The work described by these authors explores the development of thin panels that can be controlled electronically so as to provide surfaces with desired reflection coefficients. Such panels can be used as either perfect reflectors or absorbers. The development of the control system is based on the use of wave separation algorithms that separate incident sound from reflected sound. The reflected sound is then controlled to desired levels. The incident sound is used as an acoustic reference for feedforward control and has the important property of being isolated from the action of the control system speaker. The suggested control procedure makes use of a half-power FxLMS algorithm and therefore requires installation of microphones in order to be applicable and the use of low pass filters which adds significant complexity to the solution of the primary problem.

Applications in which the adaptive feedforward design can also be found are sound compensation strategies that make use of both passive and active control. These type of control designs are classified as hybrid design, as they reap the low frequency performance advantages of active control while retaining the high frequency benefits found in passive control. Because of the FxLMS design's popularity efforts have been focused on modifying the algorithm to deal with more complex control scenarios. Examples of such methods can be found in the literature that are using constraints on the filtered reference signal [Kim et al., 1994], variable leakage for approximating non-linear systems [Gontijo et al., 2006]. Finally an interesting approach is given by [Tahir Akhtar and Mitsuhashi, 2009], where by modifying the error paths and the filter of the FxLMS design it is possible to increase the robustness of the algorithm.

Probably the most significant advantage the FxLMS method has to offer is its inherent ability to control any type of disturbance input. Always when given enough time. Such an advantage is important in situations where the disturbance to be controlled is random. The greatest disadvantage of the adaptive method has it the need of a model of the feedforward path.

Furthermore, the method requires a significant amount of computational power, in other words the order of the controller and model of the forward path will be bounded by the limitations of the devices used. The limit of the size of the filter depends on the sample rate

at which the algorithm is intended to operate. With respect to the hardware facilities and desired sample rate used for experimental validation, the limit of the size of the filters was found to be around the range of 128. Finally, the small convergence rate of the algorithm causes the design procedure to take long period of times to reach its optimal performance.

### 2.3.2 Direct Velocity Feedback Control

Another approach in the field of ASAC that could reduce the inherent implementation complexity of the previous feedforward control solution has been proposed and examined by a number of researchers [Lee et al., 2002]. Specifically, this research investigated the application of a low frequency volume velocity vibration control procedure for a smart panel in order to reduce sound transmission. The control algorithm makes use of a simple velocity feedback controller, figure 2.6, in order to add damping to the resonant frequencies of the controlled panel. The addition of damping will reduce the vibration that occurs when an incident acoustic wave impacts the panel and will thereby reduce the acoustic radiation efficiency and therefore the reflected sound wave is also reduced. In contrast to the FxLMS controller this approach does not require remote measurements (microphones) nor any complicated feedforward filters to model the control path. Furthermore, stability analysis is a much simpler task based on the Nyquist criterion [Ogata and Yang, 1970]. Although this simplistic approach (simple gain control) delivers a robust and stable controller due to the collocated properties of the controller it exhibits performance limitations as to how much damping could be added. Additionally, in order to control effectively the panel's reflections multiple sensor and control points are considered on its surface and because the design procedure does not involve any optimisation the tuning is carried out manually therefore requiring considerable time and hands on experience in order to deliver a stable and efficient controller. Another restriction of the Direct Velocity Feedback Control (DVFC) method is that it reduces, simultaneously, both the reflecting and transmitted sound waves without the ability of selecting which wave to reduce, this is due to the addition of damping to the controlled plant by the feedback signal. Hence, the DVFC method does not provide the control designer freedom to which sound wave to reduce (reflecting and transmitted). Therefore, in applications where acoustic cloaking is intended (reduction of reflecting sound wave without reduction of transmitted

sound wave) DVFC is not a solution.

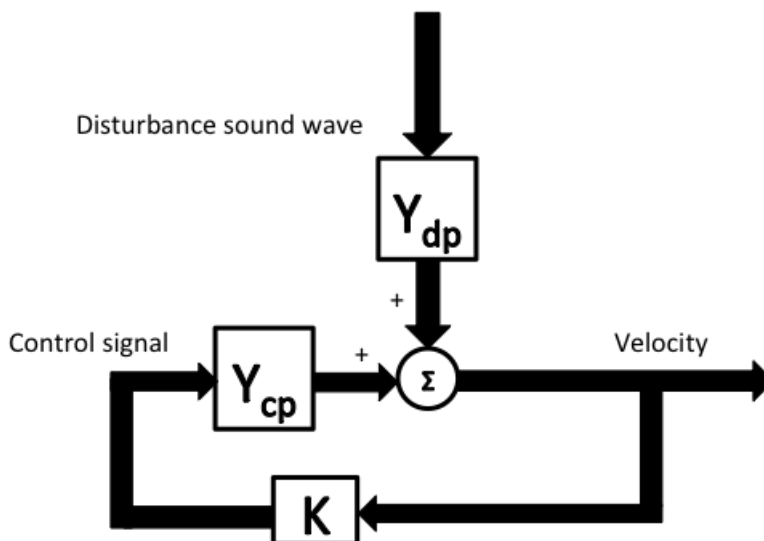


Figure 2.6: Direct velocity feedback control block diagram.  $Y_{cp}$  is the control path transfer function and  $Y_{dp}$  is the disturbance path transfer function.

### 2.3.3 Electroacoustic Absorbers Via Lead Lag Control

Finally, the most relevant scientific work to the proposed FLS PID feedback controller is a recent application in the field of ANC with the aim of developing ideal acoustic absorbers. Specifically, this novel work focuses on how to transform a loudspeaker in an active electroacoustic resonator [Lissek et al., 2011]. With the aid of sensors (microphones, optical velocity sensor) and control system, the proposed control design makes use of a simple lead-lag-gain velocity feedback controller that is able to achieve broadband sound absorption at the transducer diaphragm [figure 2.7]. This type of control in contrast with the DVFC has a more complex controller and is able to perform more effectively.

The main goal is to control the diaphragm velocity response in order to adapt the acoustic impedance of the loudspeaker to the characteristic impedance of air. Before the control design is described it is important to describe how the design intends to achieve the desired impedance matching. The reflection coefficient under normal incidence can be derived as [Kinsler et al., 1999]:

$$R(s) = \frac{p_0 c_0 - Z}{p_0 c_0 + Z} = \frac{1 - y(s)}{1 + y(s)} \quad (2.19)$$

where  $Z$  is the acoustic impedance of the reflecting element to be controlled,  $p_0$  is the density of the fluid (in this case air),  $c_0$  the speed of sound in the fluid (in this case air),  $y(s)$  is the frequency dependent formula of the velocity of the reflecting surface which in this case is the loudspeaker's diaphragm [figure 2.7]. Hence, by matching the acoustic impedance ( $Z$ ) with the specific acoustic impedance ( $p_0 c_0$ ) perfect absorption is achieved ( $R(s) = 0$ ). In order to achieve this matching, a generalised velocity response of the transducer diaphragm, which is related to the reflecting to any surrounding sound field is formed as:

$$y(s) = \rho_0 c_0 S \frac{Z_e(s) + BlC}{Z_m(s)Z_e(s) + (Bl)^2 + BlC} \quad (2.20)$$

where  $Z_e$  is the blocked electrical impedance and  $Z_m$  is the mechanical impedance of the loudspeaker,  $S$  is the effective area of the loudspeaker  $C$  is the controller to be designed to achieve impedance matching and  $B$  is the magnetic flux density and  $l$  is the effective length in meters of the electrical conductor that moves at right angles across the magnetic lines of force of flux density  $B$  [figure 2.7]. From equation (2.20) it is understood that the velocity of the diaphragm can be manipulated in such a way to alter the reflection coefficient [equation (2.19)]. From a control design perspective, the general objective is to specify control settings that [Lissek et al., 2011]:

1. meet the desired control bandwidth over which the transducer diaphragm is supposed to have prescribed behaviour,
2. ensure that the diaphragm velocity follows the time-varying reference as accurately and as fast as possible,
3. make the closed loop as insensitive as possible relative to change in the transducer parameters,
4. guarantee the stability of the closed-loop system.

Generally speaking, strict adherence to all requirements over the entire audio-frequency range

is limited by the technological design of the transducer [figure 2.7]. The block diagram of the described control design is illustrated in figure 2.8.

The disadvantage of this method is that it relies on empirical fine-tuning of the controller just as for the DVFC and therefore fails to address the ANC problems in a more general manner. Furthermore, the error signal used by the controller requires the use of a microphone and therefore increases the implementation complexity.

Ideally, the desired control design would make use only of local measurements from the controlled structure to achieve the desired impedance matching. Such an approach would be more practical for solving real life problems where additional sensors (microphones) is not an option.

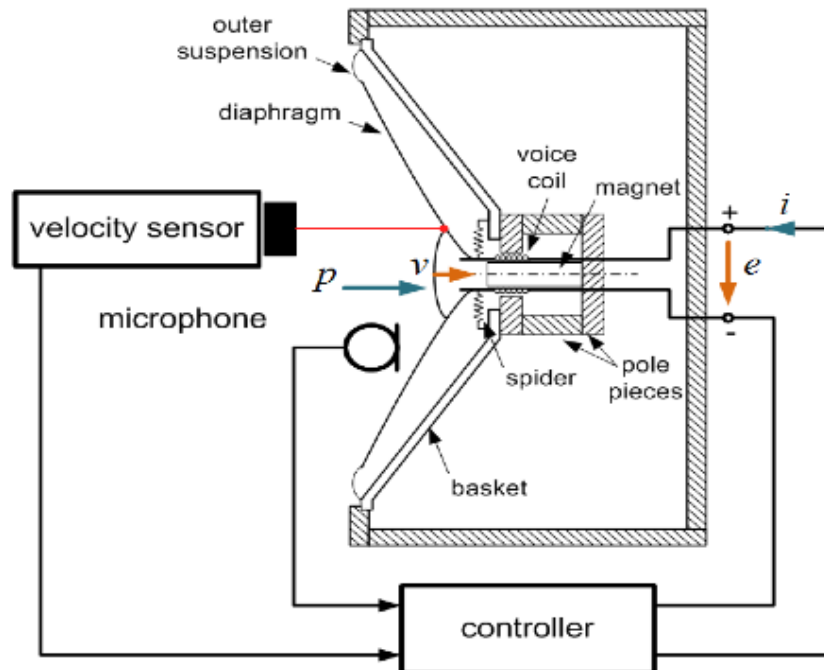


Figure 2.7: Electroacoustic absorber illustration describing the controller-sensor-loudspeaker setup [Lissek et al., 2011].

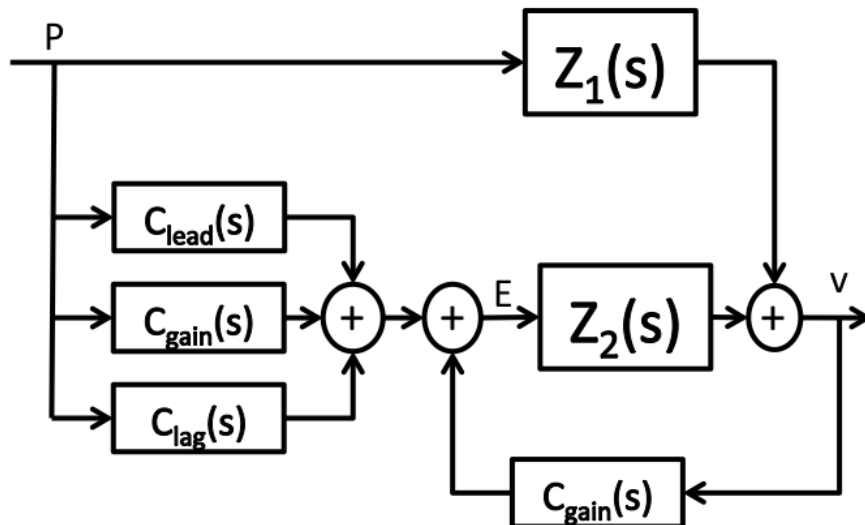


Figure 2.8: Block diagram layout for electroacoustic absorbers.  $C_{lead}(s)$  is a lead controller,  $C_{lag}(s)$  is a lag controller,  $C_{gain}(s)$  is a gain controller,  $Z_1(s)$  is the transfer function describing the path between the disturbance pressure wave ( $P$ ) and the velocity of the transducer's diaphragm and  $Z_2(s)$  is the transfer function describing the path between the control signal ( $E$ ) and the velocity of the transducer's diaphragm.

## 2.4 Candidate Controller for Cancelling Reflecting Sound Waves

The type of controller selected to achieve the desired impedance matching is the popular PID controller. This choice is done for two reasons. Firstly, PID control has been investigated thoroughly and a large number of stable and robust tuning methods have been developed for many problems [Cominos and Munro, 2002]. The second reason for choosing PID has to do with the fact that the three controller coefficients can be related to physical values of the plant (velocity, acoustic impedance etc.) and therefore the beneficial results of applying the controller can be related to the physics of the setup. The reasons of selecting PID, will become more clear in the next chapter where the feedback arrangement of the controlled device is described.

## 2.5 PID Control Designs

PID control designs have been used over the past decades. The reasons of its popularity originate at the fact that the design is inherently simple and robust to plant uncertainty. Because of its popular demand it has been investigated thoroughly by the academic community and industry is very keen on using it. If we were to define a PID controller in the frequency domain the following equation would be considered:

$$C(s) = K_p + \frac{K_i}{s} + K_d s \quad (2.21)$$

Where  $K_p$  is the proportional coefficient,  $K_i$  is the integral coefficient and  $K_d$  is the derivative coefficient. It is common to have the following realisation in order to reduce noise amplification:

$$C(s) = K_p + \frac{K_i}{s} + \frac{K_d s}{sT_n + 1} \quad (2.22)$$

The above expression, although it shares an identical frequency response at the low frequency bandwidth as equation (2.21), it also has a lowpass filter added to the derivative term in order to eliminate any magnification of noise [Cominos and Munro, 2002].  $T_n$  corresponds to the filter's time constant.

### 2.5.1 Ziegler - Nichols PID Tuning Methodology

This PID tuning method was initially proposed by Ziegler and Nichols [Ziegler and Nichols, 1942] and is formed by making use on the plant to be controlled open loop response. The tuning method relies on the concept that a great number of systems can be modelled a first order lag transfer functions with the addition of a pure time delay, example of such a model is [Cominos and Munro, 2002]:

$$G_p(s) = \frac{\alpha}{sl} e^{-st} \quad (2.23)$$

where the  $\alpha$  and  $l$  coefficients can be identified by making use of the plant's step response [Ziegler and Nichols, 1942; Cominos and Munro [2002]]. In order to obtain the parameters

for the PID controller use of the Ziegler - Nichols (ZN) step response method is required. The method is summed up in table 2.1.

After the original ZN method was published, a later version from the same authors was presented. Specifically in this variation of the design, the tuning method made use of the plant's response when the proportional term of the controller is only active (the other two terms are inactive) [Cominos and Munro, 2002]. In this case, the gain is gradually increased and eventually the closed-loop system will become critically stable. The gain that forces the closed loop system to critical stability,  $K_u$ , and the corresponding period of oscillation,  $T_u$ , are used to calculate the parameters of PID controller based on table 2.2 [Cominos and Munro, 2002].

It must be emphasised that the initial motivation of developing the ZN methods was to provide good reaction of the controlled plant to sudden variations to external inputs. Therefore, a damping criterion that was utilised in the design procedure was able to provide controlled plant with damping ratio near to 0.2 [Cominos and Munro, 2002]. But such criteria are not ideal for a large number of systems because of the unsatisfactory gain and phase margins. Furthermore, these PID tuning methods are not considered a good candidate solution on operating plants. This is due to the fact that for critical processes, sudden variations to the signal fed to the controller are not option. Furthermore, the operation at the critical stability limit generally not accepted for these processes.

For the acoustic problem under investigation, the ZN method would fail to give a fully automated design method without the additional need of fine tuning. This is due to the predefined performance specifications the method was originally developed (previous paragraph). Therefore it is not considered as a preferable choice to consider.

Table 2.1: Tuning parameters based on the ZN step response methodology [Cominos and Munro, 2002]

Controller	$K_p$	$K_i$	$K_d$
P	$1/\alpha$		
PI	$0.9/\alpha$	$3L$	
PID	$1.2/\alpha$	$2L$	$L/2$

Table 2.2: Tuning parameters based on the ZN frequency methodology [Cominos and Munro, 2002]

Controller	$K_p$	$K_i$	$K_d$
P	$0.5K_u$		
PI	$0.4K_u$	$0.8T_u$	
PID	$0.6K_u$	$0.5T_u$	$0.12T_u$

## 2.5.2 Pole Placement Method

The pole placement methods are considered popular to use when the plant that is going to be controlled has a low order. A standard way of implementing this control design method is to initial consider a second order transfer function that will describe the plant's dynamics. Having done that, the next step is to define what damping ratio and natural frequency the controlled plant should have. Once the specifications and system are know, it is possible to identify the position of the system's two poles in order to achieve the ideal closed loop performance. In order to appreciate this method let us consider a simpler problem in which we have a first order plant. The transfer function of such a plant is [Cominos and Munro, 2002]:

$$G_P(s) = \frac{K_P}{1 + sT_1} \quad (2.24)$$

When applying a PI controller the characteristic equation will be [Cominos and Munro, 2002]:

$$s^2 + s \left( \frac{1}{T_1} + \frac{K_P K_p}{T_1} \right) + \frac{K_P K_p}{T_1 T_i} = 0 \quad (2.25)$$

If we then compare the above equation with a second order frequency domain model as the one given below [Cominos and Munro, 2002]:

$$s^2 + 2\zeta\omega + \omega^2 = 0 \quad (2.26)$$

we then have [Cominos and Munro, 2002]:

$$K_p = \frac{2\zeta\omega T_1 - 1}{K_P}, \quad K_i = \frac{2\zeta\omega T_1 - 1}{\omega^2 T_1} \quad (2.27)$$

An alternative approach in implementing the pole placement design is dominant pole design. This pole placement method is usually considered when some needs to make use of a PID compensator and the plant to be controlled has high order dynamics [Cominos and Munro, 2002]. In contrast to the previous method, the dominant pole design method, as the name suggests, attempts to reposition only the system's dominant poles rather than all of the poles [Cominos and Munro, 2002].

The pole placement tuning method exhibits good design properties for plants with low order dynamics but fails to provide a good control design for a plant for higher order dynamics which is the case in most ANC problems. Furthermore, the efficiency of the tuning method relies heavily on how good the plants dynamics are modelled. These two realisations, especially the second one, lead us to considered an alternate design approach that would address the problem and is presented in the next subsection.

### 2.5.3 Frequency Loop Shaping

Recent work concerning PID controller design has shown that a robust and near-optimal controller can be developed that makes use of the frequency domain model of the system to be compensated, [Grassi et al. 2001]. The controller design is carried out in the frequency domain, hence it is natural to focus on frequency loop shaping methods which aim to provide a desirable sensitivity function,  $S(s) = \frac{1}{1+K(s)G(s)}$  and complementary sensitivity function,  $T(s) = 1 - S(s)$ . Where  $G(s)$  expresses the plant's transfer function and the controller is defined as  $K(s)$ . It is possible to describe the desired performance characteristics by setting bounds for the sensitivity and complementary sensitivity functions. In order to achieve good disturbance rejection and set point following the sensitivity function must have small values at the low frequency bandwidth. Furthermore, for good noise attenuation and robustness to model uncertainty due to un-modelled dynamics it is necessary to have the complementary sensitivity set as small values. In order to tune the controller it is common to adopt convex algorithms. A good example in which both the identification and the control design (PID) are dealt in a simple way is given by [Grassi et al. 2001]. This method is referred to as the Frequency Loop Shaping (FLS) PID tuning method. Specifically, this algorithm attempts to identify the the control coefficients  $K_p$ ,  $K_i$  and  $K_d$  in such a way that the compensated

plant is close to a desired frequency response function,  $L(s)$ , in a  $L_\infty$ , sense (the infinity norm of the difference between the compensated system and the target function is minimised, equation (2.29))[Cominos and Munro, 2002]. Here, a more specific use of the approach is made since the desired loop transfer function is defined by the impedance matching requirement. The transfer function of the controller is presented in the following form:

$$K(s) = \frac{K_1 s^2 + K_2 s + K_3}{s(\tau s + 1)} \quad (2.28)$$

with  $K_p = K_2 - K_3$ ,  $K_i = K_3$  and  $K_d = K_1 - K_2 + K_3$ .

An advantage of such parameterisation is that any function of the form  $\|W(G(s)K(s) - L(s))\|_\infty$ , which will be used as a cost function in order to tune the PID controller, where  $W$  is a weighting function to emphasise which frequencies are to be controlled [Cominos and Munro, 2002;Grassi et al., 2001]. To sum up, this tuning method can be expressed as the following minimisation problem:

$$\min_{K_1, K_2, K_3 \in \mathbb{K}} \|W(s)S_0(s)(G(s)K(s) - L(s))\|_{L_\infty} \quad (2.29)$$

where  $S_0(s)$  is the desired sensitivity function and  $\mathbb{K}$  is a convex set of constraints that are chosen by the designer in order to shape the plant's response [Grassi et al., 2001;Cominos and Munro, 2002].

Two properties of the FLS tuning method lead us in selecting it for the design of the feedback controller that will reduce the undesired reflecting sound for the ANC problem illustrated in figure 2.1:

- The FLS method is a fully automated design procedure (gradient descent optimisation) that calculates the control coefficients relatively easy regardless of the complexity of the plants dynamics.
- The FLS method makes efficient use of the desired closed loop response which in the problem investigated in this chapter is fully known.

### 2.5.4 Stability Analysis

In order to guarantee stability of the FLS design, we will derive the convex constraint that ensures the stability of the closed loop. Let  $\Delta = L - GC$  be the error between the open loop transfer function with the desired open loop transfer function. Then, by rewriting the closed-loop system in terms of the desired target function ( $L$ ) and  $\Delta$  and applying the small gain theorem [Ogata and Yang, 1970], a sufficient condition for closed-loop stability is given by [Grassi et al., 2001]:

$$\|S_0\Delta\|_\infty = \|(1 + L)^{-1}(GC - L)\|_\infty < 1 \quad (2.30)$$

Equation 2.30 can be regarded as a cost functional for solving the weighted approximation problem of  $L$  by  $GC$ .

Notice that for internal stability should contain no right-half plane pole/zero cancellations. This requirement is easily met by restricting our attention to minimum phase controllers. Such a restriction makes practical sense since the PID gains are expected to be of the same sign. Without much loss of generality, it is assumed that the PID gains are positive, implying the positivity of  $K_1$ ,  $K_2$  and  $K_3$ . All of these constraints are convex and can be easily incorporated into the optimisation process.

### 2.5.5 Robust Analysis

The controller equation (2.28) derived in section 2.5.3 will amplify measurement noise in the closed loop system if it has high gain. The effect of low signal to noise ratio on the measurements and truncation of high frequency modes can be represented as a frequency dependent uncertainty and the robust stability conditions can be determined using upper limit values on uncertainty [Skogestad and Postlethwaite, 2007].

The inequality shown in equation (2.30) guarantees closed-loop stability with the nominal plant model. For Robust stability with respect to modelling errors, the margin of the inequality (distance between the left- and right-hand side) of the inequality can increase robustness of the controller. Specifically, the dynamic uncertainty for a nominal plant model is shown in figure 2.9. Where  $\Delta_I$  is any stable transfer function such that  $\|\Delta_I\|_\infty < 1$  and  $W_I$  denotes

the frequency dependent magnitude of uncertainty. The system is robustly stable if the set of all possible perturbed plant models are stable.

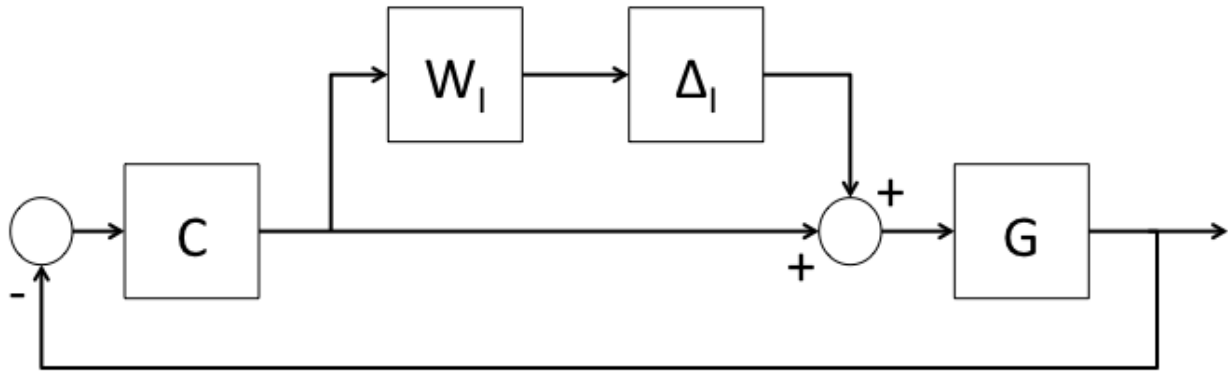


Figure 2.9: Feedback system with multiplicative uncertainty. With  $C$  being the controller block,  $W_I$  is the frequency dependent magnitude uncertainty,  $\Delta_I$  is any stable transfer function such that  $\|\Delta_I\|_\infty < 1$  and  $G$  is the plant to be controlled.

This can be verified using the Nyquist stability criterion for the set of all perturbed plant models. The nyquist plot of this set of perturbed plant models can be represented as discs of radius  $|W_I(j\omega)G(j\omega)C(j\omega)|$  centred on the nyquist contour of the open loop nominal model transfer function  $G(j\omega)C(j\omega)$ . At every frequency this disc should avoid the point  $-1$  for robust stability. This can be achieved if the distance from the critical point  $-1$  to  $G(j\omega)C(j\omega)$  is greater than the radius of the disc  $|W_I(j\omega)G(j\omega)C(j\omega)|$  which is determined by:

$$|W_I(j\omega)G(j\omega)C(j\omega)| < |1 + G(j\omega)C(j\omega)|, \quad \forall \omega \quad (2.31)$$

$$\left| \frac{G(j\omega)C(j\omega)}{1 + G(j\omega)C(j\omega)} \right| < \left| \frac{1}{W_I(j\omega)} \right|, \quad \forall \omega \quad (2.32)$$

$$|S_0(j\omega) - 1| < \left| \frac{1}{W_I(j\omega)} \right|, \quad \forall \omega \quad (2.33)$$

where  $S_0(j\omega) = \frac{1}{1+G(j\omega)}$  is the sensitivity function. By controlling limiting the sensitivity function to be small we assure robust stability of the controlled plant. Hence by including in the convex optimisation rule (equation (2.29)) the sensitivity function we can increase the robust stability of the controller.

## 2.6 Conclusions

In this chapter a brief literature review of the PNC and ANC research field was presented with emphasis on relating to problems of reduction of reflected noise. Emphasis is given on why feedback designs are considered ideal for reducing the implementation complexity compared to feedforward designs (FxLMS). The proposed method in reducing the reflections of sound inside the acoustic duct will be the impedance matching technique hence a feedback controller is required in order to achieve the desired matching. The selected controller is PID and therefore a review of popular tuning methods is included. This review emphasised on the FLS PID method, furthermore the benefits of using it to solve the impedance matching problem is also included.

In the next chapter, a model of a coupled acoustic duct, disturbance and control source system is derived. The model is used for testing the impedance matching method with FLS feedback PID control. Furthermore, in order to access the performance of the suggested solution a FxLMS design is also implemented and compared with the PID design.

# Chapter 3

## Reduction of Reflected Sound Via Local Frequency Loop Shaping Control

### 3.1 Introduction

In the previous chapter a fully automated local feedback design was proposed (FLS PID) in order to reduce the undesired reflecting sound waves inside acoustic duct systems via impedance matching of the boundary reflecting surface and the ambient fluid.

In order to assess the performance of the control design, in this chapter a simulated example for the feedback design is carried out and compared with the FxLMS controller. The reason FxLMS is selected as a control method for comparing with the proposed feedback design is due to the popularity the FxLMS algorithm has in the field of reduction of reflecting sound waves [Zhu et al., 2003]. Furthermore, such a comparison will reinforce the beneficial characteristics of the proposed novel design. The two designs implemented in this chapter will require a model of the acoustic duct. Specifically two layouts are conceived for the purpose of the designs. The FxLMS design requires a coupled acoustic duct system with two loudspeakers (disturbance and control sources), figure 3.1. The FLS design replaces the control loudspeaker with an actively controlled mass-spring-damper element, figure 3.3.

It should be mentioned that it is a necessary condition for the FxLMS control methodology to have a model of the physical system to be controlled. The most difficult part of modelling ANC problems, such as the one illustrated in figure 2.1, is the coupling of the dynamics that

occur when assembling structures together (acoustic duct, disturbance loudspeaker, reflecting boundary surface dynamics). To overcome this complexity, a lot of control schemes used in active noise control ignore the importance of a mathematical model and use black box models to deal with the lack of a validated system [Zimmer et al., 2003]. Nevertheless, a model of the plant will allow greater understanding of the dynamics of the problem; also with the presence of a model high-performance control algorithms can be achieved. Additionally, a high accuracy model will allow us to predict with confidence the experimental response of physical plant.

In contrast to the FxLMS method, the suggested FLS PID feedback design is a collocated controller and makes use solely of local measurements (velocity of terminating surface) in order to suppress the undesired reflecting sound waves that occur in the presence of an incident disturbance sound wave. This choice is done in order to keep the implementation complexity as minimal as possible and has the advantage that collocated systems are guaranteed to be (theoretically) stable regardless of the exact form of the modes of system [Preumont and Seto, 2008]. Furthermore, the local nature of the design reduces significantly the modelling required for implementing the feedback controller. Specifically, the FLS PID design requires the mobility of the controlled element. The mobility function is the transfer function that relates an applied force at one point of a mechanical system to the resulting velocity at that point.

This chapter is organised in the following manner. Initially in section §3.2, two coupled acoustic duct layouts are described and modelled. In section §3.3 the impedance matching control procedure required to achieve the reduction of the undesired reflecting sound is described and presented with respect to reflecting element considered as a boundary element for the modelled acoustic duct. In section §3.4, a separation technique that retrieves the reflecting sound wave, inside the acoustic duct, is described. In section §3.5, the steps required to implement the FxLMS and FLS designs are presented and numerical examples of the two designs are carried out. In section §3.6 the two designs are compared in terms of performance and implementation complexity. Finally, section §3.7 provides some concluding remarks with regards to the suggested design and what benefits are achieved in comparison to FxLMS design.

## 3.2 Development Of a System Model

Before the control designs are considered the first requirement that has to be met is the successful modelling of the acoustic duct and the coupling of the dynamics of the disturbance loudspeaker, the control loudspeaker and the controlled boundary element. This section of the chapter is devoted into explaining the modelling assumptions and mathematical procedure required to generate the coupled system's transfer function representation. With a model of the proposed rig (figure 3.1), it will be possible to conduct simulations and derive the controller based on the FLS PID method described in the previous chapter. Furthermore, the model will be utilised to implement the adaptive FxLMS algorithm.

### 3.2.1 Acoustic Duct Model

In order to simplify the modelling procedure it is convenient to assume a one - dimensional case. By simplifying the model its validity is limited up to a certain frequency, named the cut off frequency. Specifically, the cut off frequency is the limit at which the acoustic wave propagates only along the  $x$  - direction of the duct, figure 3.1. Below this cut off frequency, for the other directions an evanescent standing wave that attenuates exponentially is present and therefore a one dimensional model is consider a valid model for the acoustic phenomena [Kinsler et al., 1999]. The value of the cut off frequency is dictated by the geometry of the duct; for circular ducts of radius  $a$ , the cut off frequency is  $0.293c_0/a$  with  $c_0$  being the speed of sound in the medium, [Hu, 1995]. Furthermore the dynamics of the microphone velocity sensor and electrical circuit dynamics of the actuator that will deliver the control force are not considered in this chapter. Accurate transfer function models of the acoustic duct have been developed over the past decades by a considerable number of authors, [Zimmer et al., 2003; Hull et al., 1991; Pota and Kelkar, 2001; Hull and Radcliffe, 1991; Levine and Schwinger, 1948; Hu, 1995; Birdsong and Radcliffe, 1999; Lane and Clark, 1998]. In order to simplify the acoustic duct problem the following assumptions are made when modelling:

- The system is assumed to be adiabatic
- The mean flow in the duct is zero

- The duct cross section is uniform
- There are negligible air viscosity effects
- The duct has hard walls with dissipation only occurring at the termination end
- The duct diameter is small compared to the length so that wave propagation is planar

These assumptions are valid for frequencies bellow the cut off frequency [Hu, 1995].

The layout of the acoustic duct for which a model will be derived and subsequently used in simulation is shown in figure 3.1. The following fundamental equations describe the acoustic pressure inside a duct [Nelson et al., 1993, Kinsler et al., 1999]:

$$\frac{\partial^2 p(x, t)}{\partial x^2} - \left(\frac{1}{c_0}\right)^2 \frac{\partial^2 p(x, t)}{\partial t^2} = -\frac{1}{\pi A^2 \rho_0} \frac{\partial V(x, t)}{\partial t} \quad (3.1)$$

$$\rho_0 \frac{\partial u(x, t)}{\partial t} = -\frac{\partial p(x, t)}{\partial x} \quad (3.2)$$

Where  $A$  is the cross-section of the duct,  $c_0$  is the speed of sound in the medium,  $p(x, t)$  is the pressure in the duct,  $u(x, t)$  is the particle velocity,  $\rho_0$  is the density of air and  $V(x, t)$  is a volume velocity source per unit length of the duct due to the controlled boundary end surface. The control approach discussed in this chapter involves altering terminating boundary conditions in order to approximate the desired characteristic impedance. Hence, the model described in [Zimmer et al., 2003], which takes into consideration variations in the terminating boundary conditions, is ideal for use.

The Laplace transforms of equation (3.1) and equation (3.2) with respect to time is equivalent to a linear boundary value problem and can be solved with a standard Green's function method. If the solution is combined with the loudspeaker modelled dynamics a transfer function model ( $G_{dist}$ ) that links the value of the acoustic sound pressure at any location inside the acoustic duct, to the voltage applied to the disturbance loudspeaker, [Zimmer et al., 2003] (for more details see Appendix A):

$$G_{dist}(x, s) = e^{-xs/c_0} G_{d_0}(x, s) \quad (3.3)$$

$$G_{d_0}(x, s) = \frac{Bl\rho_0c_0(1 + \alpha_0(s))(1 + \alpha_L(s)e^{2(x-L)s/c_0})}{2R_{coil}Z_0(s)(1 - \alpha_0(s)\alpha_L(s)e^{-2Ls/c_0})} \quad (3.4)$$

where  $Z_0(s)$  is the acoustic impedance of the disturbance loud speaker and  $Z_L(s)$  is the acoustic impedance of the reflecting boundary,  $Bl$  is the loudspeaker's magnetic voice coil motor,  $R_{coil}$  is the loudspeaker's electrical resistance of voice coil,  $p_0$  is the density of air and  $c_0$  is the speed of sound in air. The reflecting coefficients described by  $\alpha_0(s)$  and  $\alpha_L(s)$  of the disturbance loudspeaker and reflecting boundary surface are given in equations (3.5) and (3.6).

$$\alpha_0(s) = \frac{Z_0(s) - \rho_0c_0A_D}{Z_0(s) + \rho_0c_0A_D} \quad (3.5)$$

$$\alpha_L(s) = \frac{Z_L(s) - \rho_0c_0A_D}{Z_L(s) + \rho_0c_0A_D} \quad (3.6)$$

In a similar manner, a transfer function can be developed for the control loudspeaker.

$$G_{con}(x, s) = e^{-xs/c_0}G_{co}(x, s) \quad (3.7)$$

$$G_{co}(x, s) = \frac{Bl\rho_0c_0(1 + a_L(s))(1 + a_0(s)e^{-2x(s/c)})}{2R_{coil}Z_c(s)(1 - a_0(s)a_L(s)e^{-2L(s/c)})} \quad (3.8)$$

The values of the coefficients used in equations (3.3) – (3.8) are fully described in table 3.1.

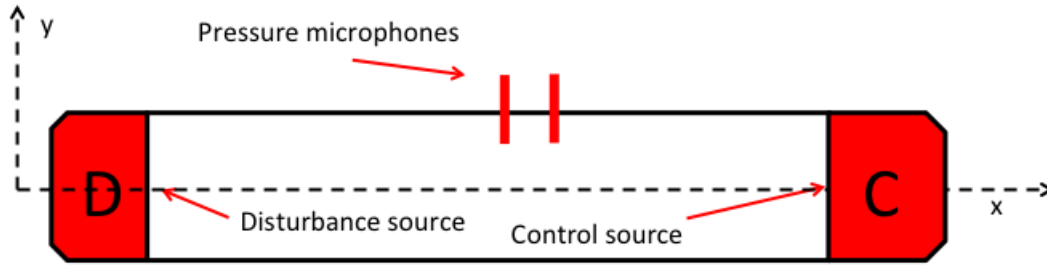


Figure 3.1: Schematic layout of acoustic duct. The acoustic duct is of length  $L$  and diameter  $r$ . A Disturbance source at one end of the duct (D) and control source at distance  $x_c$  (C). Two pressure microphones placed near the control source at distance  $\Delta x_1$  from each other and  $\Delta x_2$  from the control loudspeaker.

Table 3.1: Values of coefficients used for the simulated acoustic duct loudspeaker system

$L$	2 (m)
$r$	0.101 (m)
$\rho_0$	1.20 (kg/m <sup>3</sup> )
$c_0$	341 (m/s)
$m_D$	0.015 (kg)
$k_D$	810.87 (N/m)
$c_D$	5.23 (N/s)
$m_c$	0.015 (kg)
$k_c$	810.87 (N/m)
$c_c$	5.23 (N/s)
$R_{coil}$	6 ( $\Omega$ )
$Bl$	5.6 (N/A)
$r_D$	0.087 (m)
$A_D$	0.024 (m <sup>2</sup> )
$r_c$	0.087 (m)
$A_c$	0.024 (m <sup>2</sup> )

### 3.2.2 Disturbance Boundary

In the literature, a large number of approaches are found when dealing with the boundary value problem of an acoustic duct. Especially when attempting to model the disturbance end of the duct. One popular approach is to treat the disturbance speaker's cone velocity as the input for the plant's transfer function [Birdsong and Radcliffe, 1999; Lane and Clark, 1998]. It must be noted that feedback is introduced to the loudspeaker so that its response is close

to that of a pure volume velocity source [Zimmer et al., 2003]. Although this approach is commonly accepted, it lacks in describing the interaction that occurs between the dynamics of the loudspeaker and the acoustic duct. For this to be better appreciated, let's consider the the loudspeaker is offline, this will result in the loudspeaker to act as a mechanical mass-spring-damper element and a coupling between the duct and the element will be present [Zimmer et al., 2003]. Hence, a model that considers a pure pressure or volume velocity source for the disturbance end neglects this crucial coupling between the acoustic duct and the loudspeaker. Therefore, an ideal model for this kind of a setup would require the addition of a full electro-mechanical model of the disturbance end in order to be coupled to the duct model and properly represent the disturbance end [Zimmer et al., 2003].

If a mechanically analogous system is used to describe the impedance of the speaker, the following impedance equation can be derived [Guicking and Karcher, 1984; Guicking, 1992]:

$$Z_0(s) = \frac{\pi r^2}{A_D s} (m_D s^2 + c_D s + k_D) \quad (3.9)$$

The coefficients of equation (3.9) are related to the loudspeaker, specifically  $A_D$  is the disturbance speaker's effective cross section,  $m_D$  is the disturbance speaker's cone effective mass,  $c_D$  is the disturbance speaker's damping coefficient and  $k_D$  is disturbance speaker's cone suspension stiffness. Throughout this chapter, the values used for the coefficients of equations (3.3) - (3.9) are detailed in table 3.1.

### 3.2.3 Reflecting Boundary for FxLMS

In a similar manner to the disturbance end, the control loudspeaker is modelled as:

$$Z_L(s) = \frac{\pi r^2}{A_c s} (m_c s^2 + c_c s + k_c) \quad (3.10)$$

The coefficients of equation (3.10) are related to the loudspeaker, specifically  $A_c$  is the control speaker's effective cross section,  $m_c$  is the control speaker's cone effective mass,  $c_c$  is the control speaker's damping coefficient and  $k_c$  is control speaker's cone suspension stiffness. The values used for the coefficients found in equation (3.10) are detailed in table 3.1.

### 3.2.4 Reflecting Boundary for FLS

Because two control designs are implemented on the duct two different reflecting boundary ends are considered. Various terminating boundary conditions are employed in the literature to describe an acoustic reflecting surface. The boundary-end of the acoustic duct for the FLS design will be modelled as a simple mechanical baffle (a mechanical mass-spring-damper system) similar to that of a loudspeaker speaker figure 3.2.

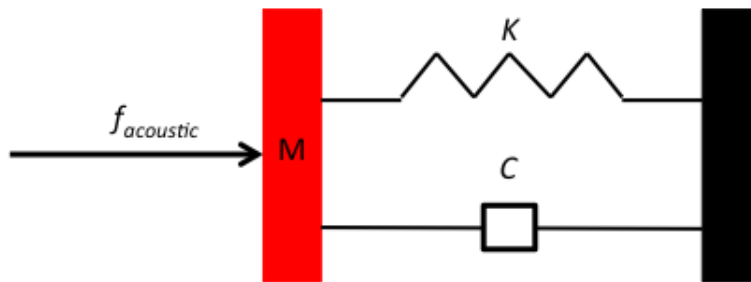


Figure 3.2: Mass-spring-damper element used to model the reflecting surface of the acoustic duct.  $M$  is the mass of the reflecting surface,  $K$  is the stiffness,  $C$  is the absolute damping,  $f_{acoustic}$  is the external force due to the acoustic wave.

The following assumptions concerning the boundary condition are considered:

- The friction between the baffle and the acoustic duct is considered equal to zero.
- The acoustic pressure leakage is not present at the connection between the duct and the boundary surface.
- The velocity sensor is considered ideal, hence no sensor dynamics are considered.
- The transducer that delivers the control force to the reflecting element is considered ideal, therefore no electrical circuit dynamics of the actuator are considered.

The frequency dependent specific acoustic impedance of a mechanical mass-spring-damper structure is the inverse function of the mobility function ( $G_{mobil}$ ) of the reflecting boundary divided by the cross section of the reflecting surface:

$$G_{mobil}(s) = \frac{s}{Ms^2 + Cs + K} \quad (3.11)$$

Hence, the mathematical formula of the specific acoustic impedance of the reflecting boundary is:

$$Z_L(s) = \frac{Ms^2 + Cs + K}{As} \quad (3.12)$$

where  $M$  is the mass,  $C$  the damping coefficient,  $K$  the stiffness coefficient of the system and  $A$  is the cross section of the acoustic tube.

At this point it must be emphasised that the impedance formula given in equation (3.12) is equivalent to the impedance formula for the loudspeaker equation (3.10). The mass-spring-damper element retains the same mechanical properties of a baffle loudspeaker setup but not the electrical circuit dynamics to drive the control force. Therefore, ideal force actuation is considered for the proposed impedance matching design.

Therefore, the final schematics of the a coupled duct system that will implement the FLS design is:

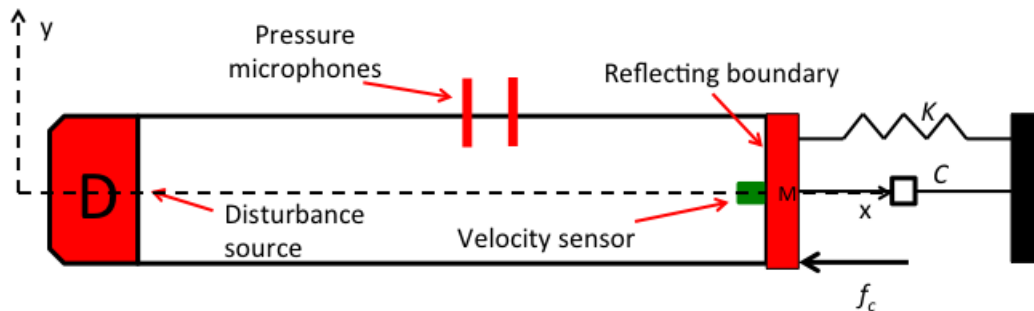


Figure 3.3: Acoustic duct for implementing the FLS design. The reflecting boundary end considered is a mass-spring-damper element (figure 3.2).

### 3.3 Impedance Matching

By definition, the characteristic impedance of a lossless fluid is the product between the density of the fluid ( $\rho_0$ ) and the speed of sound in the fluid ( $c_0$ ),  $Z_0 = c_0\rho_0$ . The specific acoustic impedance of a boundary reflecting surface  $Z$ , is the frequency dependent ratio of the total

acoustic pressure ( $p$ ) over the volume velocity ( $u$ ) of the surface. This loop-shaping method has been adopted here in order to tune the frequency response of the controlled reflecting surface's specific acoustic impedance to the characteristic impedance of the bounding fluid (target loop transfer function).

### 3.3.1 Feedback Control Arrangement

The physical implementation of a feedback PID controller on a boundary surface such as the one described in section 3.2.4 with the addition of a control force relative to the velocity of the mass is illustrated in figure 3.4. The equation of motion describing the controlled mass spring damper element is given by the following formula:

$$Ms^2x_1 = -Csx_1 - Kx_1 + f_{acoustic} - sx_1C_{cont}(s) \quad (3.13)$$

From equation (3.13) if we group on one side the terms which contain the displacement ( $x_1$ ) and leave on the other side the external input force ( $f_{acoustic}$ ) we have:

$$(Ms^2 + Cs + K + C_{cont}(s))x_1 = f_{acoustic} \quad (3.14)$$

The closed loop mobility function of the controlled structure, is the transfer function that relates the applied force ( $f_{acoustic}$ ) to the resulting velocity ( $v_1$ ). Hence, from equation (3.14) we have:

$$G_{cl}(s) = \frac{v_1}{f_{acoustic}} = \frac{sx_1}{f_{acoustic}} = \frac{s}{Ms^2 + Cs + K + sC_{cont}(s)} \quad (3.15)$$

where  $G_{cl}$  is the mobility function for the closed loop system ( $M$  is the mass,  $C$  the damping coefficient and  $K$  the stiffness coefficient),  $C_{cont}(s) = \frac{K_1s^2 + K_2s + K_3}{s(\tau s + 1)}$  is the velocity feedback controller's transfer function. It is interesting to emphasise that the mobility function closed loop dynamics (figure 3.5) can be fully influenced by a three term controller (integral, gain and derivative action). Therefore, a PID controller is an ideal candidate for altering the acoustic impedance of the controlled element. The closed loop impedance function is derived in the same manner as in an uncontrolled case and is given by:

$$Z_{cl}(s) = \frac{1}{AG_{cl}(s)} \quad (3.16)$$

Where  $A$  is the cross section of the acoustic tube.

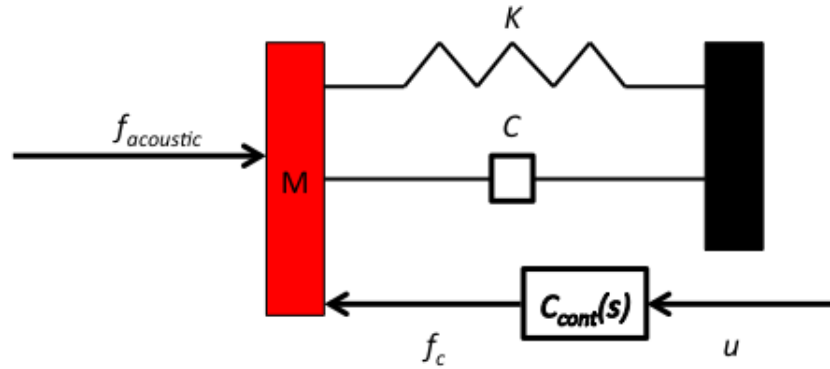


Figure 3.4: Mass-spring-damper element used to model the reflecting surface of the acoustic duct with addition of the PID feedback controller  $C_{cont}(s)$ .  $M$  is the mass of the reflecting surface,  $K$  is the stiffness,  $C$  is the absolute damping,  $f_{acoustic}$  is the external force due to the acoustic wave,  $f_c$  is the control force applied on the mass by the local velocity feedback control loop.

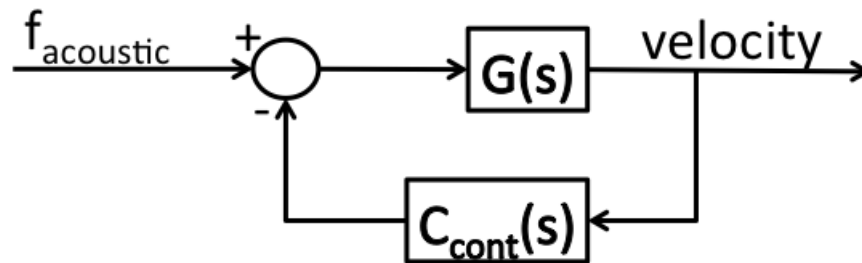


Figure 3.5: Block diagram of control loop of reflecting surface with a control force related to the velocity of the reflecting surface. The force due to the incident acoustic wave is  $f_{acoustic}$ ,  $G(s)$  is the transfer function relating the external force to the velocity of the mass of the reflecting surface ( $G(s) = \frac{s}{Ms^2 + Cs + K}$ ),  $C_{cont}(s)$  is the PID controller, equation (2.28).

### 3.3.2 FLS Minimisation for Impedance Matching

The next step is to define the terms of the minimisation rule that will allow calculation of the controller. Based on equation (2.29)  $W(s)$  is defined as a weighting function to emphasise over what frequency range the controller is to be tuned, in this simulation the range is chosen

to cover 1-1000 Hz which is the cut-off frequency at which the model of the duct is valid. Specifically, the one dimensional model can be adopted for a cylinder acoustic duct with radius  $r$ , when the we consider frequencies below the cutoff frequency which is given by the following formula [Morse and Feshbach, 1953]:  $f_{cutoff} = \frac{0.293c_0}{\alpha}$

$$f_{cutoff} = \frac{0.293c_0}{\alpha} \quad (3.17)$$

As mentioned in the previous section in order to achieve a robust controller,  $S_0(s)$  the sensitivity of the desired closed loop response is added. Because we are interested in matching the controlled surface to a specific response, the open loop system should approximate the desired response, hence  $L(s) = \rho_0 c_0$  ( $\rho_0 c_0$  is the characteristic acoustic impedance of the surrounding fluid that is assumed here to be air). Now that it is possible to calculate the PID controller coefficients, the acoustic impedance of the reflecting boundary surface of the closed loop system equation is given by:

$$Z_{cl}(s) = \frac{1}{AG_{cl}(s)} \quad (3.18)$$

where  $G_{cl}(s)$  is the closed loop transfer function of the controlled system illustrated in the block diagram in figure 3.5:

$$G_{cl}(s) = \frac{G_{mobil}(s)}{1 + G_{mobil}(s)C_{cont}(s)} \quad (3.19)$$

### 3.4 Calculation of Reflecting Sound Wave for the Coupled System

The control procedure aims to cancel the reflecting sound wave. Equation (3.3) describes the total acoustic pressure due to the disturbance speaker (incident and reflecting sound waves). Even though the suggested feedback control architecture does not require knowledge of the undesired reflecting sound wave it is necessary in order to monitor the performance of the control strategy, therefore a separation technique of the incident and reflecting sound wave is carried out and will allow us to view the control methods performance. To achieve separation

of the incoming and reflecting pressure sound waves it is necessary to recall some basic wave theory. As mentioned previously, equation (3.3) describes the total acoustic pressure due to the loudspeaker at any given location inside the acoustic duct and furthermore it is the superposition of two acoustic pressure waves, the incident  $p_i$  and the reflecting  $p_r$ . Recalling a fundamental property of waves, periodicity; [Guicking and Karcher, 1984] due to this attribute if we place in an acoustic duct two microphones with distance  $\Delta x$  from each other, as shown in figure 3.1, the separation can be achieved by using signal readings from these two sensors. In the time domain, the incident and reflecting wave have the following mathematical form [Guicking and Karcher, 1984] :

$$p_i(x, t) = p_i(kx + \omega t) \quad (3.20)$$

$$p_r(x, t) = p_r(kx - \omega t) \quad (3.21)$$

where  $k$  is the wave number and  $\omega$  is the angular frequency. The total sound pressure is the sum of both.

$$p_{tot}(x, t) = p_i(x, t) + p_r(x, t) \quad (3.22)$$

From the theoretical setup illustrated in figure 3.1, if it is assumed that microphone one is located at position  $x_1 = 0$  and microphone two is at position  $x_2 = \Delta x$  an arbitrary distance from the first one, then the two sensors will pick up the following pressure signals:

$$p_1(x_1, t) = p_i(0, t) + p_r(0, t) \quad (3.23)$$

$$p_2(x_2, t) = p_i(\Delta x, t) + p_r(\Delta x, t) = p_i(0, t + \tau) + p_r(0, t - \tau) \quad (3.24)$$

where  $\tau$  is the time required for sound to propagate the distance between the two microphones, hence  $\tau = \frac{\Delta x}{c_0}$ . If the signal from microphone 1 has a time delay of value  $\tau$  applied, the following signal is retrieved [Guicking and Karcher, 1984]:

$$p_{1\tau} = p_1(x_1, t - \tau) = p_i(0, t - \tau) + p_r(0, t - \tau) \quad (3.25)$$

By subtracting the second microphone's signal from the delayed one the following signal is acquired:

$$p_3(t) = p_{1\tau} - p_2 = p_i(0, t - \tau) - p_i(0, t + \tau) \quad (3.26)$$

The acoustic pressure derived in the previous mathematical expression contains only the incident sound wave. In a similar manner for the reflecting sound wave the following equations are valid:

$$p_{2\tau} = p_2(t - \tau) = p_i(0, t) + p_r(0, t - 2\tau) \quad (3.27)$$

$$p_4(t) = p_{2\tau} - p_1 = p_r(0, t - 2\tau) - p_r(0, t) \quad (3.28)$$

Equation (3.28) contains the superposition of terms that refer to the reflecting sound wave. The signal described by equation (3.28) in comparison with the reflecting sound wave  $p_r(0, t)$  has the same phase response. In contrast, the magnitude response of equation (3.28) is amplified by a constant gain due to the superposition of the signals from the two measurement points ( $p_{2\tau}$  and  $p_1$ ) when compared to  $p_r(0, t)$ . This constant gain does not affect the results and analysis of the simulations, hence for the rest of the thesis signal  $p_4$  will be referred to as the reflecting sound wave.

## 3.5 Implementation of Control Designs

In this section of the chapter the two methodologies (FxLMS and FLS) are implemented for an acoustic duct setup described in figure 3.1 and the two methods are compared in terms of performance and implementation complexity.

### 3.5.1 Implementation of FxLMS Control Design

For the purpose of implementing the FxLMS design the open end acoustic duct is considered, figure 3.1. The set of frequency dependent functions that will be used to describe the pressure wave for the new acoustic duct are given in the following table:

Table 3.2: Equations used to simulate conduct the FxLMS design

Mathematical Formula	Description
$G_{dist}(x, s) = e^{-xs/c_0}G_{d_0}(x, s)$	Total acoustic pressure inside the duct
$G_{con}(x, s) = e^{-xs/c_0}G_{c_0}(x, s)$	Total acoustic pressure inside the duct
$Z_0(s) = \frac{\pi r^2}{A_D s} (m_D s^2 + c_D s + k_D)$	Acoustic impedance of the disturbance loudspeaker
$Z_L(s) = \frac{\pi r^2}{A_c s} (m_c s^2 + c_c s + k_c)$	Acoustic impedance of the control loudspeaker
$p_r(x_1, s) = p_4(s)$	Acoustic pressure of the reflecting sound wave
$p_i(x_1, s) = p_3(s)$	Acoustic pressure of the incident sound wave

For each source (disturbance and control) two paths are formed, specifically a path from the source to the pressure measured at each microphone. The final block diagram that describes the plant dynamics is presented in figure 3.6:

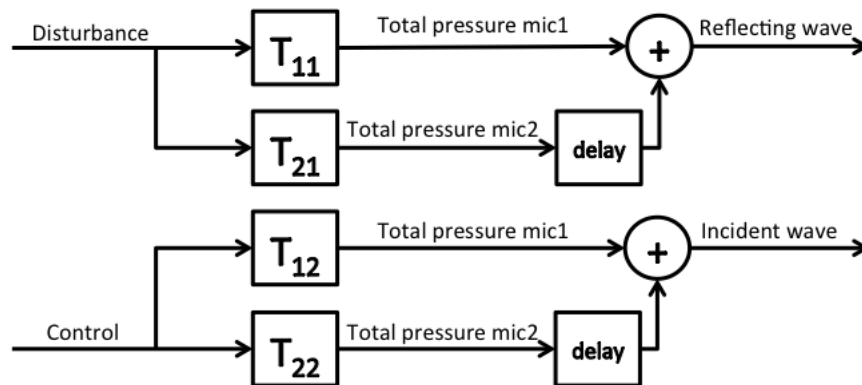


Figure 3.6: Block diagram describing the dynamics of a coupled duct system (figure 3.1). The transfer function blocks ( $T_{11}$ ,  $T_{21}$ ,  $T_{12}$  and  $T_{22}$ ) are based on equations found in table 3.2. The blocks labeled as delays are based on the separation formula described in section §3.4.

Now that the plant dynamics are modelled the next step is to formulate the FxLMS block diagram that will tune online the controller. It must be emphasised that a vital requirement for the stability of this adaptive controller is the feedforward filter placed before the updating

rule of the FxLMS controller. Figure 3.7 contains the final block diagram that will calculate the controller.

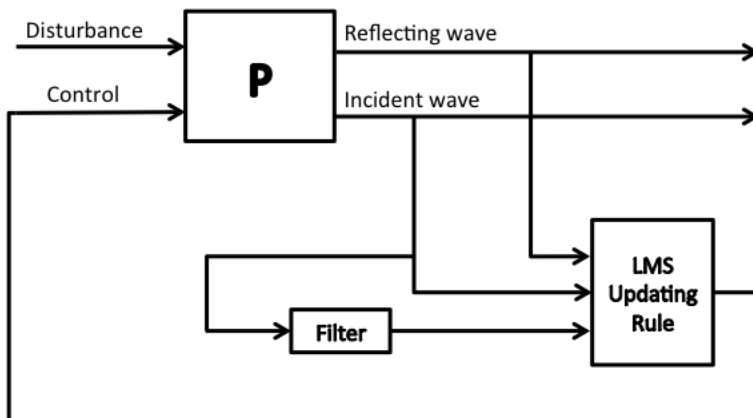


Figure 3.7: Block diagram for implementing FxLMS design.  $P$  is the *MIMO* transfer function that models the plant's dynamics. The block with label filter is a transfer function that replicates the path between control to reflecting wave. Finally the updating rule block is formulated based on the theory described in the previous chapter (section 2.3.1).

With regards to the implementation of the adaptive controller, through trial and error a 128th order adaptive controller was required in order to give the best results, additionally the convergence rate coefficient had to be kept relatively small ( $a < 0.001$ ) in order to avoid unstable response. The FxLMS design is able to provide a satisfactory reduction of the undesired reflecting sound wave, specifically in figure 3.8 the reduction begins to be evident at 20 Hz and up until 1000 Hz is able to reduce all the resonant frequencies.

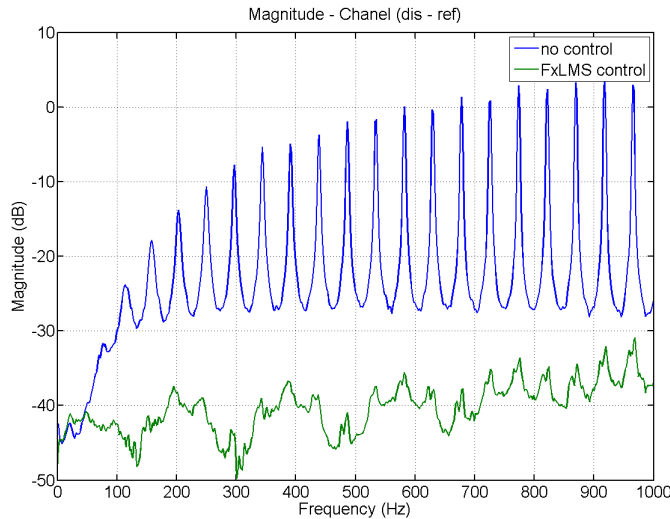


Figure 3.8: Simulated response of reflecting sound wave in an acoustic duct with an actively controlled reflecting surface as the boundary surface (green), Simulated response of reflecting sound wave in the same acoustic duct with the same reflecting surface without the active control applied (blue).

### 3.5.2 Implementation of FLS Control Design

For the purpose of implementing the FLS design the open end acoustic duct is sealed with a reflecting boundary element (figure 3.4). Hence, the acoustic duct layout used for the purpose of the proposed design is illustrated in figure 3.3.

In order to design the FLS controller the terms of the minimisation rule have to be defined. Based on the formula developed in the previous chapter the controller is formulated as:

$$\min_{K_1, K_2, K_3 \in \mathbb{K}} \|W(s)(S_0(s)G(s) - L(s))\|_{L_\infty} \quad (3.29)$$

where  $W(s)$  is defined as a weighting function to emphasise over what frequency range the controller is to be tuned, for the purpose of the numerical example the range is chosen to cover 1-1000 Hz which is the cut-off frequency at which the one dimensional model of the acoustic duct is valid. As mentioned in the previous chapter, in order to achieve a stable robust controller, the sensitivity function of the desired closed loop response is also included to the minimisation rule ( $S_0(s) = \frac{1}{1+G(s)C_{cont}(s)}$ ). Because we are interested in matching the controlled surface to a specific response, the closed loop system's impedance (equation (3.18))

should approximate the desired response, hence  $L(s) = \rho_0 c_0$  ( $\rho_0 c_0$  is the characteristic acoustic impedance of the surrounding fluid that is assumed here to be air). Now that it is possible to calculate the controller's PID coefficients, from equation (3.18) the acoustic impedance of the reflecting boundary surface of the closed loop system equation can be formulated as a transfer function. In order to calculate the optimal solution for the minimisation problem, described from equation (3.29), use of Matlab's optimisation toolbox is required. Specifically, the minimisation problem can be solved with a convex optimisation algorithm such as the gradient descent algorithm.

A simulated response of the specific acoustic impedance of the reflecting surface can be generated from equation (3.18) when the feedback control force is applied to the reflecting element. Figure 3.9 shows the acoustic impedance for the controlled and uncontrolled cases and it can be seen that the reflecting boundary surface with the aid of the controller can approximate the characteristic impedance of air across a frequency band between 200-1000 Hz, with 1000Hz being the cut off frequency at which the model is accurate (section §3.2 assumptions of modelling).

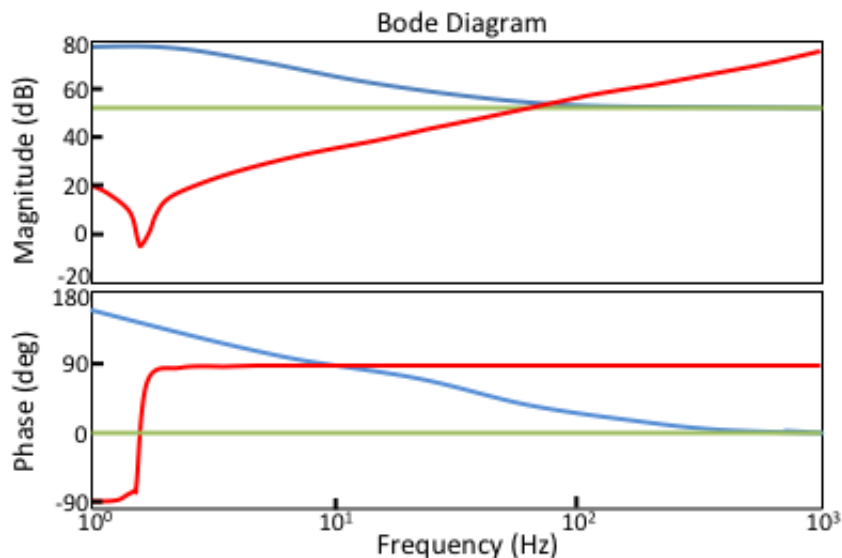


Figure 3.9: Simulated specific acoustic impedance of an actively controlled element composed of a mass-spring-damper element (blue), theoretical specific acoustic impedance of the mass-spring-damper element without control (red) and the characteristic acoustic impedance, i.e. the desired response, of air (green). For these simulations the mass of the reflecting surface is  $M = 0.02(kg)$ ,  $C = 0.05(Ns/m)$  and  $K = 10(N/m)$ .

Up to now, in this section it has been demonstrated how the FLS local velocity output feedback control design can be utilised to provide a boundary condition that will mimic the impedance characteristics of a infinity long acoustic tube and therefore reduce the undesired acoustic reflections, which is our initial intent. If equation (3.3) which describes the total acoustic pressure wave inside the ideal acoustic duct (figure 3.3) is combined with the boundary condition of loudspeaker (equation (3.9)) and the boundary condition of the controlled reflecting element (equation (3.18)) the total acoustic pressure wave at any point along the duct can be simulated for the case of applying control to the reflecting boundary. The initial problem to be solved is the reduction of the reflecting sound wave inside the acoustic duct, therefore if the expression that describes the total acoustic pressure is combined with equation (3.28), the reflecting sound wave can be simulated and thus the performance of the controller can be assessed. The boundary problem with all the equations used to derive the reflecting sound wave are summarised in table 3.3:

Table 3.3: Equations used to simulate the reflecting sound wave for the controlled case

Mathematical Formula	Description
$G_{dist}(x, s) = e^{-xs/c_0} G_{d_0}(x, s)$	Total acoustic pressure inside the duct
$Z_0(s) = \frac{\pi r^2}{A_D s} (m_D s^2 + c_D s + k_D)$	Acoustic impedance of the disturbance loudspeaker
$Z_{cl} = \frac{1}{AG_{cl}(s)}$	Acoustic impedance of the controlled surface
$p_r(x_1, s) = p_4(s)$	Acoustic pressure of the reflecting sound wave

Across the frequency range in which the control boundary approximates the characteristic acoustic impedance of air, there is a reduction in the undesired reflecting sound that arises inside an acoustic duct. The result is verified in figure 3.10, where the reflecting sound wave in the modelled acoustic duct for the case with the actively controlled boundary element and the case without the local feedback control scheme applied, is displayed. It can be observed that a significant reduction of the reflecting noise is evident in the 200 - 1000 Hz range as expected from the impedances plotted in figure 3.9. The reduction is up to 60 dB at some frequencies, in particular towards the end of the plotted range. This confirms the potential of the methodology.

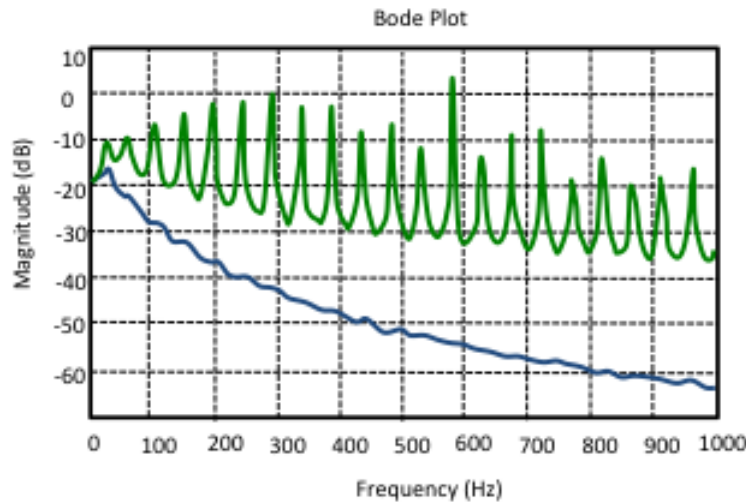


Figure 3.10: Simulated response of reflecting sound wave in an acoustic duct with an actively controlled reflecting surface as the boundary surface (blue), Simulated response of reflecting sound wave in the same acoustic duct with the same reflecting surface without the active control applied (green).

The closed loop stability of the proposed control design can be confirmed by the Nyquist

criterion for SISO plant [Ogata and Yang, 1970]. Figure 3.11 illustrates a Nyquist Diagram of the open loop system ( $G(s)C_{cont}(s)$ ) zoomed near the critical point (0,-1). There is no encirclement of the critical point and therefore closed loop stability is guaranteed.

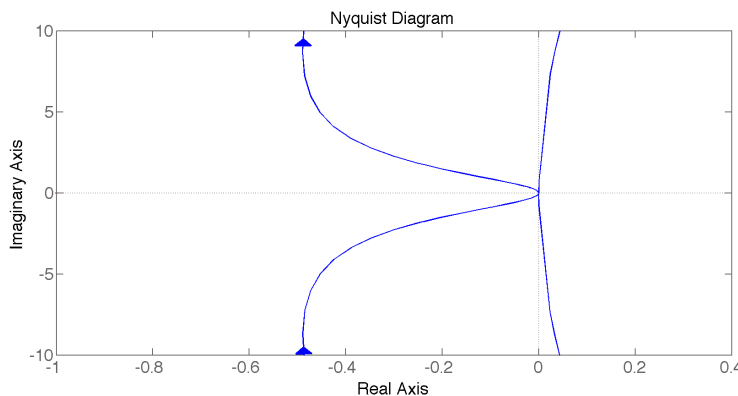


Figure 3.11: Nyquist plot open loop

### 3.6 Performance and Implementation Analysis

The two designs were able to reduce the undesired reflecting sound wave for large frequency bands. From figures 3.10 and 3.8 the FLS and FxLMS controllers give comparable results and achieve reductions over 60 dB. The significant performance differences between the two designs is observable at frequencies below 200 Hz, where the adaptive control approach is superior and achieves larger reduction of the reflecting sound wave.

The increased performance of the FxLMS design is partially due to the fact that the filter that models the path from control voltage to reflecting sound wave and the actual control path are identical (figure 4.20). In a reality such a matching will not be feasible. It must be reminded that both designs consider perfect sensing, the FxLMS design utilises perfect microphones whereas the FLS design assumes a perfect velocity sensor.

An important aspect of the FLS method that should be highlighted is the inherent implementation simplicity. The structure used to carry out the design is a mass-spring-damper element (figure 3.2) to which the sensing (velocity sensor) and actuation (control force) are both embedded, this has as a result a far more compact setup to the FxLMS design. In order to be implemented the FxLMS design requires a model of the control path (filter in

figure 4.20), the FLS controller requires no tedious modelling of the control path. Furthermore the feedback controller is designed offline (in contrast to the online formulation of the FxLMS) and therefore stability can be confirmed before implementing on a real physical problem.

Additionally, the embedded structure conceived for implementing the proposed design, approximates the concept of collocated control. This characteristic is rather important, as collocated control is able to guarantee stability even when un-modelled dynamics are not considered during the design process [?]. This aspect (collocation) of the proposed local feedback design is important as it assists the designer to implement the methodology on real physical problems where un-modelled dynamics will inevitably arise.

## 3.7 Conclusions

In this chapter a novel approach was implemented for the reduction of the reflecting sound waves in a numerical simulation of a one-dimensional acoustic duct problem, figure 3.1. This method made use of a robust and near-optimal FLS PID controller and was able to reduce the undesired reflected sound waves within a frequency bandwidth that reached the limits of the cut-off frequency (0 - 1000 Hz). In contrast to the feedforward adaptive FxLMS controller, the suggested feedback procedure is a locally based control design. The selection of this controller is done due to the good knowledge of the plants dynamics (figure 3.2) and the desired response we want the system to have (impedance of air). By utilising in a novel manner the FLS design, a impedance matching technique was developed. The advantages of such a method in comparison to a feedforward design such as the adaptive FxLMS design are:

- Significant reduction of the design complexity (no feedforward filters required)
- Implementation costs are reduced as the only measurement required for such a method is the velocity of the actively controlled surface, in contrast to expensive microphone arrangements required for FxLMS control. The cost of a miniature, lightweight, ceramic accelerometer would range between 800 - 900 pounds, whereas a set of high precision Brüel & Kjær microphones could cost well over 8000 pounds.

- Due to the local nature of the proposed design (only velocity measurements the controlled surface are required), FLS control could be a viable solution for problems that extend beyond closed acoustic cavities and remote measurements from microphones are not an option.

Finally, in contrast to the DVFC [Lee et al., 2002] and the electroacoustic absorbers [Lissek et al., 2011] the suggested feedback control design is a fully automated design and therefore requires no fine tuning methods to deliver a satisfactory result.

In the next chapter, an apparatus is modified to approximate the model plant [figure 3.1]. The test rig is used for experimental validating of the simulated results of the investigated control designs (FxLMS and FLS PID feedback control).

# Chapter 4

## Reflected Noise suppression using local acceleration feedback control

### 4.1 Introduction

In this chapter we are dealing with the development of local feedback control designs to reduce the reflecting sound wave inside an experimental pulse tube similar to the acoustic duct setup investigated in the previous chapter. The schematics of the acoustic duct considered for experimental validation of control designs is illustrated in figure 4.1.

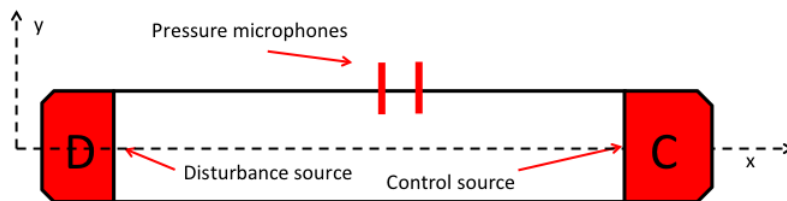


Figure 4.1: Duct setup for local feedback designs with sensor actuator dynamics embedded on one structure.

The proposed apparatus has an important alteration compared to the previous chapter. The ideal reflecting surface (mass-spring-damper element) that was used to seal the end opposite to the disturbance source, is approximated by a control loudspeaker. This alteration can be reasoned by the fact that a loudspeaker is a mechanical piston (mass-spring-damper element) with the addition of an electrical circuit to drive the speaker's baffle. Due to this

the two boundary elements (ideal surface, loudspeaker) have similar acoustic impedance functions equation 3.10 and equation 3.12. By positioning the loudspeaker at the opposite end, actuator dynamics, which in the previous chapter were not considered, are now available and included in the feedback design procedure. Furthermore, this arrangement can also be used to implement the FxLMS algorithm.

In order to implement the FLS feedback design a model of the mobility function of the control loudspeaker is required. The resulting experimental model, revealed two problems that limited the performance of the FLS feedback design significantly. The details of these two problems will be fully analysed in section §4.3. These problems lead to the benefits of an output PID controller to be rather insignificant, hence a more powerful and robust controller has to be chosen and designed for the real life problem. Specifically, a generalised  $H_2$  output feedback controller for the pulse tube setup is selected. As with the PID design, the suggested control scheme will make use solely of local measurements (acceleration) of the reflecting boundary surface (control loudspeaker's cone) in order to suppress the undesired reflecting sound waves inside the acoustic duct setup (figure 4.1).

This chapter is organised as follows: In section §4.2 a description of the experimental acoustic duct system and the modelling procedure involved to calculate the desired disturbance and control paths are provided. In section §4.3 the two fundamental problems that prevent the FLS feedback design to provide a controller with satisfactory performance are analysed. In section §4.4 the  $H_2$  output feedback control design approach that is selected to cancel the undesired reflecting sound wave is presented. In section §4.5 the results of applying the  $H_2$  controller is illustrated and the design's performance is compared with the adaptive feedforward FxLMS controller. Finally, section §4.6 provides some concluding remarks.

## 4.2 Modelling of Experimental Test Rig

This section of the chapter is devoted to describing the modelling procedure of the apparatus illustrated in figure 4.2. Figure 4.2 shows a schematic representation of the system that comprises the acoustic duct with the disturbance source, the secondary control source, the three sensors, the amplifiers, the dSpace controller board and the PC required to implement

the control strategies that are presented in this chapter. In more detail, the pulse tube setup consists of a hard walled cylinder and two loudspeakers; the first one is acting as a disturbance source and the second one is acting as the control source. The sensors required for the experiment are two pressure microphones in order to retrieve the pressure of the total standing sound wave and calculate the reflecting sound wave and an accelerometer that will measure the acceleration of the control loudspeakers cone. It is important to state that the microphones are only present so as to monitor the performance of the proposed control design and for the initial calibration; only the accelerometer is required for control system implementation.

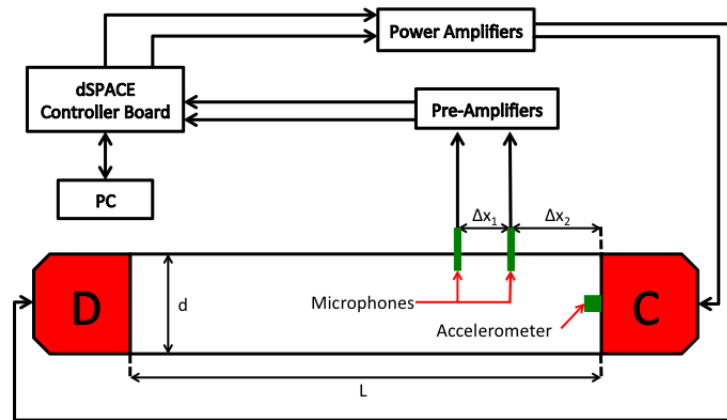


Figure 4.2: Illustration of the experimental acoustic duct of length  $L = 2.054m$  and diameter  $d = 0.099m$ . A Disturbance source at one end of the duct (D) and control source at the other end (C). Two pressure microphones (green) placed near the control source at distance  $\Delta x_1 = 0.0428m$  from each other and  $\Delta x_2 = 0.2m$  from the control loudspeaker. Accelerometer is connected to the cone of the control loudspeaker (green).

The experimental rig illustrated in figure 4.2 with all the elements (pulse tube, loudspeakers, sensors, dSPACE PPC Controller Board, Power Amplifiers and Pre-amplifiers) can be viewed in the following photos.



Figure 4.3: Picture of the experimental acoustic tube consisting of the disturbance source (near end), control source (far end) and the three sensors (two microphones and the accelerometer).

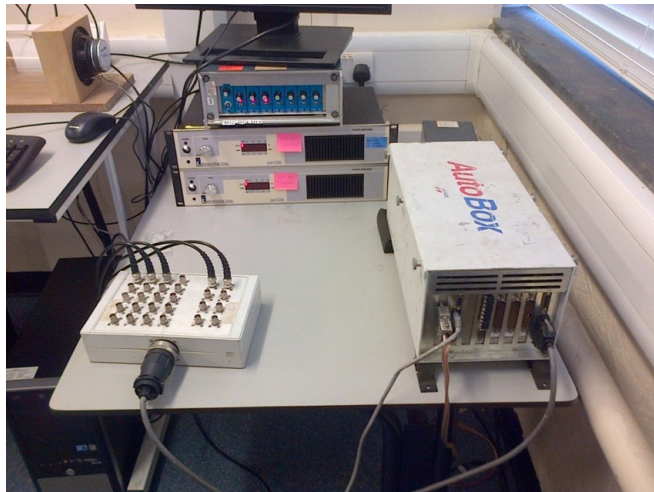


Figure 4.4: dSPACE PPC Controller Board, Power Amplifiers and Pre-amplifiers required to implement the proposed control strategy.

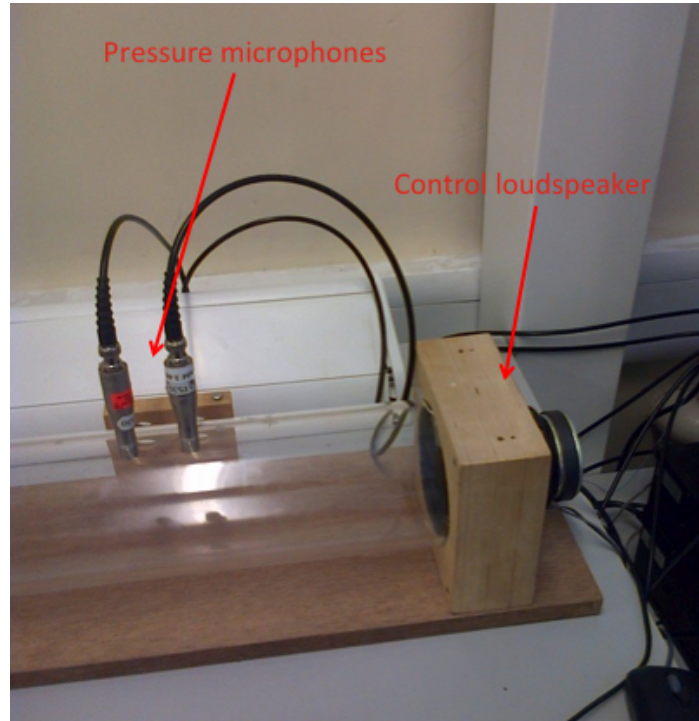


Figure 4.5: Control loudspeaker with embedded accelerometer and two non matched pressure microphones.

### 4.2.1 Matching of Acoustic Pressure Microphones

Before the models of the plant are derived, its necessary to explain the matching procedure required for the microphones. Matched microphones are rather expensive pieces of equipment, this is due to the manufacturing procedure required for their construction. For the needs of this experimental procedure a set of unmatched microphones were used. This will have as a result on the performance signal produced (corresponding to the reflecting sound wave). Therefore a calibrating procedure for the two microphones is required.

In this subsection the procedure in which we were able to effectively compensate for the unmatched microphones is described. The result of which is to have identical signals from both microphones over a large frequency range. The procedure designed to calibrate the microphones requires a random signal to be injected through the disturbance speaker and the data from both microphones collected. Once this step has been done, the microphones are repositioned in each other's location (swapped) for an additional measurement of random noise. From the two measurements the average signal and a filter that will compensate for

the phase and magnitude difference will be derived. With the addition of the filter the microphones are now matched.

In order to have a visual appreciation of the matching, two images of the signals retrieved before and after compensation are illustrated below. It must be noted that the broadband time domain signal from the microphones is far too dense and would not show clearly the impact of the compensator in achieving the desired matching, hence a discrete excitation frequency ( $f = 140 \text{ Hz}$ ) is selected for the visual confirmation. Initially the signals generated by the two microphones (as expected) are not matched (figure 4.6). Once the compensator is designed, the signal retrieved from the microphone 2 (figure 4.2) is fed to it. The compensated signal and the signal given from microphone 1 are now calibrated show the same magnitude and phase characteristics (figure 4.7).

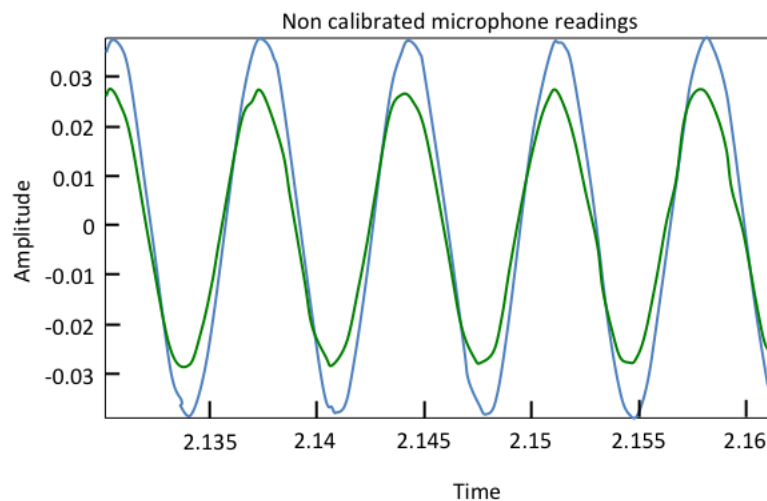


Figure 4.6: Reading from pressure microphone 1 (blue), non calibrated reading from pressure microphone 2 (green)

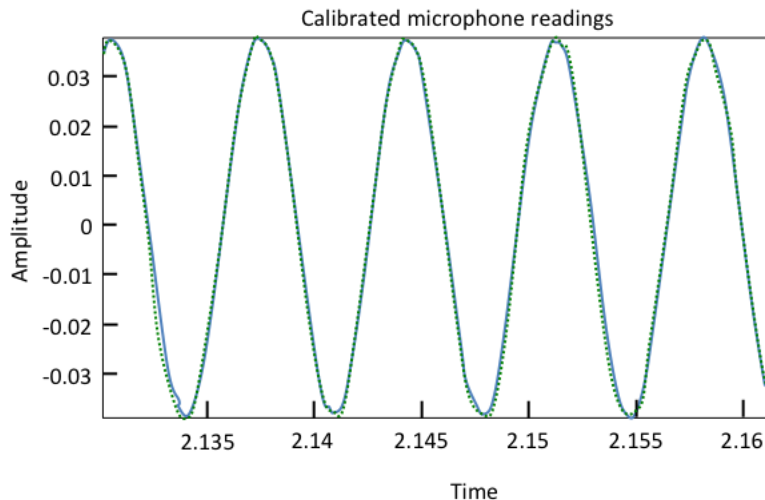


Figure 4.7: Reading from pressure microphone 1 (blue), calibrated reading from pressure microphone 2 (green dashed)

When applying the compensator, the signal recorded by both microphones are now nearly identical. Finally, because the driving signal was random white noise (covering the full frequency range needed to perform experiments) the matching of the microphones is assured over this frequency range and thus control can be safely applied on the full range of frequencies.

Because the environment will always change ( air temperature, humidity etc) the calibration of the microphones should be performed every time experiments are carried out. Furthermore, small variations of the amplifier gains due to temperature variations can also deteriorate the matching.

### 4.2.2 Separation Technique

The separation method described in section 3.4 is going to be utilised to obtain the reflecting sound wave. Due to the distance of the microphones, (figure 4.2), in order to successfully separate the standing wave in incident and reflecting the appropriate time delay required is  $\tau = \Delta x/c = 0.0428/343.3 = 0.000125$  s hence a sampling rate of 8 kHz is chosen as this corresponds to one sample time. It will be noted that in the uncontrolled state the upper measurable limit of  $P_{ref}$  is 4 kHz, but that is well beyond the duct cut-off frequency for radial modes ( $\sim 1$  kHz). The expression that describes the reflecting sound wave is given by:

$$P_{ref} = mic_{2\tau} - mic_1 = p_r(x_1, t) + p_r(x_1, t - 2\tau) \quad (4.1)$$

Where  $mic_1 = p_i(x_1, t) + p_r(x_1, t)$  and  $mic_2 = p_i(x_2, t) + p_r(x_2, t) = p_i(x_1 + \Delta x, t) + p_r(x_1 + \Delta x, t) = p_i(x_1, t + \tau) + p_r(x_1, t - \tau)$ .

### 4.2.3 Experimental Model

In order to derive a model based controller for the experimental rig the disturbance and control paths of the plant have to be modelled. In more detail the disturbance and control paths of the plant can be viewed in the block diagrams illustrated in figures 4.8 and 4.9. The reflecting sound wave measurement is present in order to monitor the performance of the control design and is retrieved with the use of the calibrating method explained in section 4.2.1 and the separating method discussed in section 4.2.2.

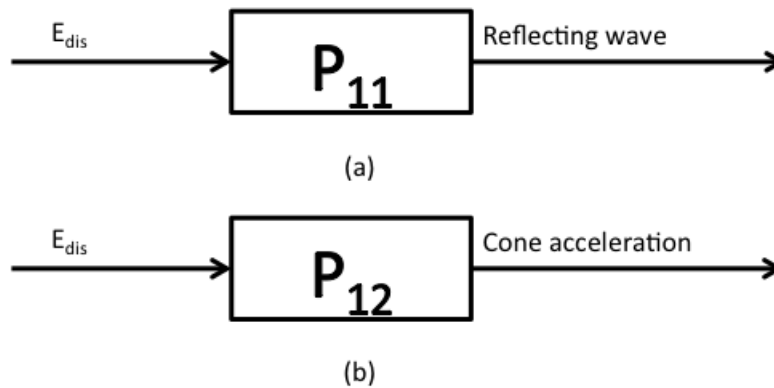


Figure 4.8: (a) Block diagram of disturbance path for the experimental pulse tube setup relating disturbance voltage (disturbance loudspeaker) with reflecting sound wave (pressure microphones) (b) Block diagram of disturbance path for the experimental pulse tube setup relating disturbance voltage (disturbance loudspeaker) with acceleration of control loudspeaker's cone (accelerometer).

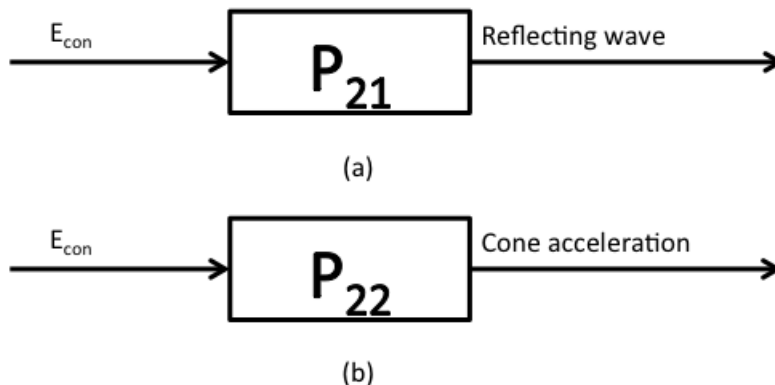


Figure 4.9: (a) Block diagram of control path for the experimental pulse tube setup relating disturbance voltage (control loudspeaker) with reflecting sound wave (pressure microphones) (b) Block diagram of control path for the experimental pulse tube setup relating disturbance voltage (control loudspeaker) with acceleration of control loudspeaker's cone (accelerometer).

If the two necessary steps (calibration and separation) are assumed, the modelling procedure is straightforward and is described in the following two steps:

- The frequency response of the system required to model the plant is acquired by injecting a random signal through each path of the plant.
- With the use of common Matlab library functions a high order (over 1000) MIMO Finite Impulse Response (FIR) discrete filter ( $f_s = 8$  kHz) is formed for each path.

The FIR models that describe the plant are illustrated in contrast with the raw data used for the modelling in figure 4.10 and figure 4.11. It can be viewed from the bode plots that the modelled plant is able to describe all the important dynamics of the system. The choice of this sampling time ( $T_s = 1/8000$  s) is not arbitrary and is related with the separation technique required for the acquisition of the reflecting sound wave (section 4.2.2). Specifically, because the distance of the two microphones is fixed at  $\Delta x = 0.0428$ , the required time for a sound wave to travel this distance is  $t = 0.00025$  s therefore in order for both microphones to measure the same travelling wave a sample time of  $T_s = 1/8000$  s is required.

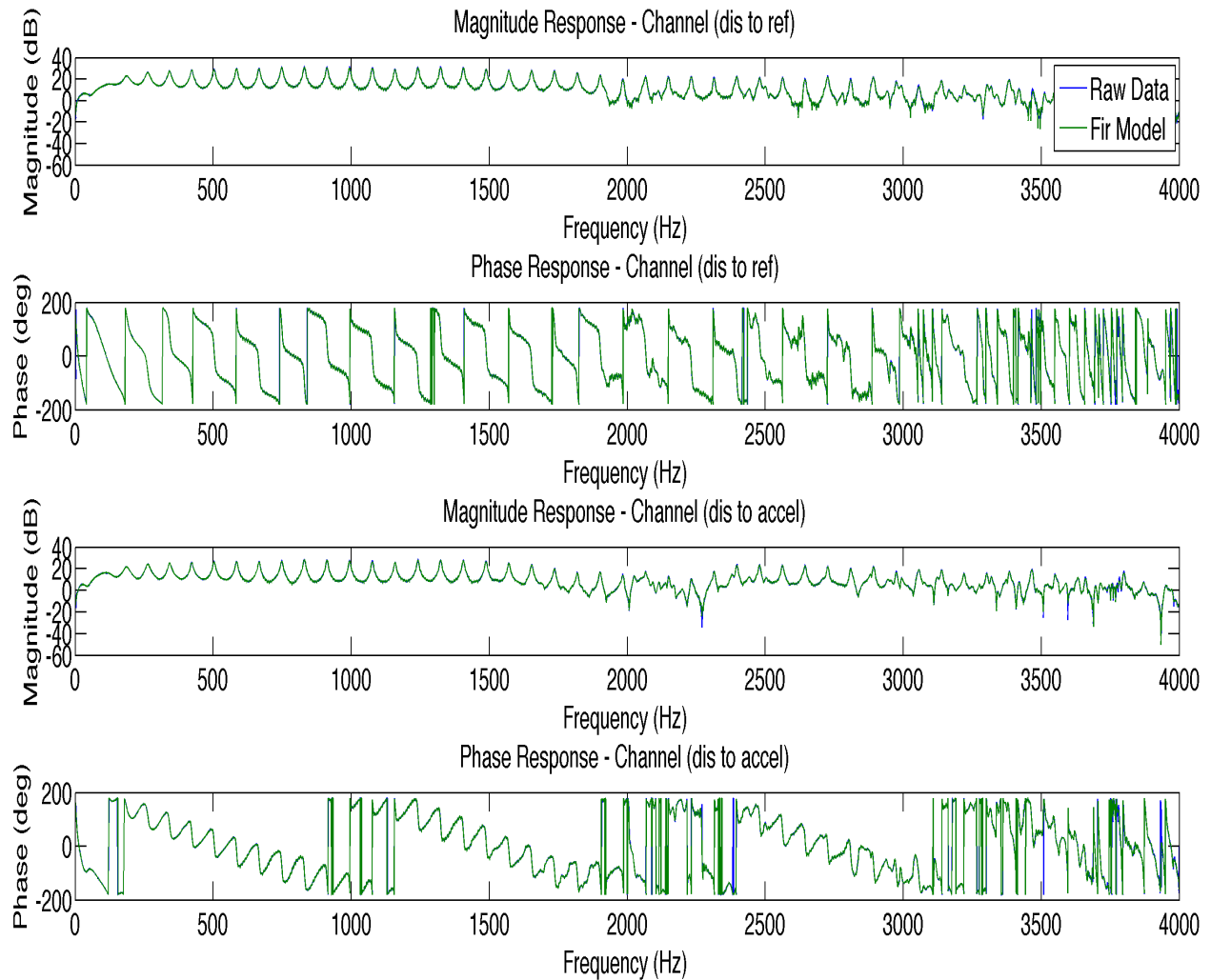


Figure 4.10: Bode plot of the raw experimental data for the disturbance paths (blue) and bode plot of the high order FIR filter fitted to the experimental data (green).

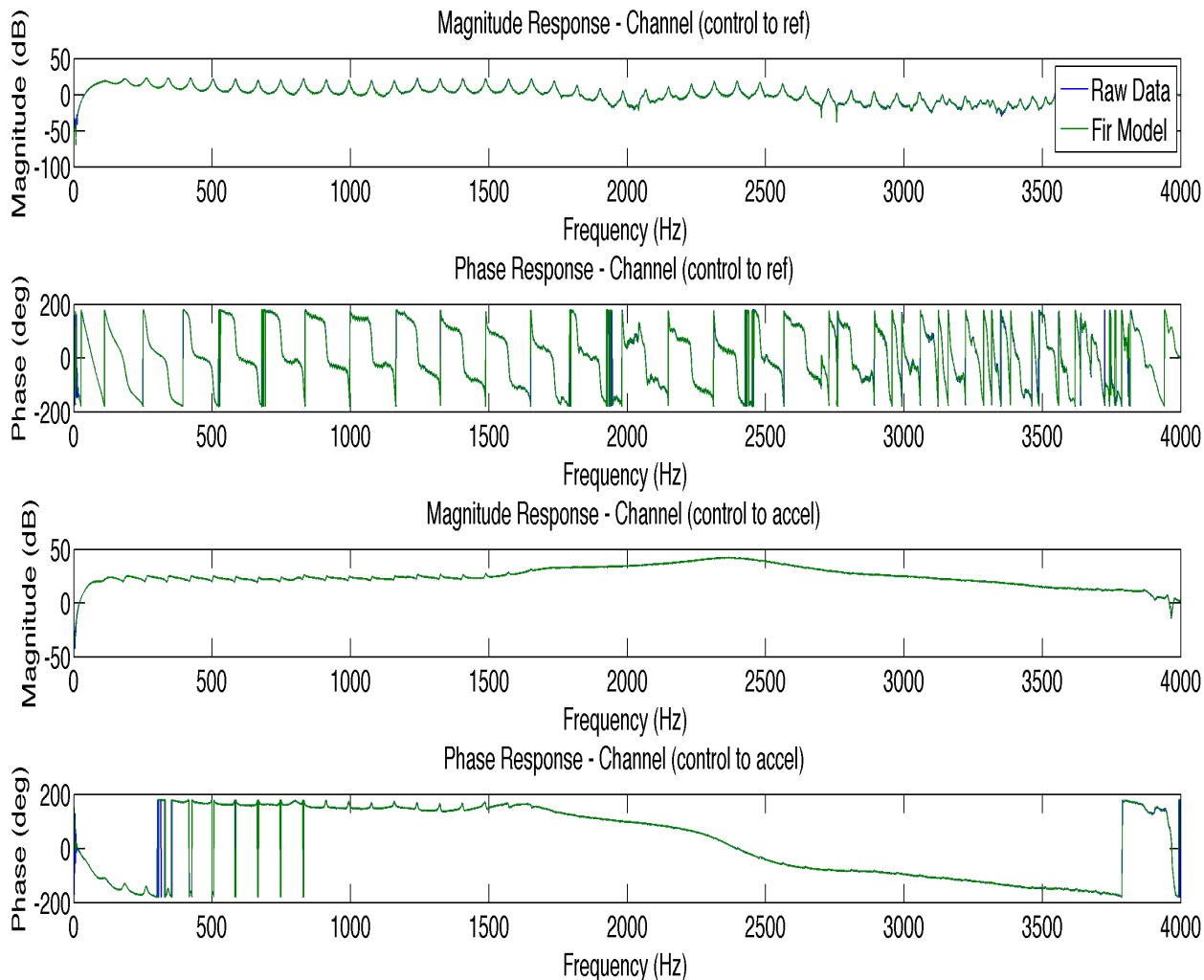


Figure 4.11: Bode plot of the raw experimental data for the control paths (blue) and bode plot of the high order FIR filter fitted to the experimental data (green).

### 4.3 Problem Implementing FLS Design

While deriving the necessary modelling procedure of the control path, two issues of concern in applying the local FLS feedback control design are discovered.

The first problem is that in the lower frequency bandwidth at which plane wave propagation is dominant (0 - 1000 Hz) the dynamics of the control plant have an increased number of acoustic resonances (figure 4.12). This is due to the coupling between the control loudspeaker and the acoustic duct. This increase of dynamics leads to rather disappointing performance (reduction of the reflecting sound wave) the PID controller can provide.

The second problem is that in contrast to the simulated problem solved earlier where only the mechanical resonance of an ideal piston was assumed as a reflecting boundary problem (figure 3.2) whereas for the experimental validation conducted in this chapter a loudspeaker is considered. This alteration increases the complexity of the control path as a electrical circuit of the loudspeaker and the power amplifiers contribute significantly to the final mobility function of the control source. The control loudspeaker used as a controlled boundary element exhibits three resonant peaks (figure 4.12). The first resonance located at  $f_1 = 68.36 \text{ Hz}$  is due to the mechanical element of the loudspeaker where as the other two located at  $f_2 = 1734 \text{ Hz}$  and  $f_3 = 2367 \text{ Hz}$  are due to the electrical circuits. These added resonances complicate the minimisation problem of the FLS PID controller (equation (2.29)) which leads to poor performance (reduction of the reflecting sound wave).

The two problems have resulted in the benefits of an output PID controller to be rather insignificant. Hence a more powerful and robust controller has to be chosen and designed for the real life problem. Specifically, a generalised  $H_2$  output feedback controller for the pulse tube setup is selected. The two arguments, which support the selection of this control design are:

- $H_2$  Feedback design constructs optimal controller.
- $H_2$  control is model based and will be able to deal with the increased complexity of the plants dynamics as it creates a controller of equal order to the model.

As with the PID design the suggested control scheme will make use solely of local measurements (acceleration) of the reflecting boundary surface (control loudspeaker's cone) in order to suppress the undesired reflecting sound waves that occur in the presence of an incident disturbance sound wave.

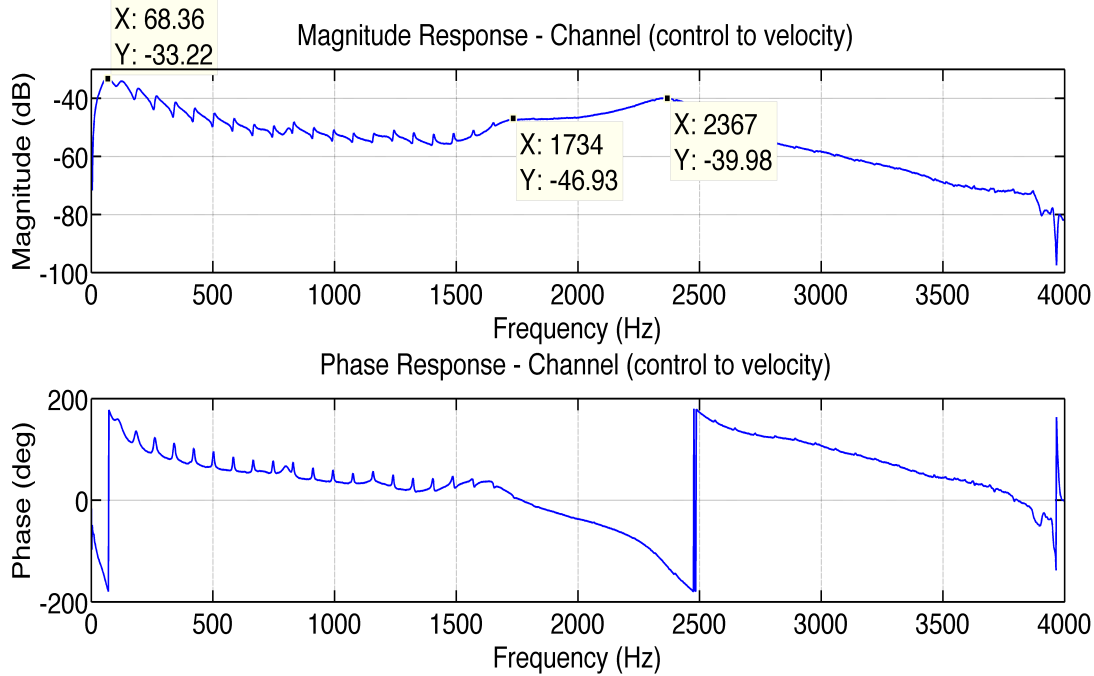


Figure 4.12: Control loudspeaker's acceleration response to random input signal.

## 4.4 Suggested Control Design

In this section a brief explanation of the control design chosen to minimise the undesired reflecting sound is presented. An  $H_2$  controller design will be considered; therefore a Linear Fractional Transformation (LFT) expression of the mathematical model is required. The architecture utilised is illustrated in figure 4.13. The process is represented as a two-input and two-output system that is labelled as  $P$  and has a feedback controller  $K$  that uses the measurable signal  $w_{loud}$  to provide the control variable  $E_{con}$ . Specifically, the two inputs are the voltage of the disturbance loudspeaker  $E_{dis}$  and the voltage of the control loudspeaker  $E_{con}$ . Additionally, the two outputs are the signal retrieved from the separation technique (section 4.2.2) that describes the total reflecting sound wave  $P_{ref}$  and  $w_{loud}$  the signal retrieved from the sensor embedded on the control loudspeaker's cone and which describes the acceleration of the cone. The matrix representation of the open loop system is therefore:

$$\begin{bmatrix} P_{ref} \\ w_{loud} \end{bmatrix} = \begin{bmatrix} P_{11} & P_{12} \\ P_{21} & P_{22} \end{bmatrix} \begin{bmatrix} E_{dis} \\ E_{con} \end{bmatrix} \quad (4.2)$$

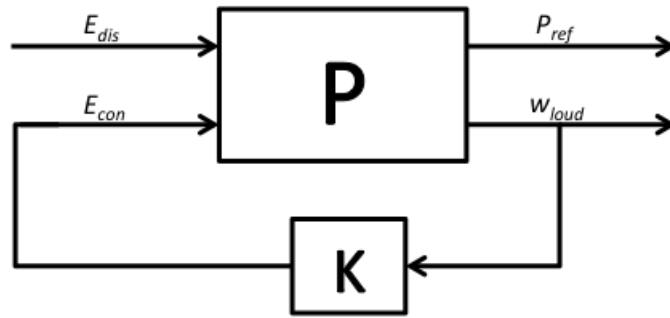


Figure 4.13: LFT control architecture described by a MIMO generalised process ( $P$ ) and a output feedback controller ( $K$ ). Inputs of the generalised process are the voltage of the disturbance loudspeaker ( $E_{dis}$ ) and the voltage of the control loudspeaker ( $E_{con}$ ), furthermore the outputs are the undesired reflecting sound wave signal ( $P_{ref}$ ) to be minimised and the acceleration signal of the control loudspeaker's baffle ( $w_{loud}$ ).

The next step is to formulate the  $H_2$  problem, based on equation (4.2) with the LFT description used for the overall system (figure 4.13).

#### 4.4.1 Output Feedback Control Design Method

The goal is to minimise the performance measurement, which for the case considered here is the reflected sound wave in the duct ( $P_{ref}$ ). In particular the controller is to be designed to minimise the  $H_2$  norm of the closed loop transfer function between the disturbance input ( $E_{dis}$ ) and the performance output ( $P_{ref}$ ). For reasons of consistency with the control literature a discrete state space representation of the system is adopted. Specifically,  $x(k) \in \mathbb{R}^n$  is the state vector,  $d(k)$  is the disturbance input (disturbance voltage  $E_{dis}$ ),  $z(k)$  is the performance or error output (reflecting sound wave  $P_{ref}$ ) and  $y(k)$  is the measurement output (acceleration of loudspeaker cone  $w_{loud}$ ) [Skogestad and Postlethwaite, 2007]:

$$\left. \begin{aligned} x(k+1) &= Ax(k) + B_1d(k) + B_2u(k) \\ z(k) &= C_1x(k) + D_{11}d(k) + D_{12}u(k) \\ y(k) &= C_2x(k) + D_{21}d(k) + D_{22}u(k) \end{aligned} \right\} \quad (4.3)$$

The equivalent compact matrix representation is given by:

$$P = \left[ \begin{array}{c|cc} A & B_1 & B_2 \\ \hline C_1 & D_{11} & D_{12} \\ C_2 & D_{21} & D_{22} \end{array} \right] \quad (4.4)$$

Let  $z = F_l(P, K)$  where  $F_l(P, K) = P_{11} + P_{12}K(I - P_{22}K)^{-1}P_{21}$ .

The design of the optimal feedback controller is based on the popular two Riccati function method [Doyle et al. [1989]]. In order to generate the controller the general  $H_2$  algorithm requires the following assumptions to be valid [Skogestad and Postlethwaite, 2007]:

1.  $(A, B_2, C_2)$  is stabilisable and detectable
2.  $D_{12}$  and  $D_{21}$  have full rank.
3.  $\begin{bmatrix} A - j\omega I & B_2 \\ C_1 & D_{21} \end{bmatrix}$  has full column rank for  $\omega$ .
4.  $\begin{bmatrix} A - j\omega I & B_1 \\ C_2 & D_{21} \end{bmatrix}$  has full column rank for  $\omega$ .
5.  $D_{11}$  and  $D_{22}$  are zero.
6.  $D_{12} = \begin{bmatrix} 0 \\ I \end{bmatrix}$  and  $D_{21} = \begin{bmatrix} 0 & I \end{bmatrix}$ .
7.  $D_{12}^T C_1 = 0$  and  $B_1 D_{21}^T = 0$ .
8.  $(A, B_1)$  is stabilizable and  $(A, C_1)$  is detectable.

Given the assumptions are satisfied, a stabilising controller  $K_{opt}(j\omega)$  exists if and only if:

1.  $X_1 \geq 0$  is a solution to the algebraic Riccati equation:

$$A^T X_1 + X_1 A + C_1^T C_1 + X_1 (-B_2 B_2^T) X_1 = 0$$

2.  $Y_1 \geq 0$  is a solution to the algebraic Riccati equation:

$$A Y_1 + Y_1 A^T + B_1 B_1^T + Y_1 (-C_1^T C_1) Y_1 = 0$$

In conclusion, the optimal controller is then given by the following formula:

$$K_{opt}(j\omega) = \left[ \begin{array}{c|c} \hat{A}_2 & -L_2 \\ \hline F_2 & 0 \end{array} \right] \quad (4.5)$$

where  $\hat{A}_2 = A + B_2 F_2 + L_2 C_2$ ,  $L_2 = -Y_1 C_2^T$  and  $F_2 = -B_2^T X_1$ .

It must be added, that in the case where assumptions 5,6 and 7 are not met, an appropriate transformation of the state space problem is possible and will allow the designer to form an optimal controller [Green and Limebeer, 2012].

#### 4.4.2 Offline Calculation of Output Feedback Controller

Ideally the described methodology would be adequate to develop an optimal feedback controller but as mentioned in the previous section a sampling rate of 8 kHz is required which in turn requires a high order discrete FIR filter (greater than 1000) in order to model the plant dynamics accurately across a broad band of frequencies. The high order of the model in combination with the sampling rate initially prohibits the design of a practical broadband feedback controller. To overcome this problem an FIR model of significantly lower order is fitted to the plants dynamics to cover the frequency bandwidth of specific interest and this model will be used to derive the feedback controller. The desired bandwidth chosen to operate the controller is from 0-250 Hz. Two reasons led to such a choice. Firstly the frequency band is located at relatively low frequencies where ANC is proven to provide significantly better performance compared to traditional passive means. Secondly the range of such a band would include the 1st dominant acoustic resonance (186 Hz). The reduced order models for the disturbance paths and the control paths are illustrated with red colour in figure 4.14, figure 4.15, figure 4.16 and figure 4.17. Additionally in these figures the experimental dat is included (blue colour) and the high order model (green colour) fitted to the entire frequency range. The low order transfer functions fitted to the control path data (figure 4.16 and figure 4.17) do not model ideally the high frequency dynamics (close to 250 Hz). The poor modelling at these frequencies is of little importance as the intended resonance to be controlled is located at  $f = 186$  Hz and beyond this resonance a low pass filter will be applied in order to guarantee no excitation of un-modelled dynamics of the plant

at higher frequencies. Having acquired a controller for the reduced order model of the plant with lower sampling resolution (0.5 kHz) the next step is to transform this to operate with a sample rate of 8 kHz to enable application to the experimental rig.

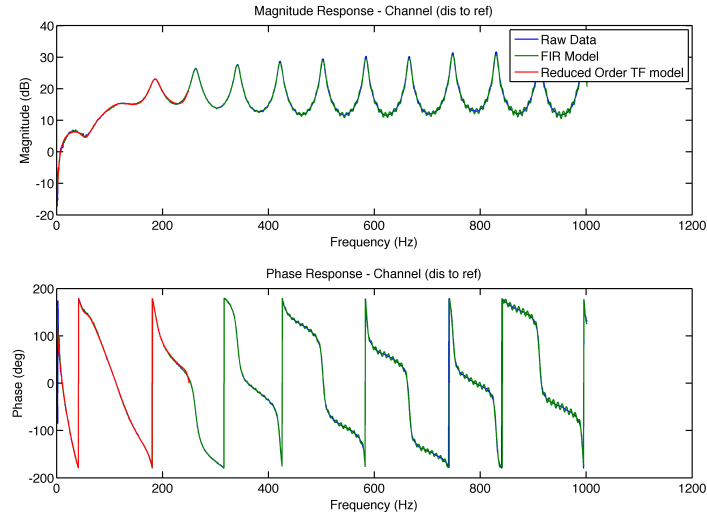


Figure 4.14: Disturbance path (disturbance to reflecting sound wave). Bode plot of the raw experimental data (blue), bode plot of the high order FIR filter fitted to the experimental data (green) and bode plot of the reduced order FIR filter fitted to the experimental data (red).

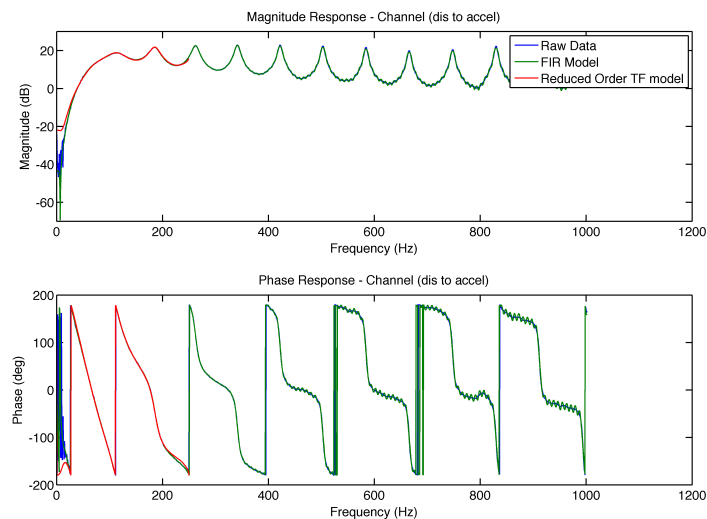


Figure 4.15: Disturbance path (disturbance to acceleration). Bode plot of the raw experimental data (blue), bode plot of the high order FIR filter fitted to the experimental data (green) and bode plot of the reduced order FIR filter fitted to the experimental data (red).

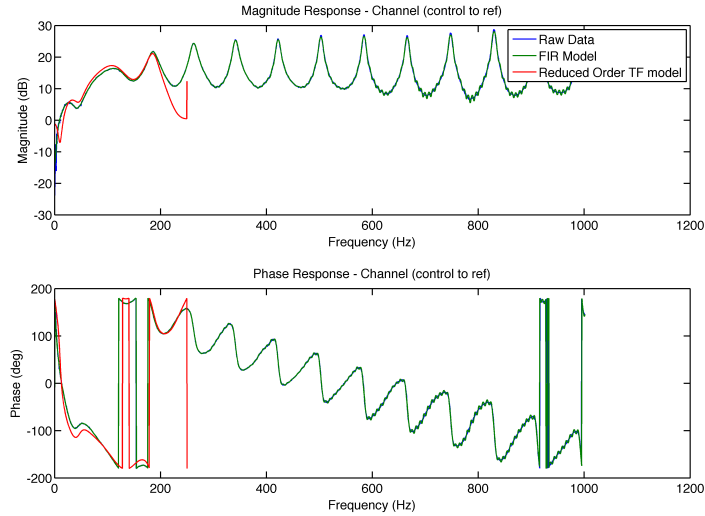


Figure 4.16: Control path (control to reflecting sound wave). Bode plot of the raw experimental data (blue), bode plot of the high order FIR filter fitted to the experimental data (green) and bode plot of the reduced order FIR filter fitted to the experimental data (red).

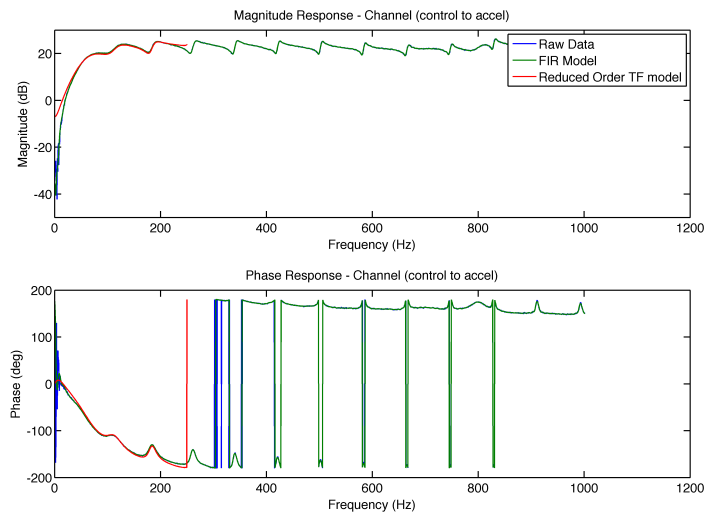


Figure 4.17: Control path (control to acceleration). Bode plot of the raw experimental data (blue), bode plot of the high order FIR filter fitted to the experimental data (green) and bode plot of the reduced order FIR filter fitted to the experimental data (red).

The overall procedure of calculating the acceleration feedback controller offline is presented in a schematic form in figure 4.18.

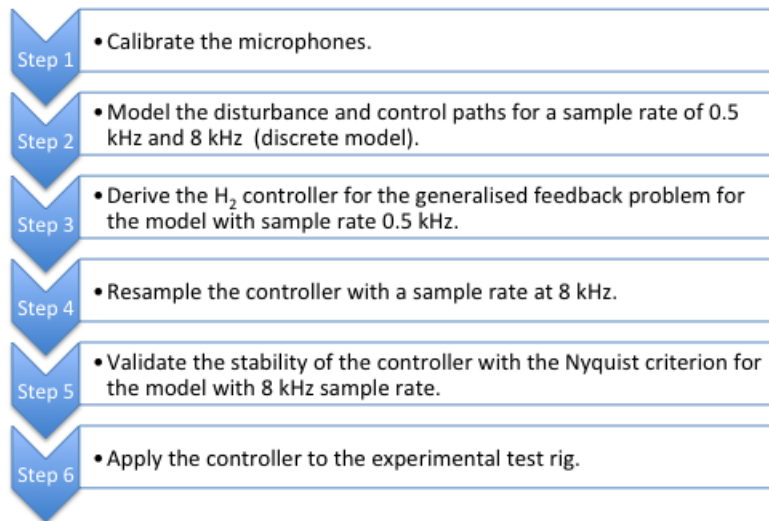


Figure 4.18: Offline  $H_2$  control design for reduction of reflecting noise inside an experimental acoustic duct.

### 4.4.3 FxLMS Control Design for Experimental Implementation

In order to evaluate the level of performance of the  $H_2$  feedback design it is necessary to compare the design with a well established control design. Therefore, just as in the previous chapter, the FxLMS method is chosen and implemented on the apparatus. The FxLMS algorithm has already been fully described (section 2.3.1) when implemented for the simulated plant. In this subsection the steps required to implement the adaptive controller are summed up in schematic form in figure 4.19. The stability and the performance of the design are affected by the magnitude of the convergence rate ( $\alpha$ ) and the order of the controller. Hence, through trial and error the stability and good performance (reduction of the reflecting sound wave) can be achieved.

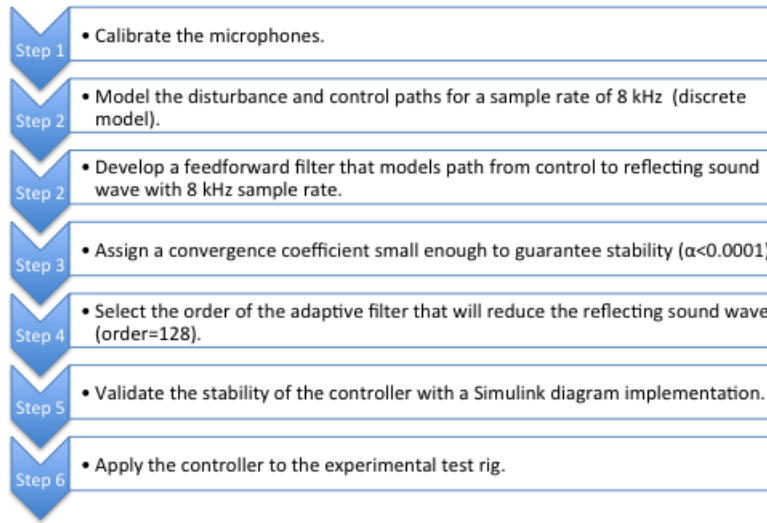


Figure 4.19: Offline  $H_2$  control design for reduction of reflecting noise inside an experimental acoustic duct.

In addition to the steps required to implement the FxLMS design (figure 4.19) the block diagram utilised for the purpose of tuning the adaptive controller is presented in figure 4.20.

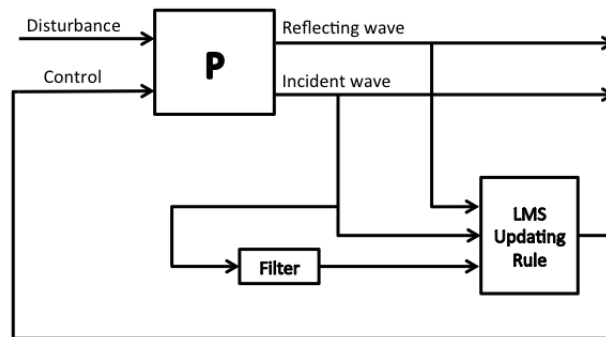


Figure 4.20: Block diagram for implementing FxLMS design.  $P$  is the *MIMO* plant's dynamics. The block with label filter is a transfer function that replicates the path between control to reflecting wave. Finally the updating rule block is formulated based on the theory developed in the previous chapter (section 2.3.1).

## 4.5 Results and Analysis

In this section the experimental implementation of the two designs is presented.

With regards to the the  $H_2$  controller, the high precision modelling of the control path to acceleration, figure 4.11, allows us to inspect the stability of the proposed control design

before it is actually applied directly on the pulse tube preventing any potential damage to the equipment. Although the investigated plant is modelled with a MIMO system the actual control feedback signal is of dimension equal to one, therefore the closed loop system's stability can be confirmed by the Nyquist criterion regarding SISO systems [Ogata and Yang, 1970].

With the FxLMS algorithm, in order to achieve a stable response with good reduction of the undesired reflecting sound wave a convergence coefficient of  $\alpha = 0.00001$  and a 256th order controller were selected. It must be emphasised that these values were determined based on experimental testing.

Before the results are presented it should be noted that theory suggests that acoustic resonances (modes) in duct setups such as in figure 4.2 are found at frequencies given by the formula  $f_n = \frac{nc_0}{2L}$  [Beranek, 1986]. Therefore, for the given dimensions of the duct there should be two acoustic resonances positioned below 250 Hz and additionally a resonance due to the disturbance loudspeaker ( $70Hz$ ). During the experimental validation work for the  $H_2$  controller for this chapter, the 1st acoustic mode ( $\sim 90Hz$ ) was not observable, figure 4.23. The difficulty in observing the first acoustic mode was solved in later experimental validation work (Chapter 5).

### 4.5.1 Experimental Implementation of $H_2$ Design

Initially, the stability of the design is verified for a simulated response of the open loop system, figure 4.21. The next and final step required to confirm the stability of the proposed control design is to plot the Nyquist diagram of the open loop system with the use of raw data, figure 4.22. The nyquist diagram of the open loop system does not encircle the critical point  $(-1, 0j)$  and therefore closed loop stability is guaranteed [Ogata and Yang, 1970]. It should be noted that for all the simulations considered in this chapter a positive feedback control loop is used and as a result of this assumption the open loop system's equation is given by:

$$G_{open}(s) = -P_{22}K(s) \quad (4.6)$$

where  $P_{22}$  is the control path between the control signal  $E_{con}$  and the acceleration of control loudspeaker's cone  $w_{loud}$  and  $K(s)$  is the  $H_2$  feedback controller. The differences viewed between the Nyquist diagrams for the simulated and experimental data (figure 4.21 and figure 4.22) are due to the minor differences of the high order FIR filters designed to model the dynamics of the plant.

The performance of the  $H_2$  control design is demonstrated with a simulated and experimental response of the plant, figure 4.24 and figure 4.23. The simulated response predicts with high accuracy the experimental response of the test rig, verifying the accuracy and efficacy of the plant's models used in the design procedure. Because the controller is designed based on a reduced order model for a frequency band between 0-250 Hz the beneficial effect of the  $H_2$  feedback controller is most clearly observed with a significant 10 dB reduction at the acoustic resonance at  $f = 185Hz$ . Since this is the only significant acoustic resonance within the design bandwidth the higher order modes remain unaffected. Depending on the application and disturbance source, the higher order modes could be included by systematically extending the order of the model and controller. Although the use of a feedforward technique such as FxLMS is likely to produce a better broad-band performance, the approach presented here has great potential in producing a practically viable and low cost distributed ANC system using easily accessible local measurements. The suggested  $H_2$  design reduces the implementation and computational complexity required by the standard FxLMS approach.

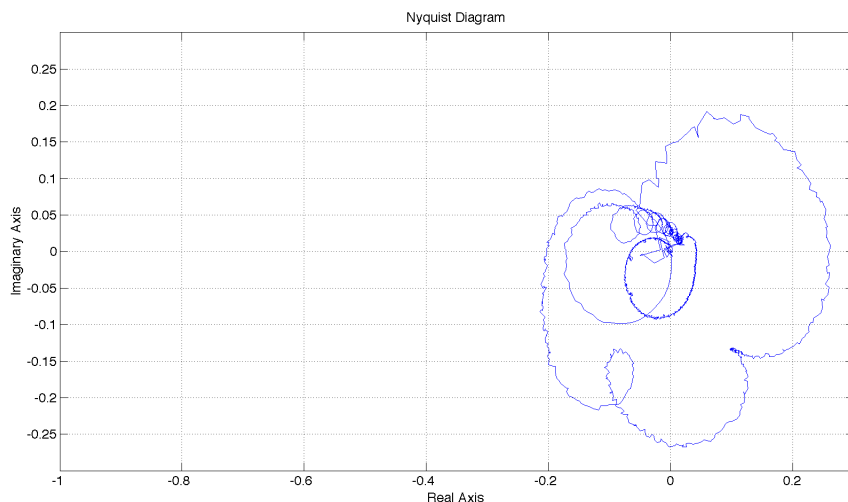


Figure 4.21: Nyquist plot of open loop with  $H_2$  feedback control for simulated response

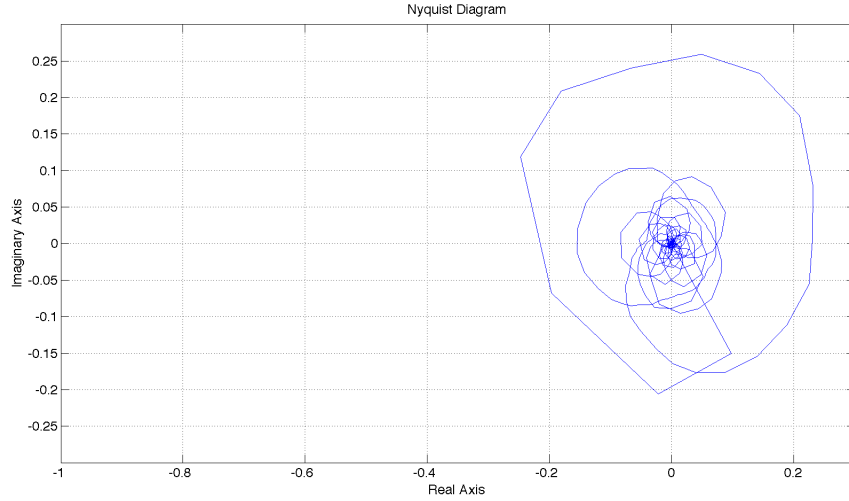


Figure 4.22: Nyquist plot of open loop system with  $H_2$  output feedback control for experimental response

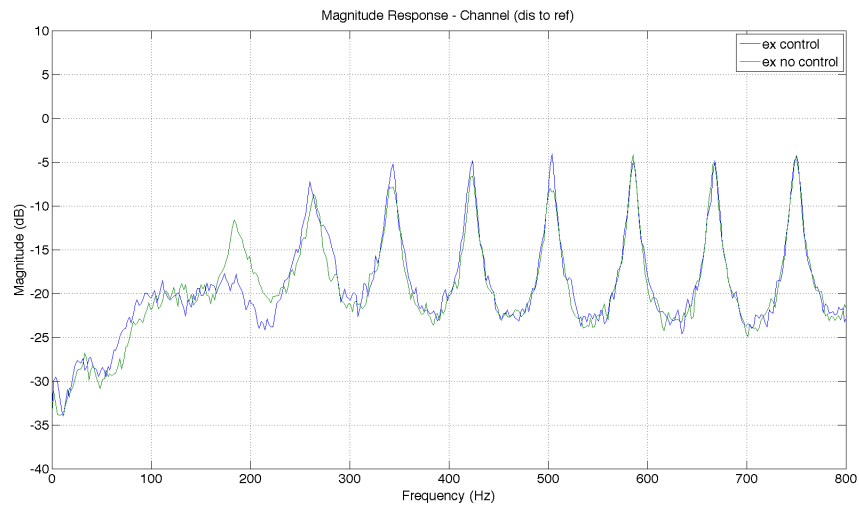


Figure 4.23: Magnitude of the power spectral density of the reflecting sound wave without and with  $H_2$  output feedback control for experimental data (green, blue). In the legend ex control stands for experimental response with controller and ex no control stands for experimental response without control.

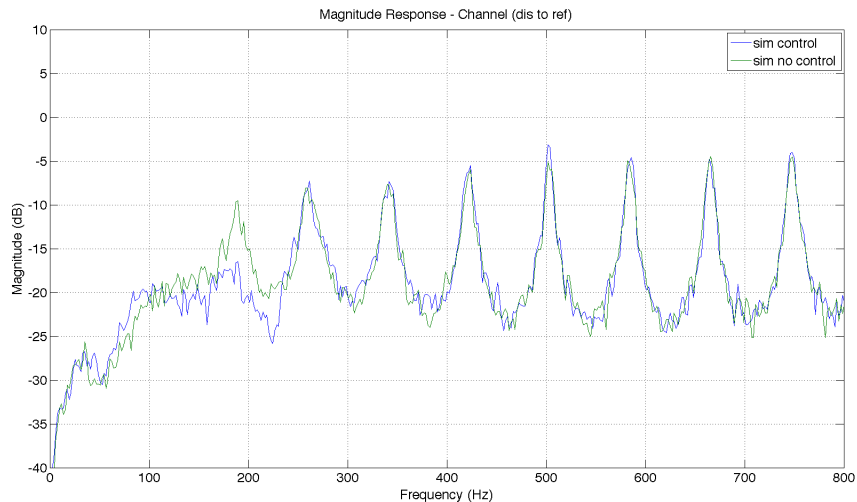


Figure 4.24: Magnitude of the power spectral density of the reflecting sound wave without control and with  $H_2$  output feedback control for simulated response (green, blue). In the legend box sim control stands for simulated response with controller and sim no control stands for simulated response without control.

## 4.5.2 Experimental Implementation of FxLMS Design

The stability of the FxLMS controller can be assessed by illustrating the time domain response of the plant while the controller is activated (figure 4.25).

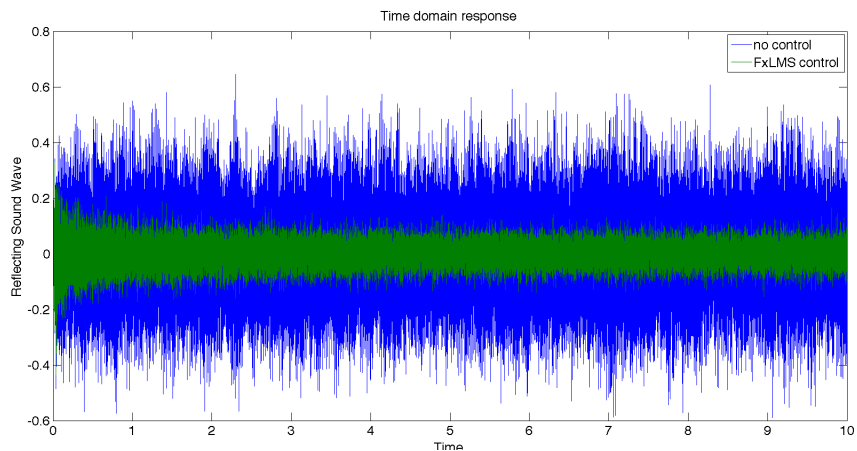


Figure 4.25: Time domain response of the reflecting sound wave. The FxLMS controller is tuned online.

In order to evaluate the level of performance of the FxLMS controller applied on the apparatus, the magnitude of the reflecting wave's power spectral density is illustrated in

figure 4.26. By selecting an order of 256 for the adaptive controller, the design reduces the reflecting sound wave for a bandwidth of 100–800 Hz. The high order of the controller allows a significant reduction of the reflecting sound wave. Specifically in figure 4.26, a minimum reduction of  $15dB$  and maximum of  $30dB$  can be viewed after the first acoustic resonance ( $185Hz$ ).

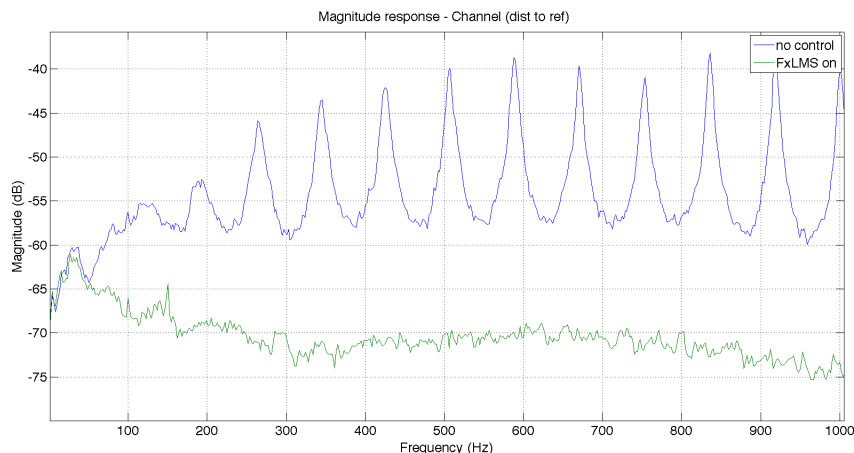


Figure 4.26: Magnitude of the power spectral density of the reflecting sound wave without control and with FxLMS feedforward control for experimental response (blue, green)

### 4.5.3 Comparison

Both control designs ( $H_2$  and FxLMS) were successfully implemented on the experimental acoustic duct (figure 4.3). In this subsection a comparison of the two control approaches is carried out. Specifically the comparison is done in terms of performance, implementation complexity and cost efficiency.

With regards to performance it can be viewed clearly that the FxLMS controller is able to reduce the undesired reflecting sound wave significantly more than the  $H_2$  local controller (figure 4.23 and figure 4.26). Furthermore the adaptive controller is able to apply control to a larger bandwidth compared to the  $H_2$  feedback controller. The reason the  $H_2$  controller has a smaller bandwidth is because the low order models designed to describe the plant's dynamics up to 250 Hz.

However, in terms of reduce implementation complexity, the  $H_2$  control design is far more superior. Specifically, the FxLMS controller requires:

- An up to date feedforward filter of the control path.
- Experimental validation of the convergence coefficient ( $\alpha$ ).
- Experimental validation of the optimal order of the adaptive control.
- The stability of the design can only be addressed online.
- Real time measurements of the remote variables (incident and reflecting sound wave)

In order to appreciate the benefits when selecting the  $H_2$  design, a summary of them is listed below:

- To run the controller in realtime, the  $H_2$  design requires for implementation only a local signal from the accelerometer embedded on the control loudspeaker, whereas the adaptive controller requires the signal from a pair of high precision pressure microphones that results in a considerable increase of cost and implementation complexity. The  $H_2$  requires the error signal only during the control design.
- The stability analysis of the  $H_2$  design is much simpler to carry out in comparison to the FxLMS approach and can be calculated analytically offline (figure 4.22).
- The  $H_2$  controller is a fully automated design and does not require any fine tuning of parameters such as the convergence rate (FxLMS) and therefore has less design complexity.

In conclusion, the feedback design is a much more cost and resource efficient approach in comparison to the adaptive controller. This design option is more favourable when global measurements (microphones) are not feasible for control implementation.

## 4.6 Conclusions

In this chapter a systematic approach to the design of an ANC system was developed in order to achieve reduction of the reflected sound waves in an experimental one-dimensional acoustic duct problem. Initially, the intent was to design a PID controller with use of the FLS

tuning method. During the modelling of the plant's dynamics, two problems were discovered and prohibited the FLS method to perform satisfactory (section §4.3). Specifically:

- The lower frequency bandwidth at which plane wave propagation is dominant (0 - 1000 Hz) the dynamics of the plant are rather complex (figure 4.12) and a simple PID controller leads to rather disappointing performance.
- The control loudspeaker used as a controlled boundary element, exhibits three resonant peaks (figure 4.12). These added resonances complicate the minimisation problem of the FLS PID controller which leads to poor performance (reduction of the reflecting sound wave).

In order to bypass this problem, a control design method that makes use of a robust and near-optimal  $H_2$  generalised feedback controller was developed. The  $H_2$  controller was able to successfully reduce significantly the undesired reflected sound wave within a design frequency bandwidth in both a simulated and experimental environment. In contrast to the classical FxLMS adaptive feedforward control approach, the suggested feedback control procedure is a locally based collocated design and therefore as theory suggests, is guaranteed to be stable [Preumont and Seto, 2008]. The approach utilises only a local measurement of the acceleration of the boundary-reflecting surface (in the experimental case considered here, the control loudspeaker's cone) in order to produce the control signal and does not therefore during implementation require any remote measurements. The performance of the control design was compared with a standard FxLMS design. The FxLMS as expected, provided a better performance, this is due to the feedforward nature of the adaptive controller. However to achieve the good performance of the adaptive controller a tedious design procedure which required a number of trial tests on the test rig it's self in order to guarantee stability had to be conducted. In practice, the  $H_2$  design reduces the physical size, cost and intrusion of the control system and moreover reduces the complexity of the compensator together with the associated computational burden.

In the next chapter an alternative feedback control approach named Remote Geometric Control will be considered and compared with the  $H_2$  design. Specifically, the designs are implemented on the apparatus (figure 4.3) and insight into the benefits and trade-offs when

considering the Geometric approach are made.

# Chapter 5

## Remote Geometric Control Design for Suppression of Reflected Noise

### 5.1 Introduction

In the previous chapter an automated  $H_2$  feedback controller was developed in order to reduce the reflections of sound for an acoustic duct problem. This method in contrast to the popular FxLMS algorithm relies on local measurements (accelerometer) in order to deal with reduction of the global measurement (reflected sound wave). Although the performance of the feedback controller is inferior to the FxLMS approach, the suggested design relies on local measurements which reduces implementation complexity and cost.

The next logical step is to attempt to improve the performance (controlled bandwidth and reduction of the reflected sound) of the feedback design while retaining its beneficial local characteristics. In order to do so, in this chapter a systematic remote geometric approach to generate a feedback controller for remote attenuation (reflecting sound wave) is adopted and compared to the  $H_2$  controller. Specifically the geometric controller has been proposed and validated via experiment on a physical arrangement for the purpose of remote Active Vibration Control (AVC) [Daley and Wang, 2008; Ubaid et al., 2011; Ubaid et al., 2012]. Based on this method, it is feasible to achieve attenuation of the vibration at remote points of a physical structure by applying a controller that is tuned in terms of optimally selecting a parameter. In order to have a stable design it is necessary to use the complement minimum

phase expression of the local control path when implementing the geometric feedback design [Daley and Wang, 2008; Ubaid et al., 2011; Ubaid et al., 2012]. Specifically, this local path (transfer function) comprises the link between the voltage of the control loudspeaker and the acceleration of the loudspeaker's baffle. The investigated methodology leads to a compensator which is classified as a stable and stabilising controller. Furthermore, it can achieve the desired output reduction at the remote points of the apparatus setup.

This chapter is organised as follows: In section §5.2 the remote geometric control design approach that is selected to cancel the undesired reflecting sound wave is presented. In section §5.3 the results of applying the geometric controller is illustrated and the design's performance is compared with the  $H_2$  feedback controller. Finally, section §5.4 provides some concluding remarks.

## 5.2 Control Design

The geometric design investigated in this chapter intends to improve the performance of the  $H_2$  feedback design in terms of reduction of the reflected noise and the number of acoustic resonances controlled (control bandwidth). The geometric design was originally developed to deal with reduction of vibration on complex interconnected structures at remote points, where application of control is not an option. Specifically, in many cases due to harsh environmental conditions the controller can not be position at the point of interest for control, an example of such a case is the propeller of a submarine. Therefore, remote control is deployed. The main problem that arises when trying to reduce vibrations with active means at a specific point on such structures is the risk of enhancement of vibration at additional positions of the physical structure [Post and Silcox, 1990; Daley and Wang, 2008; Ubaid et al., 2011; Ubaid et al., 2012].

The initial geometric method addressed the problem of reducing vibrations simultaneously at local and remote points of a physical arraignment with the use of one sensor and one actuator positioned close to each other for set of excitation frequencies [Daley and Wang, 2008]. Having achieved this, the next step was to extend the design for the broadband case [Wang and Daley, 2010]. In order to achieve reduction of vibrations for any random band

of frequencies, the controller design has to invert the transfer function that describes the local control path of the plant. It must be noted that this procedure can lead to an unstable design if the inverted function is a non minimum phase transfer function. In order to solve this problem a design freedom was introduced to parameterise the attenuation of local and remote vibrating positions in which the compensator was designed with the use of a minimum phase complement transfer function, hence no unstable transfer function occurs while inverting approximation of the control path [Daley and Wang, 2008;Ubaid et al., 2011;Ubaid et al., 2012]. Furthermore, a low pass filter was introduced in the design procedure that allowed the designer to better the robustness of the controller when dealing with un-modelled dynamics found at high frequencies [Ubaid et al., 2011;Ubaid et al., 2012]. Specifically, the presence of the filter achieves a roll off of the closed loop gain at the high frequency band without affecting the performance of the controller at the lower frequency bandwidth at which it is designed to attenuate vibrations [Ubaid et al., 2011;Ubaid et al., 2012].

The architecture utilised by the design is the same one previously described for the  $H_2$  controller and is illustrated in figure 4.13. The process is represented as a two-input and two-output system that is labelled as  $P$  and has a feedback controller  $C$  that maps the measurable signal  $w_{loud}$  to the manipulated variable  $E_{con}$ . Specifically, the two inputs are the voltage of the disturbance loudspeaker  $E_{dis}$  and the voltage of the control loudspeaker  $E_{con}$ . Furthermore, the two outputs are the total reflecting sound wave  $P_{ref}$  (remote measurement) which is to be minimised and  $w_{loud}$  (local measurement) the acceleration of the control loudspeaker's cone. The matrix representation of the open loop system is therefore:

$$\begin{bmatrix} P_{ref} \\ w_{loud} \end{bmatrix} = \begin{bmatrix} P_{11} & P_{12} \\ P_{21} & P_{22} \end{bmatrix} \begin{bmatrix} E_{dis} \\ E_{con} \end{bmatrix} \quad (5.1)$$

In the following subsection, the remote geometric feedback control design is introduced for application of attenuation of reflecting sound waves inside acoustic ducts. The controller that will be designed and realised on the experimental apparatus is expected to achieve reduction of the reflecting sound wave.

### 5.2.1 Remote Geometric Feedback Control

In the plant defined in 5.1, the goal is to construct a feedback controller  $C(j\omega)$  by making use of only the output signal from the control loudspeaker (acceleration) in order to accomplish reduction of the reflecting sound wave at the remote location where the two microphones are positioned inside the acoustic duct. As this is a traveling wave, this effectively leads to a global reduction in this wave. By applying the feedback controller to the plant,  $E_{con}(j\omega) = -C(j\omega)w_{loud}(j\omega)$ , the system's closed loop will have an output function at for points near the actuator that delivers the control force (local) and near the sensors that measure the output of the plant (remote) and are given by the following two equations [Ubaid et al., 2011;Ubaid et al., 2012]:

$$L_{cl}(j\omega) = \left[ 1 - \frac{P_{22}(j\omega)C(j\omega)}{1 + P_{22}(j\omega)C(j\omega)} \right] P_{21}(j\omega)E_{dis}(j\omega) \quad (5.2)$$

and

$$R_{cl} = \left[ 1 - \frac{P_{22}(j\omega)C(j\omega)}{1 + P_{22}(j\omega)C(j\omega)} \frac{P_{21}(j\omega)P_{21}(j\omega)}{P_{11}(j\omega)P_{22}(j\omega)} \right] P_{11}(j\omega)E_{dis}(j\omega) \quad (5.3)$$

The design freedom parameter used to calculate the stable controller is defined as  $\gamma$  and is associated to the sensitivity function  $S(j\omega)$  by the following expression [Ubaid et al., 2011;Ubaid et al., 2012]:

$$\gamma(j\omega) = \frac{1}{g_{AP}(j\omega)f_{LP}(j\omega)} [S(j\omega) - 1] \quad (5.4)$$

where  $g_{AP}(j\omega)$  is a all pass transfer function which is constructed by using the right half-plane zeros given from  $P_{22}(j\omega)$ . Furthermore, a filter is included in order to improve the robustness of the design at frequencies outside of the controller's region of control,  $f(j\omega)$ , and can be a low pass or a bandpass [Ubaid et al., 2011;Ubaid et al., 2012]. Having introduced the  $\gamma$  - parameter it is now possible to express both local and remote outputs in equation (5.2) and equation (5.3) in terms of this parameter as [Ubaid et al., 2011;Ubaid et al., 2012]:

$$L_{cl}(j\omega) = [1 + \gamma(j\omega)g_{AP}(j\omega)f_{LP}(j\omega)] P_{21}(j\omega)E_{dis}(j\omega) \quad (5.5)$$

and

$$R_{cl} = \left[ 1 + \gamma(j\omega)g_{AP}(j\omega)f_{LP}(j\omega)\frac{P_{21}(j\omega)P_{21}(j\omega)}{P_{11}(j\omega)P_{22}(j\omega)} \right] P_{11}(j\omega)E_{dis}(j\omega) \quad (5.6)$$

In equation (5.5) and equation (5.6) the magnitude of the expressions inside the brackets in the right hand side define the attenuation of both the local and remote output [Ubaid et al., 2011;Ubaid et al., 2012]. Furthermore, because the magnitudes are functions of frequency they can be expressed as circles at each individual frequency in a  $\gamma - plane$  (this is why the proposed design is named geometric) [Ubaid et al., 2011;Ubaid et al., 2012]. From this geometric representation it is possible to visualise the reduction problem. Specifically, when considering values of  $\gamma$  inside the circle we will have a reduction of the output (either local or remote) [Ubaid et al., 2011;Ubaid et al., 2012]. Around the frequency range  $[\omega_L, \omega_H]$ , the geometric feedback controller could be able to achieve simultaneous reduction in both the remote (reflecting sound wave) and the local (acceleration) outputs. Although it would be ideal to reduce both outputs (local and remote) in order to minimise the risk of structural failure due to fatigue, in many cases dual reduction might not be an option because the two  $\gamma - locus$  do not overlap (figure 5.1). When the two circles overlap (figure 5.2) dual reduction is feasible by choosing a  $\gamma - point$  that lies inside both loci. The distance of the  $\gamma - point$  from the centre of each circle, dictates the amount of reduction the feedback controller will achieve for each output. Hence, there is a trade-off between which output and what reduction can be achieved. Because the main intent of this experiment is to reduce the reflecting sound wave (remote output), priority in selecting the  $\gamma - point$  is given to points that lie inside the locus described for the remote output, equation (5.8). Additionally, if the selected  $\gamma - point$  satisfies inequality equation (5.7) dual reduction (local and remote) is achieved.

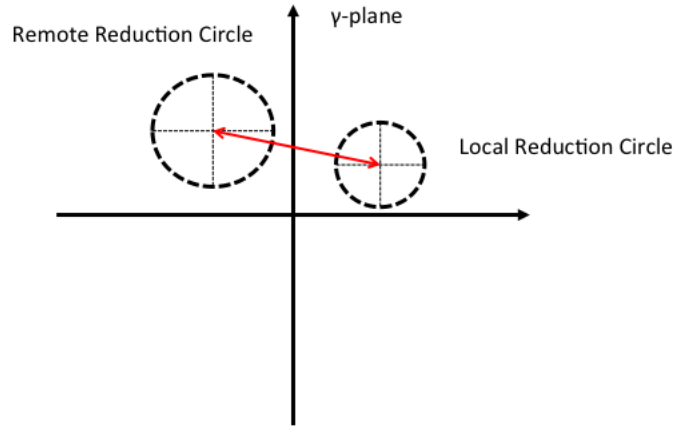


Figure 5.1:  $\gamma$  – *plane* with remote and local output reduction circles for single frequency. In this illustration the distance between the two centres is greater than the sum of the radius of the two locus (red line).

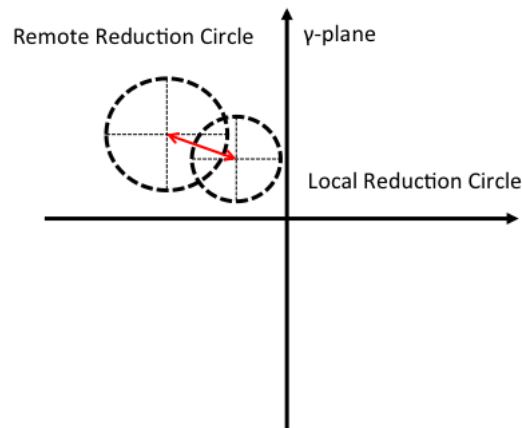


Figure 5.2:  $\gamma$  – *plane* with remote and local output reduction circles for single frequency. In this illustration the distance between the two centres is smaller than the sum of the radius of the two locus (red line).

$$\left| \gamma(j\omega_i) + \frac{1}{g_{AP}(j\omega_i)f_{LP}(j\omega_i)} \right| < \left| \frac{1}{g_{AP}(j\omega_i)f_{LP}(j\omega_i)} \right| \quad (5.7)$$

$$\left| \gamma(j\omega_i) + \frac{1}{g_{AP}(j\omega_i)f_{LP}(j\omega_i)} \frac{P_{11}(j\omega)P_{22}(j\omega)}{P_{21}(j\omega)P_{12}(j\omega)} \right| < \left| \frac{1}{g_{AP}(j\omega_i)f_{LP}(j\omega_i)} \frac{P_{11}(j\omega)P_{22}(j\omega)}{P_{21}(j\omega)P_{12}(j\omega)} \right| \quad (5.8)$$

From the previous two inequalities if select to interpolate  $\gamma$  – *points* which satisfy them

with a stable transfer function  $\gamma_k(j\omega)$  the controller can be implemented as [Ubaid et al., 2011;Ubaid et al., 2012]:

$$C(j\omega) = -\frac{\gamma_k(j\omega)f_{LP}(j\omega)}{[1 + \gamma_k(j\omega)g_{AP}(j\omega)f_{LP}(j\omega)]g_{MP}(j\omega)} \quad (5.9)$$

where  $g_{MP}(j\omega)$  is the minimum phase complementary transfer function of the local control path,  $P_{22}(j\omega)$ . If the minimum phase counter part is not considered, an unstable controller results. The technique of generating  $g_{MP}(j\omega)$  is based on manually reflecting the non-minimum phase zeros from the RHP to the LHP (figure 5.3).

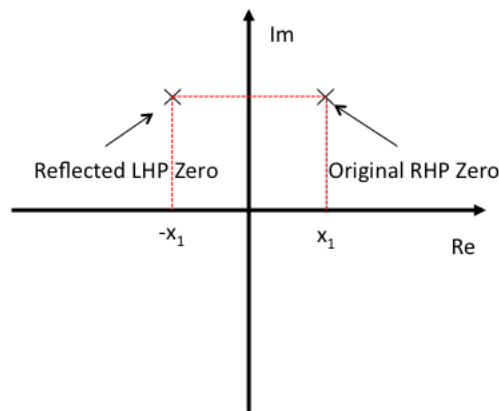


Figure 5.3: Minimum phase reflecting technique

Now that the candidate  $\gamma$  - *points* have been identified, based on equation (5.9) a set of discrete points of the ideal controller is available. The next step is to develop an automated interpolation methodology of these points and generate the transfer function of the feedback controller. The Nevanlinna - Pick interpolation algorithm is selected and described in the following subsection.

### 5.2.1.1 Nevanlinna - Pick Interpolation Method

In order to form the geometric feedback controller, a number of *points* in the  $\gamma$  - *plane* for each disturbance frequency have to be interpolated by a frequency dependent function  $\gamma_k(s)$ , which has to be stable. This interpolation step is carried out by using the Nevanlinna - Pick (N - P) algorithm [Delsarte et al., 1979;Ubaid et al., 2011;Ubaid et al., 2012]. This problem can be specified as followed:

*Problem:* Given  $l$  distinct points  $p_1, \dots, p_l$  in the Right Half Plane (RHP)  $P^+$  and a set of complex numbers  $X_1, \dots, X_l$ , calculate a frequency dependant function  $\gamma_k(s)$  that is analytic in  $P^+$  and in which the following is satisfied [Ubaid et al., 2011;Ubaid et al., 2012]:

$$\sup |\gamma_k(s)| \leq 1 \quad (5.10)$$

such that  $\gamma_k(p_j) = X_j$ , for all  $j = 1, \dots, l$ . Such a problem will be solvable if and only if the related Pick matrix [Ubaid et al., 2011;Ubaid et al., 2012]:

$$P = \left[ \frac{1 - X_n \overline{X_m}}{p_n + \overline{p_m}} \right]_{n,m=1}^l \quad (5.11)$$

is a positive definite matrix.

With the symbol  $\bar{\bullet}$  we define the complex conjugate operator.

Based on the problem definition given above, the location of the  $s_i$  points should be in the RHP and the set of  $\gamma$  – *points* should be approximated on the imaginary axis of the complex  $\gamma$  – *plane* [Ubaid et al., 2011;Ubaid et al., 2012]. In order to shift the  $s_i$  points into the RHP the use of a transformation is required. Specifically, *Lemma 2* from [Ferrerres and Puyou, 2005] is utilised. The *Lemma* states the following:

*Lemma:* A stable frequency dependant function (transfer function) will exist for the given optimal  $\gamma$  – *data* values (located at  $l$  discrete frequencies  $\omega_i$ ,  $j = 1, \dots, l$ ) iff the following Pick matrix:

$$P = \left[ \frac{1 - U_m \overline{U_n}}{s_n + \overline{s_m}} \right]_{n,m=1}^l \quad (5.12)$$

is a positive definite matrix. In which:

$U_j = \frac{\gamma_j}{M}$  and  $s_j = \sigma + j\omega$ , for  $j = 1, \dots, l$ . Where  $M$  is the maximum modulus of the interpolated transfer function and  $\sigma$  a positive real number.

By fluctuating the values of  $M$  and  $\sigma$  one can affect the positive definiteness of the Pick matrix [Ubaid et al., 2011;Ubaid et al., 2012]. In order to acquire a stable controller with good sound attenuation it is necessary to conduct a fine tuning. As a rule of thumb it should mentioned that when selecting  $\sigma$  to be small we should expect  $\gamma_k(j\omega)$  (the interpolated function) to have poles that will be at close proximity to the  $j\omega$  – *axis* of the  $\gamma$  – *plane*

[Ubaid et al., 2011;Ubaid et al., 2012]. If a small  $\sigma$  value is chosen, the transfer function  $\gamma_k(j\omega)$  will exhibit oscillations in tis frequency response and result to gain and phase crossover phenomena [Ubaid et al., 2011;Ubaid et al., 2012]. If small  $\sigma$  values are chosen, the resulting transfer function for frequency points that are not interpolated will have parts outside the loci defined from equation (5.7) and equation (5.8) and lead to a poor controller in term of noise reduction [Ubaid et al., 2011;Ubaid et al., 2012]. If instead of selecting a small value for  $\sigma$  we chose a greater value, the resulting transfer function from the N-P method will approximate more efficiently the non interpolated frequencies but will require large  $M$  values in order to satisfy the positive definite Pick matrix criteria [Ubaid et al., 2011;Ubaid et al., 2012]. However, for greater values of  $M$  are a risk in causing the design to go unstable. Specifically, the the nyquist contour of  $\gamma_k(j\omega)g_{AP}(j\omega)f_{LP}(j\omega)$  may encircle the critical point and result in a unstable loop which can be seen from equation (5.9) [Ubaid et al., 2011;Ubaid et al., 2012]. A good tuning rule would be to iteratively increase the value of  $M$  so that the pick matrix is positive definite for every specific value of  $\sigma$  until the controller stability condition is violated [Fu, 1991].

*Algorithm:*

**Step 1:** compute the elements of Fenyves array  $R$  [Ubaid et al., 2011;Ubaid et al., 2012].

$$R_{i,k} = \frac{s_k + \overline{s_{i-1}}}{s_k - s_{i-1}} \frac{R_{i-1,k} - R_{i-1,i-1}}{1 - R_{i-1,k} \overline{R_{i-1,i-1}}}, \quad 2 < i < m, \quad i < k < m \quad (5.13)$$

where  $R_{1,k} = U_k$  , for  $1 < k < m$  .

**Step 2:** Estimate  $U_1(s)$  from [Ubaid et al., 2011;Ubaid et al., 2012]:

$$U_i(s) = \frac{P_{i,i} + U_{i+1}(s) \frac{s-s_i}{s+\overline{s_i}}}{1 + \overline{P_{i,i}} U_{i+1}(s) \frac{s-s_i}{s+\overline{s_i}}}, \quad i = m, m-1, \dots, 2, 1 \quad (5.14)$$

**Step 3:** The stable bounded real analytic interpolating function for the set of data points  $(s_j, U_j)$  and its complex conjugate  $(\overline{s_j}, \overline{U_j})$ , is given by [Ubaid et al., 2011;Ubaid et al., 2012]:

$$\gamma_k(s) = M \times \frac{1}{2} \left[ U_1(s + \sigma) + \overline{U_1(s + \sigma)} \right] \quad (5.15)$$

This algorithm is valid given any initial stable bounded analytic function  $U_{i+1}(s)$  in equation (5.14) [Ubaid et al., 2011;Ubaid et al., 2012].

As a result of this interpolating method for every point that is interpolated a minimum of four poles and zeros will be added to the final transfer function  $\gamma_k(j\omega)$  [Ubaid et al., 2011;Ubaid et al., 2012]. This realisation will increase the order of the controller,  $C(j\omega)$  (equation (5.9)) [Ubaid et al., 2011;Ubaid et al., 2012]. With regards to the number of  $\gamma$  – *points* required to design a controller that will reduce the reflecting sound wave, a rule of thumb is to select a single frequency point near each resonance intended for reduction. By doing so, the interpolating problem is kept simple as possible and therefore a stable and robust controller is achieved. It must be emphasised that this rule is primarily empirical and is based on the simulations and experimental results for the specific acoustic problem.

### 5.2.2 Stability Analysis

The conditions for the closed loop stability and controller stability on the selection of  $\gamma$  – *points* is considered in this subsection. If the formula of the controller (equation (5.9)) is rearranged to form a relation between the design freedom parameter and the complementary sensitivity function the following equation is derived:

$$\gamma_k(j\omega)g_{AP}(j\omega)f_{LP}(j\omega) = -\frac{g_{MP}(j\omega)C(j\omega)}{1 + g_{MP}(j\omega)C(j\omega)} \quad (5.16)$$

It can be observed that since  $g_{AP}(j\omega)f_{LP}(j\omega)$  is stable, selecting *points* in the  $\gamma$  – *plane* as the mapping of a function which is stable (in a similar fashion to the approach proposed by Wang and Daley, 2010) guarantees closed loop stability.

Since  $g_{MP}(j\omega)$  has no RHP zero(s), a controller given by equation (5.9) is stable if  $\gamma_k(j\omega)$  is a stable transfer function and the Nyquist contour of  $\gamma_k(j\omega)g_{AP}(j\omega)f_{LP}(j\omega)$  does not enclose the critical point. This has implications near the resonant frequency of an acoustic mode. The optimal  $\gamma$  – *point* for remote attenuation close to a resonant frequency approaches  $[g_{AP}(j\omega)f_{LP}(j\omega)]^{-1}$ . This means that when a controller is to be designed for attenuation near resonant frequencies the polar plot of  $\gamma_k(j\omega)g_{AP}(j\omega)f_{LP}(j\omega)$  approaches the critical point and would therefore have very low gain and phase margins close to this frequency. Hence, when  $\gamma$  – *points* are to be selected for attenuation near a resonant frequency, which will usually be the case, then it becomes important to define some additional constraints so that

$\gamma_k(j\omega)g_{AP}(j\omega)f_{LP}(j\omega)$  in the disturbance frequency bandwidth does not risk encirclement of the critical point.

The polar plot of  $\gamma_k(j\omega)g_{AP}(j\omega)f_{LP}(j\omega)$  will not enclose the  $-1$  point and hence the controller will be stable if, at the phase crossover frequency  $\omega_{cp}$  the condition:

$$Re(\gamma_k(j\omega)g_{AP}(j\omega)f_{LP}(j\omega)) > -1 \quad (5.17)$$

is satisfied (crossover frequency is when  $Im(\gamma(j\omega_{cp})g_{AP}(j\omega_{cp})f_{LP}(j\omega_{cp})) = 0$ ). The frequency response of  $\gamma_k(j\omega)g_{AP}(j\omega)f_{LP}(j\omega)$  at the phase crossover frequency can be written in cartesian form as the products of the frequency response of  $\gamma_k(j\omega)$  and  $g_{AP}(j\omega)f_{LP}(j\omega)$  evaluated at  $\omega_{cp}$  as:

$$\begin{aligned} \gamma_k(j\omega)g_{AP}(j\omega)f_{LP}(j\omega) &= \\ &= [Re(\gamma_k(j\omega)) + jIm(\gamma_k(j\omega))] [Re(g_{AP}(j\omega)f_{LP}(j\omega)) + jIm(g_{AP}(j\omega)f_{LP}(j\omega))] \end{aligned} \quad (5.18)$$

Multiplying the terms inside the brackets and rearranging as the summation of real and imaginary parts:

$$\begin{aligned} \gamma_k(j\omega)g_{AP}(j\omega)f_{LP}(j\omega) &= \\ &= [Re(\gamma_k(j\omega)) Re(g_{AP}(j\omega)f_{LP}(j\omega)) - Im(\gamma_k(j\omega)) Im(g_{AP}(j\omega)f_{LP}(j\omega))] + \\ &\quad + j [Re(\gamma_k(j\omega)) Im(g_{AP}(j\omega)f_{LP}(j\omega)) + Im(\gamma_k(j\omega)) Re(g_{AP}(j\omega)f_{LP}(j\omega))] \end{aligned} \quad (5.19)$$

At the phase crossover frequency  $Im(\gamma_k(j\omega)g_{AP}(j\omega)f_{LP}(j\omega)) = 0$ , therefore equating the imaginary term on the right hand side of equation (5.19) to zero gives:

$$Re(\gamma_k(j\omega)) Re(g_{AP}(j\omega)f_{LP}(j\omega)) - Im(\gamma_k(j\omega)) Im(g_{AP}(j\omega)f_{LP}(j\omega)) = 0 \quad (5.20)$$

The controller is stable if at the phase crossover frequency  $Re(\gamma_k(j\omega)g_{AP}(j\omega)f_{LP}(j\omega)) > -1$ , which from the real term of equation (5.19) can be stated as:

$$Re(\gamma_k(j\omega)) Re(g_{AP}(j\omega)f_{LP}(j\omega)) - Im(\gamma_k(j\omega)) Im(g_{AP}(j\omega)f_{LP}(j\omega)) > -1 \quad (5.21)$$

Substituting  $Im(\gamma_k(j\omega))$  from equation (5.20) in equation (5.21) gives:

$$Re(\gamma_k(j\omega)) > \frac{-Re(g_{AP}(j\omega)f_{LP}(j\omega))}{[Re(g_{AP}(j\omega)f_{LP}(j\omega))]^2 + [Im(g_{AP}(j\omega)f_{LP}(j\omega))]^2} \quad (5.22)$$

The Blaschke product  $g_{AP}(j\omega)$  has unity magnitude at all frequencies and the weighting filter is chosen such that in the design frequency bandwidth it does not affect the magnitude:

$$|g_{AP}(j\omega)f_{LP}(j\omega)| = |g_{AP}(j\omega)||f_{LP}(j\omega)| \quad \omega \in [\omega_L, \omega_H] \quad (5.23)$$

Due to the inclusion of a band pass filter ( $f_{LP}(j\omega)$ ) when forming the controller, the gain outside the frequency band  $[\omega_L, \omega_H]$  is small and thus further ensures the design is not critically stable. Therefore, equation (5.22) reduces to:

$$Re(\gamma_k(j\omega)) > -Re(g_{AP}(j\omega)f_{LP}(j\omega)) \quad (5.24)$$

Similarly, substituting  $Re(\gamma_k(j\omega))$  from equation (5.20) in equation (5.21) leads to the expression:

$$Im(\gamma_k(j\omega)) < Im(g_{AP}(j\omega)f_{LP}(j\omega)) \quad (5.25)$$

A controller given in equation (5.9) will therefore be both stable and stabilising if the  $\gamma$  – *points* are selected from a mapping of a stable transfer function  $\gamma_k(j\omega)$  and either of the conditions equation (5.24) or equation (5.25) is satisfied.

### 5.2.3 Implementation of the Geometric Design

The modelling of the control path ( $P_{22}$ ) required a 7 – *th* order transfer function to be fitted to the experimental data (figure 5.4). The order of the model is based on trial simulations. It was noticed that by increasing the order of the model beyond seven had insignificant impact on the resulting controller and therefore the transfer function was kept to a low order. Due to RHP zeros a minimum phase transfer function is designed,  $g_{MP}$ , in order to guarantee stability of the controller. For the geometric controller to be compared with the  $H_2$  feedback design, the  $\gamma$  – *points* points selected must be at frequencies near the acoustic resonance (185 Hz and 230 Hz) of the reflecting sound wave (figure 5.5). Through trial and error it was found that to reduce the magnitude at the acoustic resonances, a single pair of  $\gamma$  – *points*

is sufficient to provide a stable and robust controller.  $M$  and  $\sigma$  are found with fine tuning. Finally, because the controller is intended to focus its action in the lower frequency band a low pass filter ( $f_{LP}(j\omega)$ ) with a cut-off frequency at 250 Hz is designed and utilised for the final form of the controller. It must be noted that the design procedure takes place in the continuous domain and therefore a discretisation of the controller ( $f_s = 8 \text{ kHz}$ ) is required for application on the experimental rig.

Now that the overall implementation procedure for the design has been fully described, it is convenient to group the steps into a list (figure 5.6) just as it was done for the  $H_2$  and FxLMS designs.

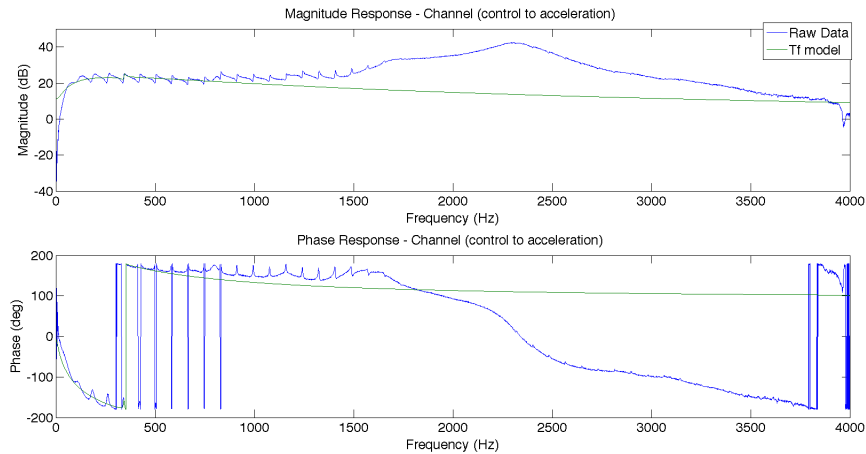


Figure 5.4: Bode plot of the raw experimental data for the control paths (blue) and bode plot of the high order FIR filter fitted to the experimental data (green).

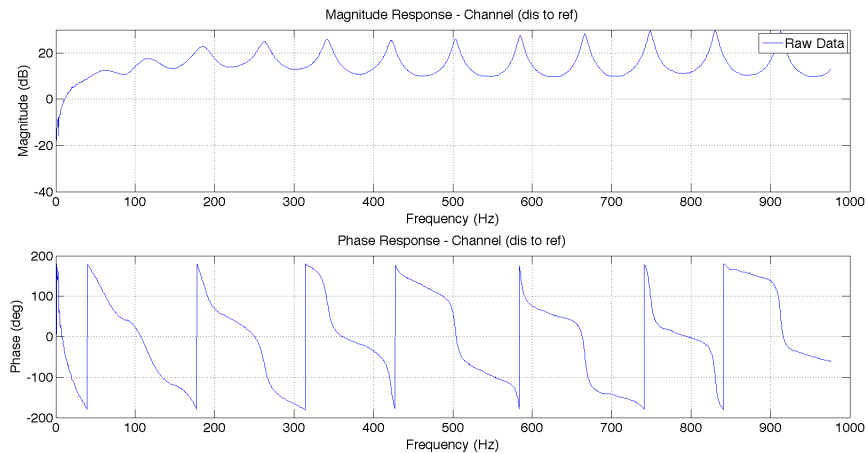


Figure 5.5: Bode plot of the raw experimental data for the disturbance paths (blue) and bode plot of the high order FIR filter fitted to the experimental data (green).

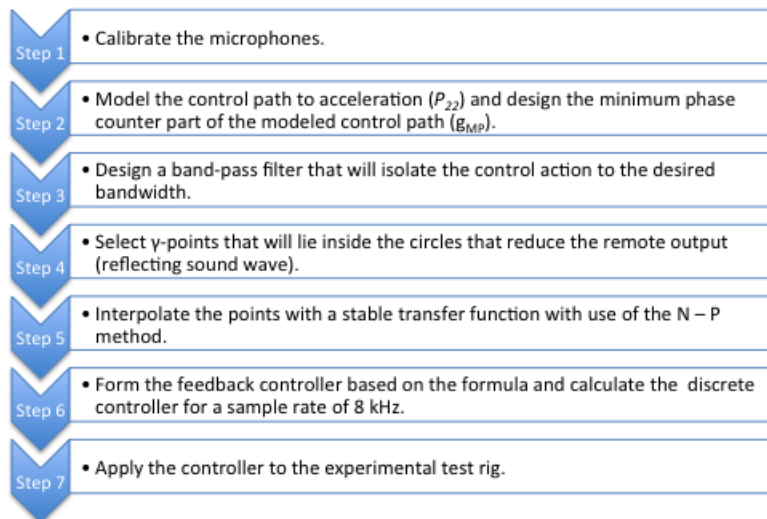


Figure 5.6: Remote geometric feedback control design procedure

## 5.3 Results and analysis

In this section the experimental implementation of the two designs is presented.

Because the two design share the same block setup (figure 4.13) the evaluation of the stability and the performance of these designs is carried out in an identical manner. Hence, the high precision modelling of the control path to acceleration (figure 5.4) allows us to inspect

the stability of the proposed control design before it is actually applied directly on the pulse tube preventing any potential damage to the equipment. As in the previous chapter, the plant is modelled with a MIMO system but the actual control feedback signal is of dimension equal to one, therefore the closed loop system's stability can be confirmed by the Nyquist criterion regarding a SISO systems [Ogata and Yang, 1970].

The feedback loop considered in this chapter is positive, therefore just as in the previous chapter the open loop system's equation is given by:

$$G_{open}(s) = -P_{22}C(s) \quad (5.26)$$

where  $P_{22}$  is the control path between the control signal  $E_{con}$  and the acceleration of control loudspeaker's cone  $w_{loud}$  and  $C(s)$  is the feedback controller.

It must be pointed out that the experimental data retrieved for the purpose of designing the remote geometric design exhibit a newly observed acoustic resonant frequency at 115 Hz [figure 5.5]. This peak was not observable in the previous experiment conducted while comparing the  $H_2$  and FxLMS designs [figure 4.23]. This resonant frequency is of acoustic nature and can be confirmed by the formula [Beranek et al., 1954]:

$$f_n = \frac{nc_o}{2L} \quad (5.27)$$

From equation (5.27) the predicted acoustic resonances are given in table 5.1. There is a small variation between the actual and predicted acoustic resonances. This is due to two reasons. The apparatus has flexible sub woofers for boundary ends and the length of the duct is slightly increased due to the attachment of the two loudspeakers. Nevertheless, the predicted resonances allows us to classify the origin of the newly observed peak as of acoustic nature.

Table 5.1: Predicted resonant frequencies for an acoustic duct of length 2.054m

$f_1$	83.7 Hz
$f_2$	167.5 Hz
$f_3$	251 Hz
$f_4$	335 Hz

The reason that could have affected the observation of the peak could have been a small variation in the amplifiers gains (figure 4.4) to which the microphones are connected to (figure 4.5). Hence, this would affect the precise measurement of the first acoustic resonance. Due to the difficulty to observe the specific resonance consistently, in this chapter the control designs will focus control effort beyond this acoustic resonance peak.

### 5.3.1 Experimental Implementation of $H_2$ Design

The stability of the design is verified by plotting the Nyquist diagram of the open loop system with the use of experimental data, figure 5.7. Based on the Nyquist stability criterion for SISO, it is clearly viewed in the Nyquist diagram that no encirclement of the critical point  $(-1, 0j)$  occurs for the open loop system. Therefore closed loop stability is guaranteed for the  $H_2$  local feedback design.

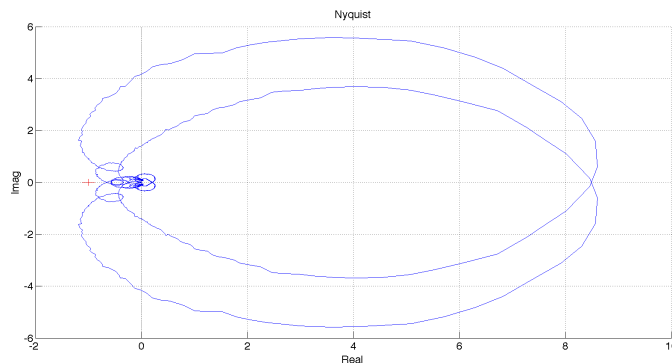


Figure 5.7: Nyquist plot of open loop system with  $H_2$  output feedback control for experimental response

The performance of the  $H_2$  control design is demonstrated with the experimental response of the plant figure 5.8. Because the controller is designed based on a reduced order model for a frequency band between 150-300 Hz the beneficial effect of the  $H_2$  feedback controller is most

clearly observed with a 5 dB reduction at the acoustic resonance at 185 Hz. Furthermore the  $H_2$  controller enhances the resonant frequency at 115 Hz.

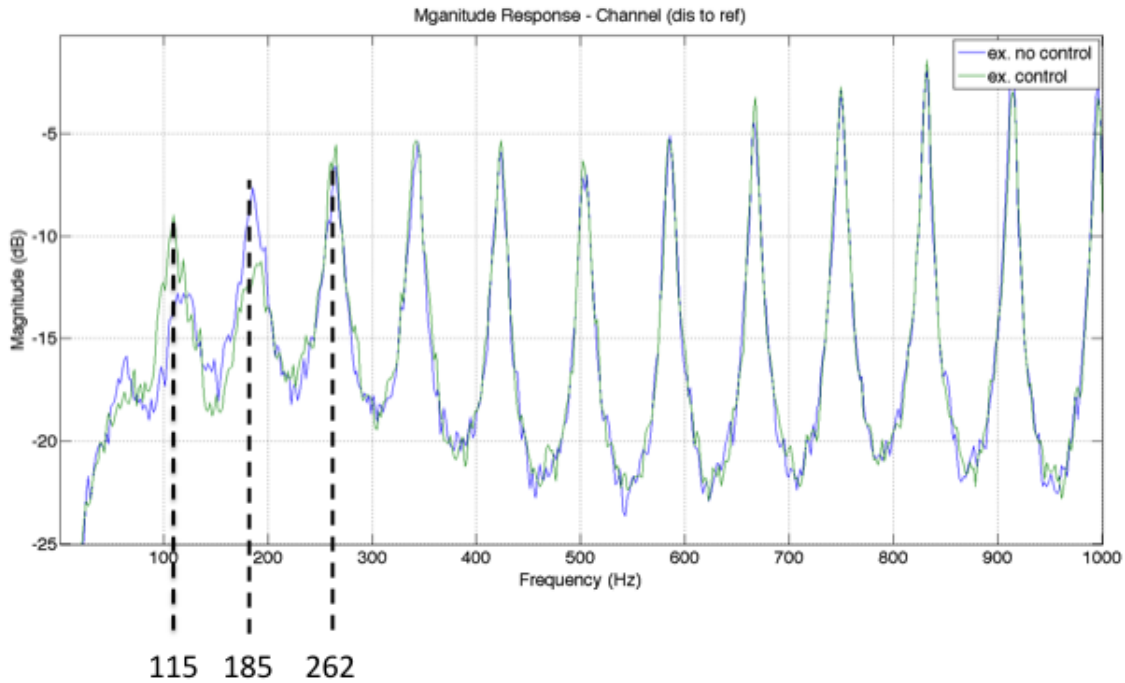


Figure 5.8: Magnitude of the power spectral density of the reflecting sound wave without and with  $H_2$  output feedback control for experimental data (blue, green).

### 5.3.2 Experimental Implementation of Geometric Design

The stability of the design is verified by plotting the Nyquist diagram of the open loop system with the use of experimental data, figure 5.9. It is clearly viewed from the Nyquist plot that the controller is stable (no encirclement of the critical point  $(-1, 0j)$  occurs for the open loop system).

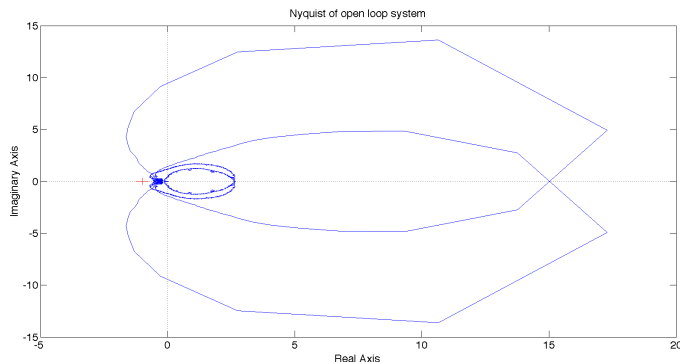


Figure 5.9: Nyquist plot of open loop system with remote geometric feedback control for experimental response

The performance of the remote geometric control design is demonstrated with the experimental response of the plant (figure 5.10). The controller is designed for a frequency band between 150-300 Hz the beneficial effect of the remote geometric feedback controller is most clearly observed with a 7 dB reduction at the acoustic resonances at 185 Hz and at 262 Hz.

The acoustic resonance at 115 Hz is magnified just as the  $H_2$  controller does. Additionally, the Geometric approach increases the acoustic resonances at the frequency band 300 - 600 Hz by 1-3dB. An explanation to this can be given if we recall that the Remote Geometric design requires the formulation of a bandpass filter. When forming the filter it was realised that there is a trade-off between the roll-off (which reduces enhancement of uncontrolled frequencies) and the stability margins of the design. Hence, by increasing the bandpass filter's roll-off, it is possible to eliminate the acoustic resonance excitations but this will increase the risk of the system going unstable.

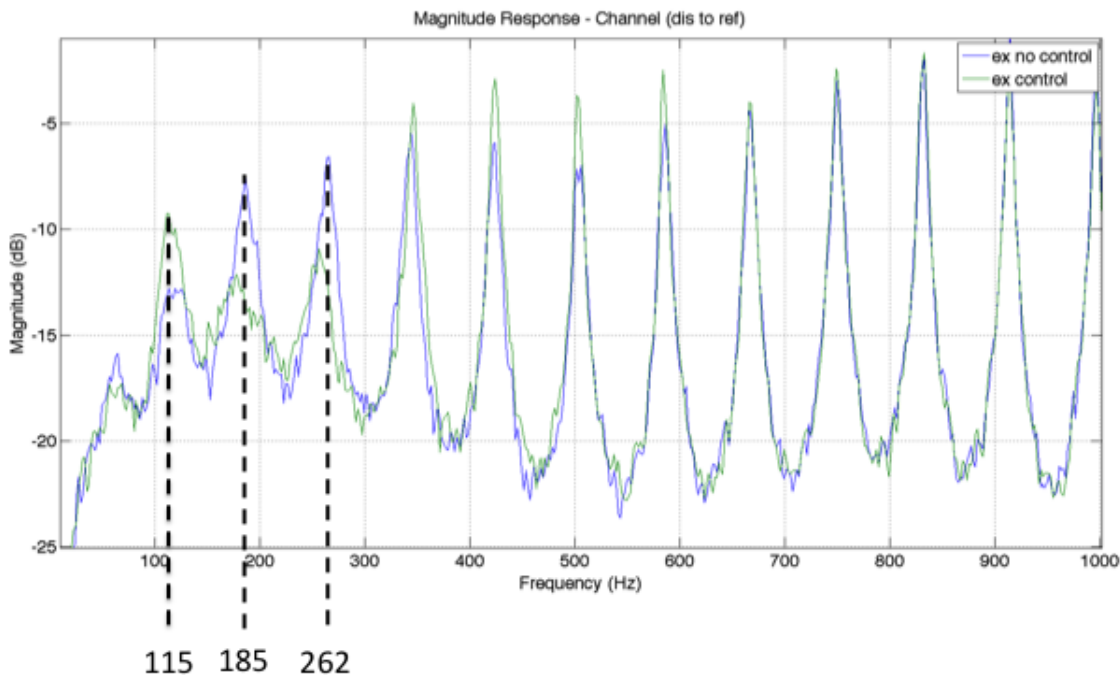


Figure 5.10: Magnitude of the power spectral density of the reflecting sound wave without and with remote geometric feedback control for experimental data (blue green).

### 5.3.3 Comparison

Now that the two feedback controllers have successfully been implemented on the apparatus the final step is to compare the two designs. In order to compare the performance of the two designs, the magnitude of the experimental responses are plotted on the same figure, figure 5.11. From the magnitude plot it is clear that the the performance of the designs are comparable up to 200 Hz, beyond that frequency the remote geometric control is able to achieve reduction of the next acoustic resonance (at 262 Hz). In terms of achieved performance at the controlled bandwidth (150 - 300 Hz) the geometric controller delivers better results than  $H_2$  approach.

On the other hand, the Remote Geometric controller excites acoustic resonances beyond the control bandwidth [figure 5.11]. This negative result is due to the bandpass filter required for the formulation of the Remote Geometric feedback controller.

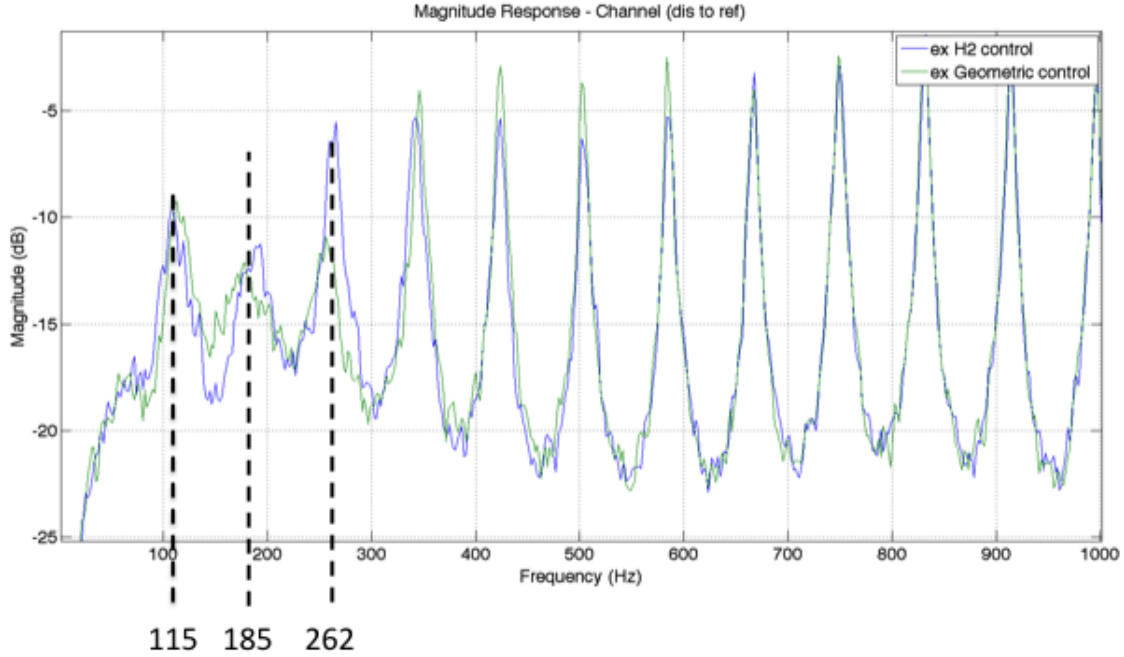


Figure 5.11: Magnitude of the power spectral density of the reflecting sound wave with remote geometric feedback control and with  $H_2$  output feedback control for experimental data (green, blue).

With regards to design complexity, the geometric design in comparison with the  $H_2$  design requires additional manual fine tuning of the  $M$  and  $\sigma$  values in order to achieve good stability and robust performance. The additional complexity is regarded as a minor burden when the overall results are considered.

Probably the most important benefit when considering the geometric design is the design freedom of choosing which output(s) are to be reduced. Because the main objective of this thesis is to reduce the reflecting noise, priority is given to selecting  $\gamma$  – *points* inside the loci intended for remote reduction (5.8). In contrast to the  $H_2$  design the geometric design is free to focus all control effort solely in reducing the reflecting sound. For us to visualise the previous statement, if equation (5.16) is rearranged the following function of the  $\gamma_k(j\omega)$  is given:

$$\gamma_k(j\omega) = -\frac{g_{MP}(j\omega)C(j\omega)}{1 + g_{MP}(j\omega)C(j\omega)} \frac{1}{g_{AP}(j\omega)f_{LP}(j\omega)} \quad (5.28)$$

Equation 5.28 is a function that generates  $\gamma$  – *values* regardless of the method used to design

the controller. Hence, it is possible to compare the two controllers (geometric and  $H_2$ ) in terms of the  $\gamma$ . In order to visualise how critical this is with regards to the performance of the design, in the following figure the  $\gamma$ -values of the two controllers (5.28) are plotted with the addition of the local and remote loci, figure 5.12. The red crosses are the geometric controller's points and the red squares the  $H_2$ . The blue circles are the local locus (equation (5.7)) and the green the remote locus (equation (5.8)). From the illustration it can be viewed, as expected, the remote controller's  $\gamma$ -values lie inside near the centre of the remote circles. For the  $H_2$  controller a more conservative approach of  $\gamma$ -values is formed, specifically the points lie in the intersection of the two remote and local loci, hence the performance (reduction of remote output) of this design is restricted. The reason the  $H_2$  controller delivers points at the intersection and not closer to the centres of the remote reduction locus is because of one additional requirement which this design satisfies to increase stability and robustness, which is minimal control effort. Specifically, the minimisation rule used to derive the  $H_2$  controller includes also the control path in order to final controller [Doyle et al., 1989].

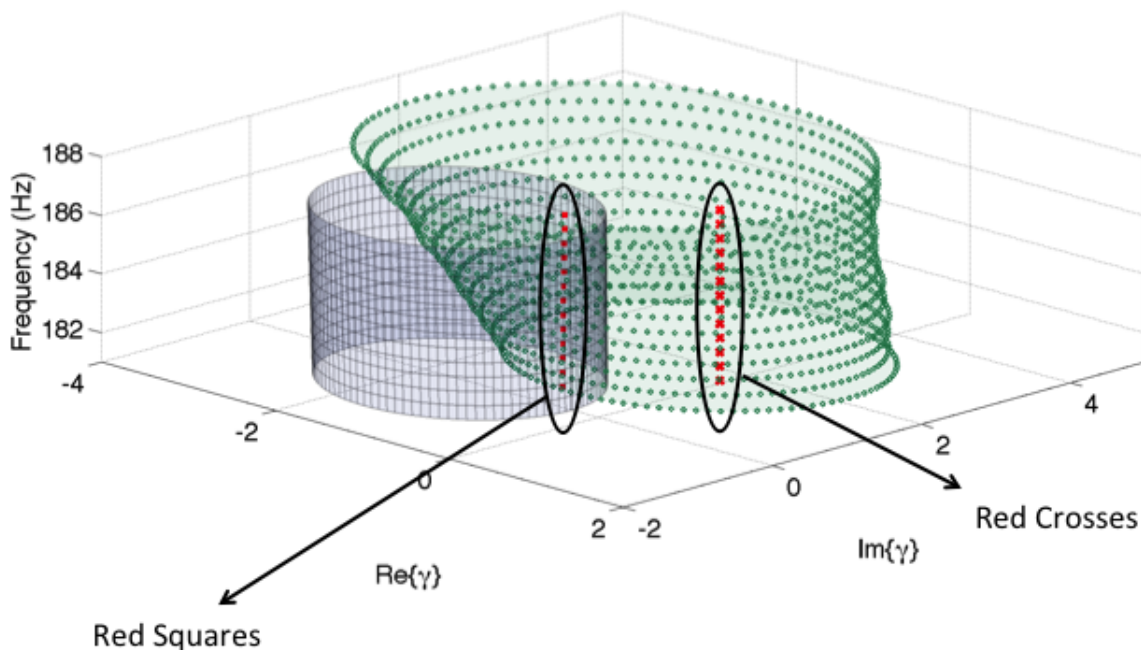


Figure 5.12: Remote measurement reduction loci (green circles). Local measurement reduction loci (blue circles).  $\gamma$ -values for  $H_2$  controller (red squares).  $\gamma$ -values for Remote geometric controller (red crosses).

A more clear appreciation of the previous finding can be given if the local loci is omitted from the plot and the centres of each circle is included in the plot. From figure 5.13 it can be observed that the Geometric controller's  $\gamma$  - values are significantly closer to the optimal remote reduction points (blue squares) than the  $H_2$  controller's  $\gamma$  - values. Additionally, in order to quantify the findings illustrated in figure 5.13 the distance (Euclidian norm) of each  $\gamma$  - value (red squares and red crosses) and the corresponding optimal reduction point (blue squares) have been calculated and presented in figure 5.14. From the measured distances it is obvious that Geometric controller's  $\gamma$  - values lies closer to the optimal remote reduction points.

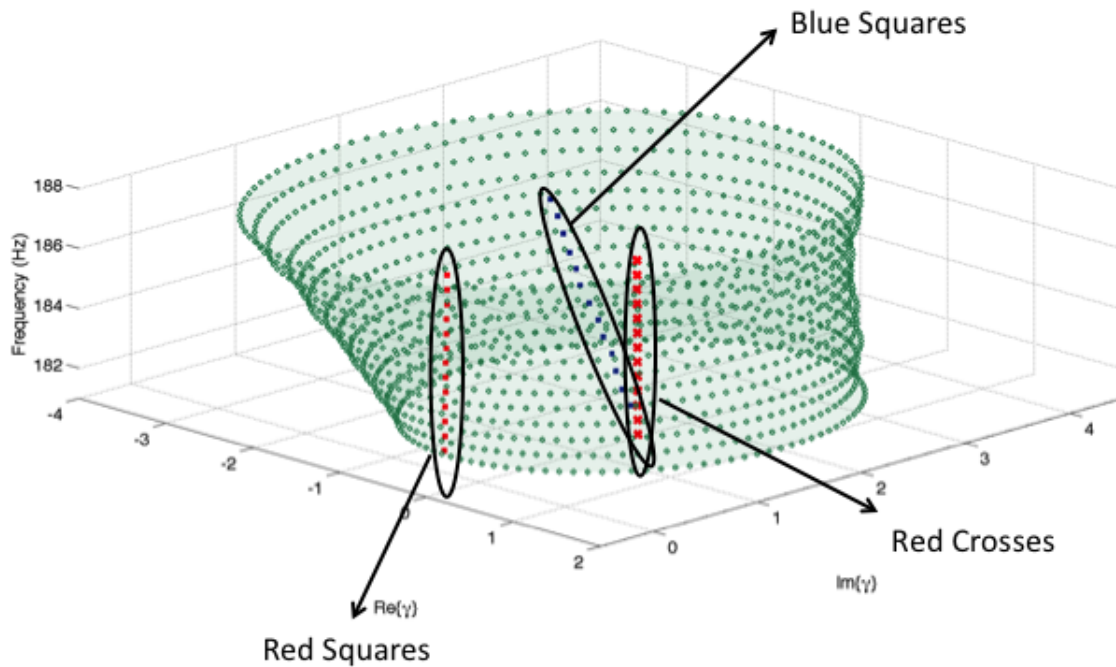


Figure 5.13: Remote measurement reduction loci (green circles).  $\gamma$  - points for optimal remote reductio (blue squares).  $\gamma$  - values for  $H_2$  controller (red squares).  $\gamma$  - values for Remote geometric controller (red crosses).

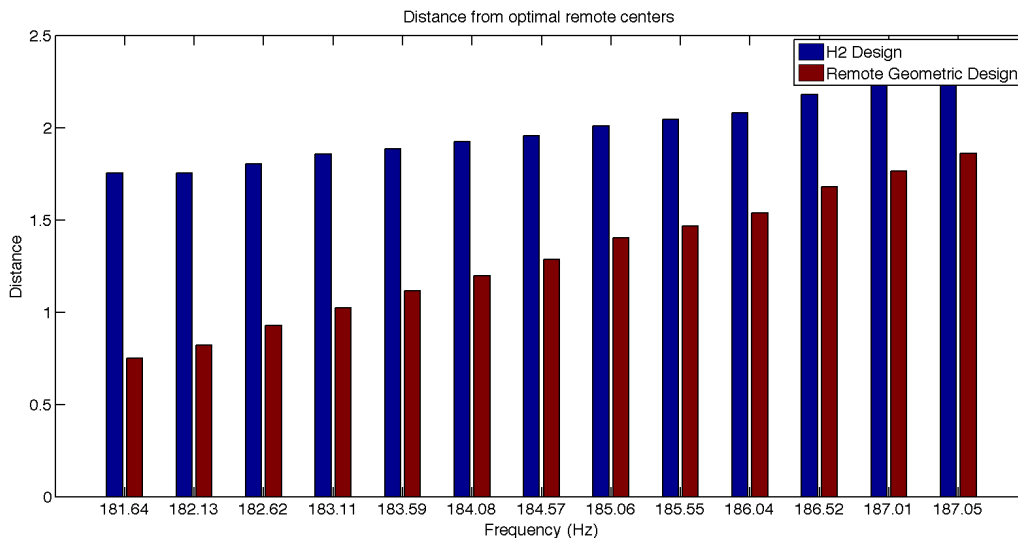


Figure 5.14: Distance (Euclidian norm) of the optimal remote reduction points and the  $\gamma$  - values for the  $H_2$  and Geometric designs

## 5.4 Conclusions

In this chapter a remote geometric feedback control design that was originally developed for AVC problems is introduced and applied in a novel manner for the one-dimensional acoustic duct problem. The method makes use of a design freedom parameter  $\gamma$  (equation (5.4)). In order to generate the geometric controller (equation (5.9)) an interpolation technique is also introduced (Nevanlinna - Pick).

Because the remote geometric method is a feedback design, it retains the same advantages of the  $H_2$  design when compared to the adaptive feedforward FxLMS algorithm. Specifically, the geometric control procedure is a locally based collocated design and therefore as theory suggests is guaranteed to be stable [Ubaid et al., 2011; Ubaid et al., 2012]. As the approach utilises only a local measurement (acceleration) in order to produce the control signal it does not during implementation require any remote measurements (microphones) other than during identification of the control path for controller design. Hence, the implementation complexity and cost are significantly reduced.

The most important benefit when considering the geometric design, in contrast to the  $H_2$  feedback design, is the design freedom of choosing which output(s) are to be reduced (remote

or local). This design freedom allows control to be focused to the primary problem, reduction of reflecting sound (remote output). Therefore, with regards to performance (i.e. reduction of reflecting sound wave) the geometric design provides better results compared to the  $H_2$  design (figure 5.11). This result is not a surprise when the  $\gamma$  – values for the two controllers (geometric and  $H_2$ ) are plotted and compared to the the optimal values (figure 5.13 and figure 5.14).

In the next chapter an investigating of an altered version of the Geometric design will be presented. Specifically, this novel design will make use of a parallel feedback controller architecture in order to independently control selected acoustic resonance peaks.

# Chapter 6

## Selective Resonance Geometric Control Design for Suppression of Reflected Noise

### 6.1 Introduction

Up to now, the reduction of the undesired reflecting sound wave was focused on a single narrow frequency band located at the lower frequencies (Remote Geometric Control,  $H_2$  Control). By doing so it was shown with numerical and experimental validation that a pair of resonant peaks could be compensated (Remote Geometric Control). When attempting to control additional peaks (three or more) by widening the bandwidth the resulting controller either fails to reduce them or even worse, leads to an unstable open loop system. A question that arises now is if it is possible to select which two resonant peaks are reduced?

If we consider the Geometric approach, the natural intuitive way is to expand the frequency band intended to apply control sufficiently enough to include the intended resonant peaks to be reduced and select  $\gamma$  - *points* near the two resonances intended for reduction. The issue that arises when increasing the frequency band of the design, is that the locus for remote reduction formed by the design freedom parameter  $\gamma$  might form a complicated spiral shape (figure 6.10). This issue, in combination with the number of optimal reduction points (centres of the  $\gamma$  - *circles*) which require interpolating, leads to an ill posed problem which the Nevanlinna - Pick method can not solve adequately in order to design a stable transfer function  $\gamma_k(j\omega)$  required to form the feedback controller.

Hence, instead of increasing the frequency bandwidth in order to include multiple resonant peaks and risk ending up with a difficult interpolating problem, an alternative approach is to design independently two controllers that will reduce the desired resonant peaks. This approach provides the designer the benefit in selecting which resonant peaks will be controlled. The only issue that arises with regards to the independent controllers is the stability analysis of the design. Because the controllers are designed without knowledge of the presence of the additional dynamics, the overall closed loop system is in risk of becoming unstable. In order to mitigate this problem, the designer is required to apply a combination of low and high pass filters with high roll-off that will isolate the control signal of each compensator to the desired frequency regions.

This chapter is organised as follows: In section §6.2 the selective remote geometric control design approach that is selected to cancel multiple resonant acoustic peaks is presented. In section §6.3 the results of applying the proposed design is illustrated and the design's performance is compared with the standard remote geometric design. Finally, section §6.4 provides some concluding remarks.

## 6.2 Control Design

The control design investigated in this chapter (Selective Resonance Geometric Control) intends to formulate independently two feedback controllers that will reduce targeted acoustic peaks. In order to formulate the two controllers the suggested design procedure makes use of the remote geometric control design that was extensively investigated in the previous chapter.

Specially, once the two controllers are designed with use of the remote geometric algorithm, the next step is to formulate the overall feedback controller that will be used to generate the feedback control signal. In order to do so, the original feedback block diagram is altered by adding a parallel feedback path used for the second control design (section 6.2.1).

It must be noted that during the control design procedure the two controllers neglect the presence of one another and as a result, the stability of the closed loop system can be at risk. Therefore, in order to guarantee stability of the design, two band-pass filters that will isolate each controller's effect to the frequency range initially intended for compensation are

included with the feedback controllers (section 6.2.2).

### 6.2.1 Parallel Feedback Control Arrangement

As mentioned earlier the control design requires an alteration of the original feedback arrangement. The new architecture utilised by the selective resonance geometric design is a generalised feedback block diagram with two controllers situated in parallel, figure 6.1. The plant is again represented as a two-input and two-output system that is labelled as  $P$  but now has a feedback controller  $K = K_1 + K_2$  that maps the measurable signal  $w_{loud}$  to the manipulated variable  $E_{con}$ . Specifically, the two inputs are the voltage of the disturbance loudspeaker  $E_{dis}$  and the voltage of the control loudspeaker  $E_{con}$ . Furthermore, the two outputs are the total reflecting sound wave  $P_{ref}$  (remote measurement) which is to be minimised and  $w_{loud}$  (local measurement) the acceleration of the control loudspeaker's cone. The matrix representation of the open loop system is therefore:

$$\begin{bmatrix} P_{ref} \\ w_{loud} \end{bmatrix} = \begin{bmatrix} P_{11} & P_{12} \\ P_{21} & P_{22} \end{bmatrix} \begin{bmatrix} E_{dis} \\ E_{con} \end{bmatrix} \quad (6.1)$$

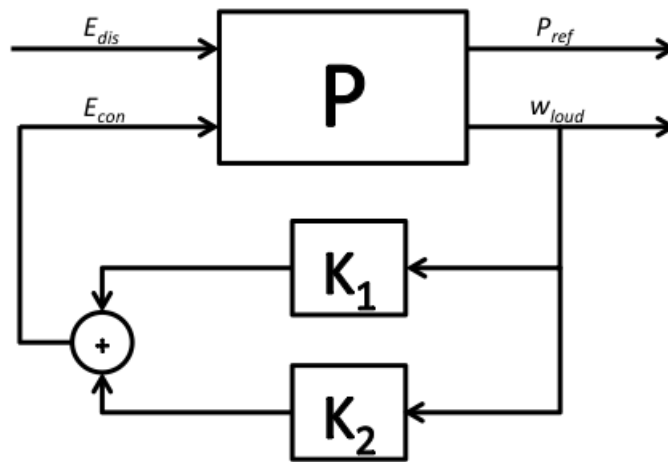


Figure 6.1: LFT control architecture described by a MIMO generalised process ( $P$ ) and two output feedback controller ( $K_1$  and  $K_2$ ) connected in parallel. Inputs of the generalised process are the voltage of the disturbance loudspeaker ( $E_{dis}$ ) and the voltage of the control loudspeaker ( $E_{con}$ ), furthermore the outputs are the undesired reflecting sound wave ( $P_{ref}$ ) to be minimised and the velocity of the control loudspeaker's baffle ( $w_{loud}$ ).

## 6.2.2 Stability Assurance

As mentioned earlier in this chapter a filtering procedure is required in order to assure stability of the closed loop. Specifically, two bandpass filters are designed and applied. Additionally from trial simulations, it was discovered that a stable loop was achieved only when the resonant peaks that were selected to be reduced were not consecutive, this is primarily due to the two filters overlapping and not having enough roll-off to isolate the control effort from each controller at the predetermined frequencies intended for control.

## 6.2.3 Implementation of Selective Resonance Geometric Design

Just as in the original remote geometric design investigated in the previous chapter, modelling of the control path ( $P_{22}$ ) is required. Hence, a 7 – *th* order transfer function is fitted to the experimental data (figure 6.2). Additionally, due to RHP zeros the minimum phase transfer function is designed,  $g_{MP}$ , in order to guarantee stability of the controllers.

For the selective resonance geometric controller to be compared with the original geometric design, the  $\gamma$  – *points* points selected must be at frequencies near the acoustic resonances intended to be reduced of the reflecting sound wave (figure 6.3). For the purpose of this chapter, the acoustic resonances selected for control are at 185 and 350 Hz. The values of  $M$  and  $\sigma$  are again found based on fine tuning. Finally, because the controller is intended to focus its action at the two resonances located at 185 and 350 Hz, two second order band pass filters around these resonant frequencies are designed and utilised for the final form of the two controllers. Again, as the design procedure takes place in the continuous domain, a discretisation of the controller ( $f_s = 8 \text{ kHz}$ ) is required for application on the experimental rig.

The steps required to construct the final controller for implementation on the acoustic pulse tube are grouped and presented in figure 6.4.

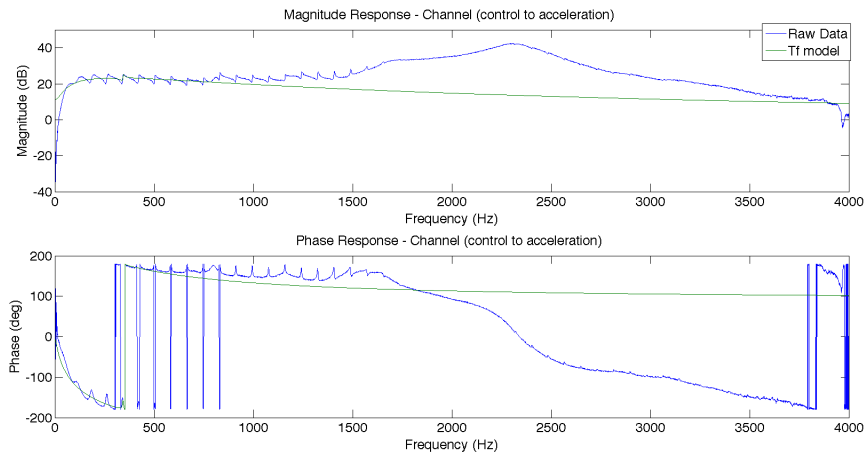


Figure 6.2: Bode plot of the raw experimental data for the control paths (blue) and bode plot of the high order FIR filter fitted to the experimental data (green).

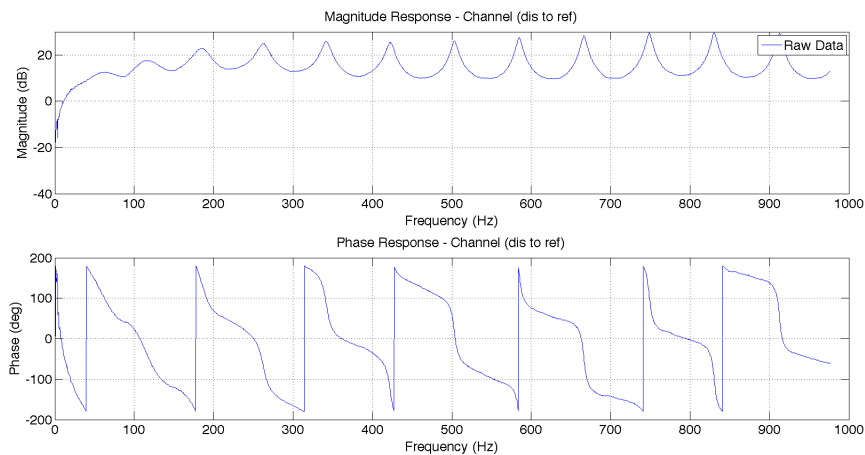


Figure 6.3: Magnitude response of the raw experimental data for the disturbance path (disturbance voltage to reflecting sound wave).

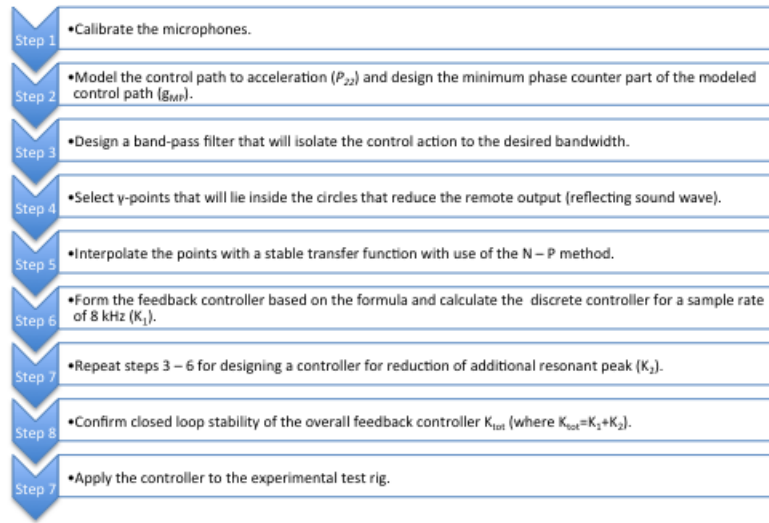


Figure 6.4: Selective resonance geometric feedback control design procedure.

## 6.3 Results and Analysis

In this section the results of the experimental implementation for the conventional remote geometric design and the selective resonance geometric design are presented.

Although the block diagram for the selective resonance geometric design, figure 6.1, differs from the original block layout initially considered for the remote geometric feedback design, the evaluation of the stability and the performance of these designs is carried out in a nearly identical manner. Specifically, due to the parallel connection of the feedback controllers, the open loop transfer function for the selective resonance design is:

$$G_{open}(s) = -P_{22}(K_1(s) + K_2(s)) \quad (6.2)$$

where  $P_{22}$  is the control path between the control signal  $E_{con}$  and the acceleration of control the loudspeaker's cone  $w_{loud}$  and  $K_1(s)$  and  $K_2(s)$  are the independently designed geometric feedback controllers. It should be noted that for all the simulations considered in this chapter a positive feedback control loop is considered. Just as in the previous chapters, the closed loop system's stability can be confirmed by the Nyquist criterion [Ogata and Yang, 1970].

The open loop transfer function for the standard geometric design is:

$$G_{open}(s) = -P_{22}K(s) \quad (6.3)$$

Where  $K(s)$  is the geometric controller designed to compensate for both selected resonances. In conclusion, the difference between the stability criterion of the two designs is found in the choice of controller. For the selective case the controller considered is the addition of the two parallel controllers ( $K_1$  and  $K_2$ ), whereas for the standard case the single feedback controller ( $K$ ).

### 6.3.1 Experimental Implementation of Remote Geometric Control

The stability of the design is verified by plotting the Nyquist diagram of the open loop system with the use of experimental data, figure 6.5. Based on the Nyquist stability criterion for a SISO system, it is clearly observed in the Nyquist diagram that no encirclement of the critical point  $(-1, 0j)$  occurs for the open loop system. Therefore closed loop stability is guaranteed for the  $H_2$  local feedback design.

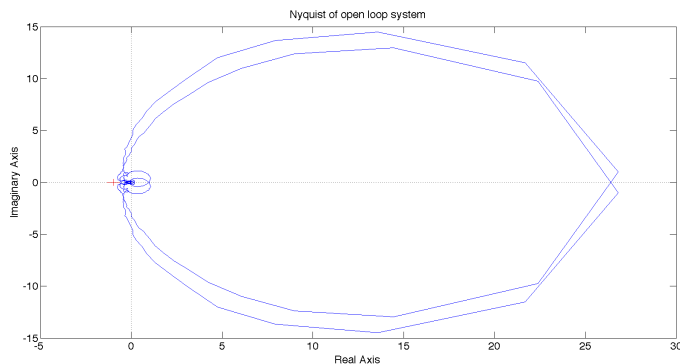


Figure 6.5: Nyquist plot of open loop system with  $H_2$  output feedback control for experimental response.

The performance of the standard remote geometric control design is demonstrated with the experimental response of the plant in figure 6.6. As expected the second (185 Hz) and fourth (350 Hz) resonant peaks are reduced when applying the remote geometric feedback controller. Specifically for the peak at 185 Hz a 5 dB reduction is achieved and for the peak at 350 Hz a 6 dB reduction is achieved. A negative result of the application of the feedback controller is the significant increase (8 dB) of the third acoustic resonance (262

Hz). Furthermore, a small enhancement of the magnitude at the lower frequencies evident especially at the first acoustic resonance at 115 Hz.

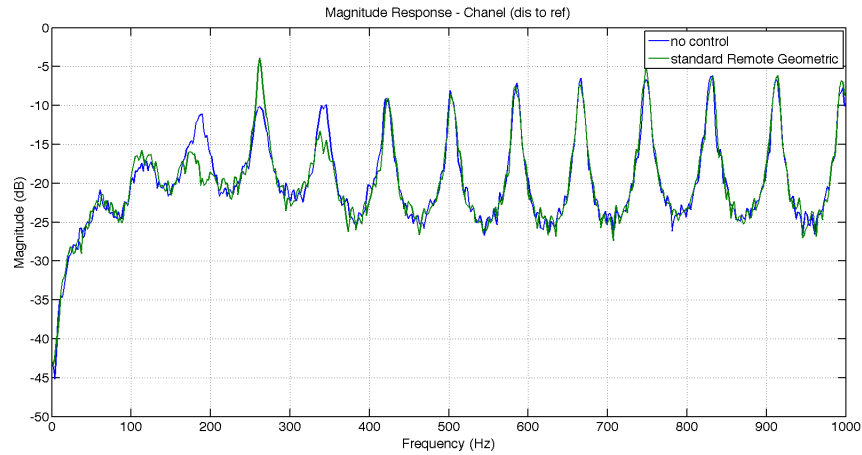


Figure 6.6: Magnitude of the power spectral density of the reflecting sound wave without and with standard remote Geometric output feedback control for experimental data (blue,green).

### 6.3.2 Experimental Implementation of Selective Resonance Control

The stability of the design is verified by plotting the Nyquist diagram of the open loop system with the use of experimental data, figure 6.7. It is clearly observed from the Nyquist plot that the controller is stable.

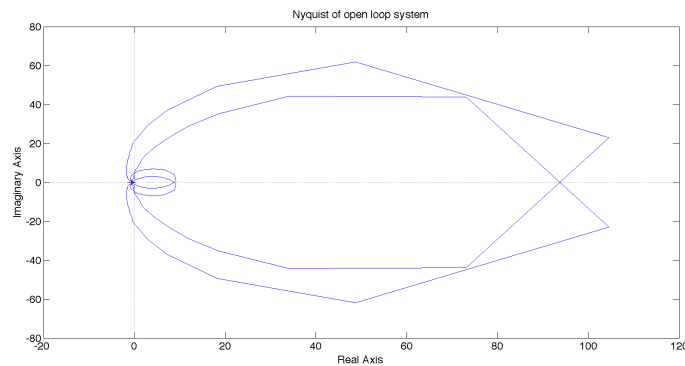


Figure 6.7: Nyquist plot of open loop system with remote geometric feedback control for experimental response.

The performance of the selective resonance geometric control design is demonstrated with the experimental response of the plant figure 6.8. Just as in the standard geometric design

the second (185 Hz) and forth (350 Hz) resonant peak are reduced when applying the selective resonance geometric feedback controller. Specifically for the peak at 185 Hz a 5 dB reduction is achieved and for the peak at 350 Hz a 6 dB reduction is achieved. Additionally, a small enhancement in the magnitude at the lower frequencies is evident. However, in contrast to the standard Geometric design the acoustic resonant peak at 262 Hz is not increased.

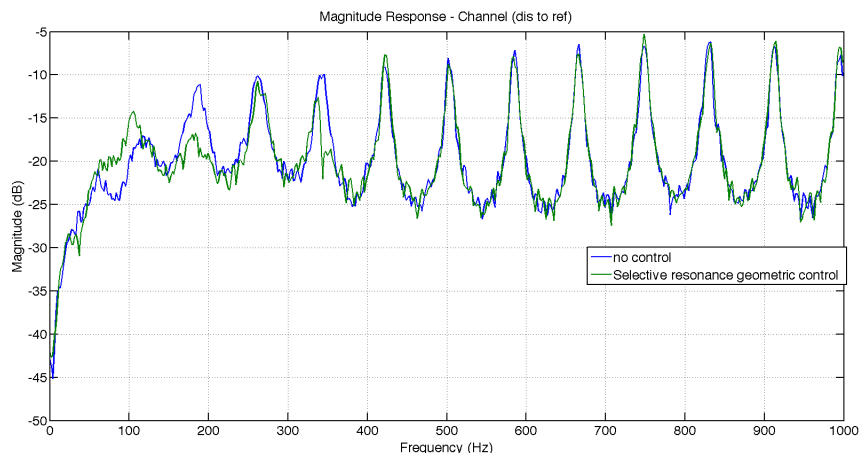


Figure 6.8: Magnitude of the power spectral density of the reflecting sound wave without and with selective resonance geometric feedback control for experimental data (blue,green).

### 6.3.3 Comparison

In order to compare the performance of the two designs the magnitude of the experimental responses are plotted on the same diagram (figure 6.9). From figure 6.9 it is clear that the the performance of the designs are almost identical at the resonant peaks intended for reduction. The significant difference that can be observed in the magnitude plot is that the standard remote geometric design is exciting the resonant peak at 262 Hz (8 dB increase) whereas the selective resonance approach does not enhance this resonance frequency.

For us to visualise the previous statement, we make use of equation (5.28), which is a function that generates the  $\gamma$  – values regardless of the method used to design the controller. Hence, its possible to compare the two controllers (remote geometric and selective resonance geometric) in terms of the  $\gamma$  – values. From figure 6.10 it can be observed that the  $\gamma$  – values resulting for the two designs show the same arrangement near 185 and 342 Hz (therefore nearly identical performance), but at 262 Hz the standard geometric implementation the

$\gamma$  – values are not inside the remote reduction locus (green circles figure 6.10). In order to quantify the previous statement the distance of the  $\gamma$  – values from the optimal remote reduction points in terms of the Euclidian norm for each controller is illustrated in figure 6.11. The increase of the distance at frequencies around 262 Hz, for the standard Geometric design, explains why there is an excitation of the reflecting sound wave at this acoustic resonance. The selective resonance approach is able to 'keep' the  $\gamma$  – values inside or near the remote reduction locus. The reason the standard geometric implementation does not keep the  $\gamma$  – values inside the remote locus is because of the 'wavy' nature of the optimal remote points, leading to an interpolation problem that is difficult to realise a stable transfer function. In order to avoid this problem the interpolation problem is segmented into individual tasks for which the fitting procedure is much simpler to deal with and a better controller (performance-wise) is designed.

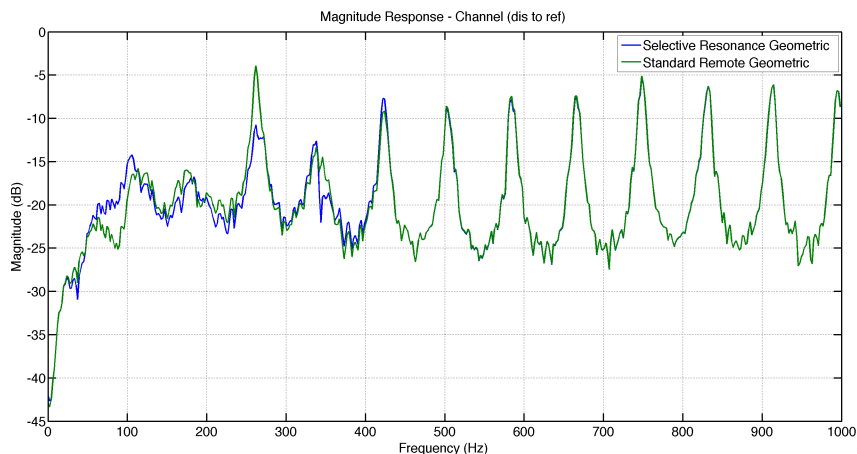


Figure 6.9: Magnitude of the power spectral density of the reflecting sound wave with standard geometric feedback control and with selective geometric control for experimental data (green, blue).

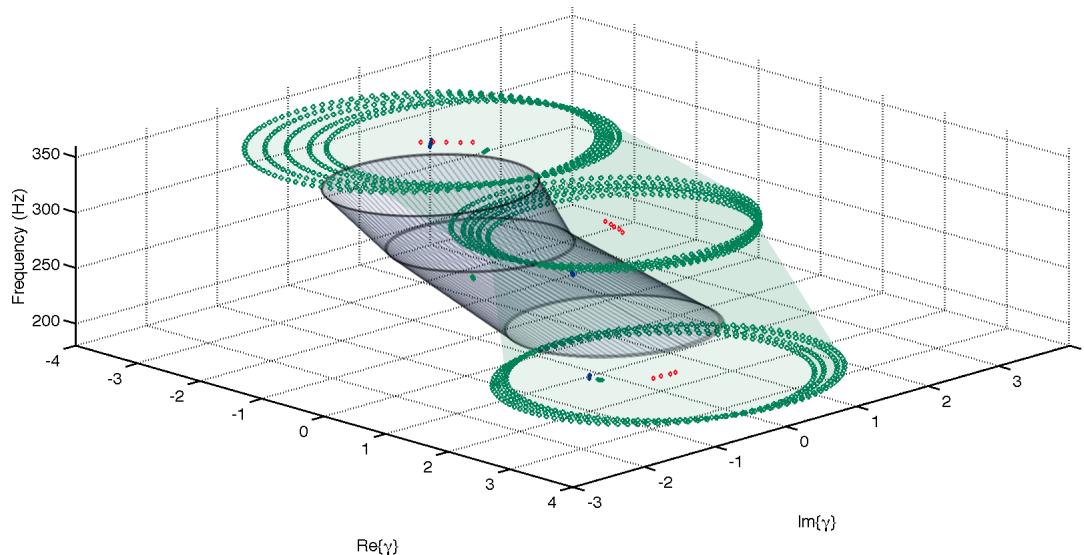


Figure 6.10: Remote measurement reduction loci (green circles). Local measurement reduction loci (blue circles).  $\gamma$ -values for selective Geometric controller (blue squares).  $\gamma$ -values for Remote geometric controller (green squares). Optimal reduction points (red crosses).

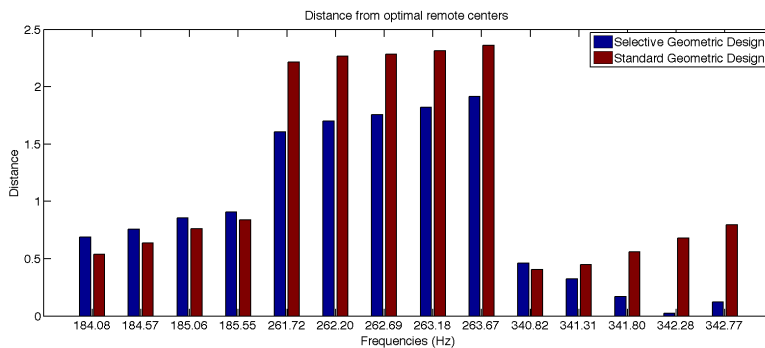


Figure 6.11: Distance (Euclidian norm) of the optimal remote reduction points and the  $\gamma$ -values for the Selective Geometric and Standard Geometric designs.

## 6.4 Conclusions

In this chapter the remote geometric feedback control design is compared with a new version named selective resonance geometric feedback control design. The newly introduced method constructs two remote geometric controllers to deal with two resonant acoustic peaks. The controllers are then connected in parallel and feed the control signal to the plant.

Although this alteration is minor it provides better performance than the standard remote

geometric approach (figure 6.9). It is argued that the main reason the selective approach can deliver a better response than the standard geometric design is that the interpolation problem is over demanding for the Nevanlinna - Pick method to deal with when intending to compensate multiple resonant peaks. By segmenting the problem the interpolation required to construct the controller is much simpler and therefore the final controller performs better. It must be noted that the newly develop approach requires some fine tuning with regards to the stability of the closed loop system as the parallel controllers neglect each others presence.

The next chapter investigates an alternative means of delivering the control signal. Instead of considering a loudspeaker as a boundary element a thin panel with a collocated sensor actuator position on it (Smart panel) is used. The reason for considering an alternative controlled boundary is primarily due to the practical difficulties of installing control loudspeakers to real life environment problems. The smart panels setup has an inherent installation simplicity that could be ideal for real life problems beyond the experimental rig. It must be noted that all of the results are conducted in a simulated environment, due to limited time and resources.

# Chapter 7

## Reflecting panel work

### 7.1 Introduction

Up to now all the control designs, whether it is a feedback controller or a feedforward controller, share one common characteristic, they all make use of a loudspeaker to deliver the control signal. Recent work in the field of ANC has been focused on designing actuator setups that will enable ASAC of low frequency noise radiated by vibrating plates, [Lee et al., 2002]. Specifically, this research investigates the application of a low frequency volume velocity vibration control procedure for a smart panel in order to reduce sound transmission. The control algorithm makes use of a simple velocity feedback controller in order to add damping to the resonant frequencies of the controlled panel. The addition of damping will reduce the vibration that occurs when an incident acoustic wave impacts the panel and will thereby reduce the acoustic radiation efficiency. Such an electroacoustic device is ideal for real life problems. In contrast to a loudspeaker, a plate's dimensions can easily be adjusted to satisfy the needs of a reflecting noise reduction problem (i.e. covering large surfaces with an actively controlled plate).

In this chapter, the aim is to develop a local SISO feedback controller for an acoustic duct system as illustrated in figure 7.1. The control scheme will make use solely of local measurements (velocity of terminating surface) of the reflecting boundary surface in order to suppress the undesired reflecting sound waves that occur in the presence of an incident disturbance sound wave. Specifically, two local broadband feedback controllers are developed

and compared in simulations. For the first compensator an  $H_2$  optimisation approach is used whereas for the second compensator a Remote Geometric Design is considered.

This chapter is organised as follows: In section §7.2 a model that has been developed to take into account the fully coupled response between the disturbance source, the control unit, the reflecting panel and the acoustic duct. The dynamic effects of the principal components of the proof-mass actuator, i.e. base mass, suspension spring and proof-mass, have been taken into account. In section §7.3 the  $H_2$  output feedback control design approach that is selected to cancel the undesired reflecting sound wave is presented and also the Remote Geometric design is reintroduced as an additional candidate control design. In section §7.4 the results of applying the  $H_2$  and Remote Geometric controller are illustrated and the design performances are compared. Finally, section §7.5 presents a summary of concluding remarks; which highlights the principal advantages of the developed feedback control laws on a flat panel.

## 7.2 Development of a System Model

In this section a detail mathematical model of a semi-infinite duct is derived with reference to the fundamental equations of physics that describe such problems.

### 7.2.1 Model Assumptions

As mentioned in the introduction, the system plant that is investigated is a result of coupling a semi-infinite acoustic duct, a reflecting boundary panel and the sensor and actuator dynamics (figure 7.1). The model developed to calculate the acoustic pressure inside a rectangular duct requires some key assumptions that will ease the mathematical formula. The assumptions are summed in the following list:

- The acoustic duct considered is of constant rectangular cross section with dimensions  $L_x$  and  $L_y$ .
- The walls are considered perfectly rigid.
- Only waves propagating in the  $z$ -direction will be investigated (one-dimensional model).

- The acoustic waves considered are plane waves and harmonic.

Furthermore, the boundary conditions assumed for the mathematical model are:

- The open end is sealed with a smart panel structure that can be modelled as a thin plate simply supported to the edges of the rectangular duct.
- The control force is generated by an inertial actuator placed in the centre of the panel. The position to place the controller in the centre is done because the first mode shape of the panel [figure 7.3] will contribute the most to the resulting sound wave from the panel. Hence, the selection of the centre of the panel is the ideal point of sensing and control.
- The velocity measurement is assumed to be acquired by an ideal sensor (perfect sensing).
- A loudspeaker as a source is considered at point  $z = 0$ .

In the following paragraphs, the fundamental equations that describe each element of the coupled plant are mentioned and the final model is derived.

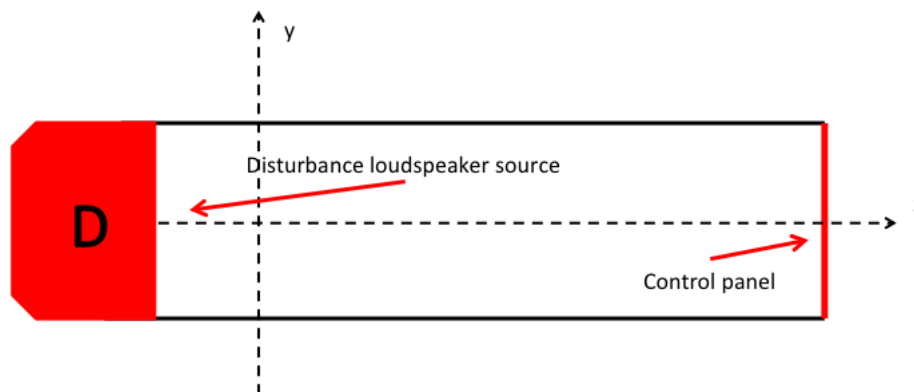


Figure 7.1: Rectangular acoustic duct with a disturbance loudspeaker source at position  $z = 0$  (red) and a simply supported boundary reflecting panel at position  $z = L$  (red). Two ideal microphones are positioned at point  $z_1 = L - 0.1$  and  $z_2 = L - 0.1 - \Delta z$ .

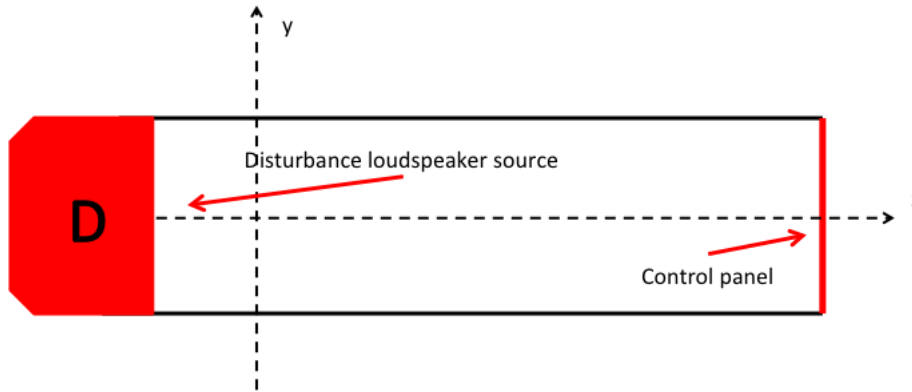


Figure 7.2: Primary mode shape of thin acoustic panel

### 7.2.2 Duct Model

As mentioned in the assumptions for the duct, only plane wave propagation in the  $z$  direction will be considered. Furthermore, a one dimensional model is valid below the first cut-off frequency:  $2\alpha < \lambda$  (where  $\lambda$  is the wave length and  $\alpha$  is  $\min\{L_x, L_y\}$ ). Hence, just as in Chapter 3, the fundamental one-dimensional Helmholtz equation describes the problem [Kinsler et al., 1999]:

$$\frac{\partial^2 p(z, t)}{\partial z^2} - \left(\frac{1}{c_0}\right)^2 \frac{\partial^2 p(z, t)}{\partial t^2} = -\frac{1}{A^2 \rho_0} \frac{\partial V(z, t)}{\partial t} \quad (7.1)$$

where  $c_0$  is the velocity of sound in air,  $\rho_0$  is the density of air and  $A$  is the cross sectional area of the rectangular acoustic duct. Equation 7.1 describes the time spatial dependency of the pressure plane wave and involves two waves (Incident and Reflecting) that travel in the positive and negative direction along the  $z$  - axis.

It is also necessary to define the linear Euler equation which is valid for acoustic processes of small amplitude as the one dealt within this work. This equation will enable coupling of the boundary conditions to the one dimensional equation and ultimately solve the overall problem [Kinsler et al., 1999]:

$$\rho_0 \frac{\partial u(z, j\omega)}{\partial t} = -\frac{\partial P(z, j\omega)}{\partial z} \quad (7.2)$$

The transfer function that describes the disturbance path between the disturbance voltage and the total acoustic pressure is given by [Zimmer et al., 2003]:

$$G_{dist}(z, s) = e^{-zs/c_0} G_{d_0}(z, s) \quad (7.3)$$

$$G_{d_0}(z, s) = \frac{Bl\rho_0c_0(1 + \alpha_0(s))}{2R_{coil}Z_0(s)(1 - \alpha_0(s)\alpha_L(s)e^{-2Ls/c_0})(1 + \alpha_L(s)e^{2(z-L)s/c_0})} \quad (7.4)$$

The reflecting coefficients  $\alpha_0(s)$  and  $\alpha_L(s)$  of the disturbance loudspeaker and reflecting boundary surface are given in equations (7.5) and (7.6),  $Z_0(s)$  is the acoustic impedance of the disturbance loud speaker and  $Z_L(s)$  is the acoustic impedance of the reflecting boundary panel.

$$\alpha_0(s) = \frac{Z_0(s) - \rho_0c_0A_D}{Z_0(s) + \rho_0c_0A_D} \quad (7.5)$$

$$\alpha_L(s) = \frac{Z_L(s) - \rho_0c_0A}{Z_L(s) + \rho_0c_0A} \quad (7.6)$$

In similar manner, a transfer function can be developed for the control reflecting panel.

$$G_{con}(z, s) = e^{-z-L} G_{co}(z, s) \quad (7.7)$$

$$G_{co}(z, s) = \frac{F_{con}(s)\rho_0c_0(1 + a_L(s))(1 + a_0(s)e^{-2z(s/c)})}{Z_L(s)(1 - a_0(s)a_L(s)e^{-2L(s/c)})} \quad (7.8)$$

The frequency dependent transfer function  $F_{con}(s)$  describes the driving control force

applied to the panel due to the inertia actuator (Appendix A). The values of the coefficients used in equations (7.3) – (7.7) are fully described in table 7.1.

Table 7.1: Values of coefficients used for the simulated rectangular acoustic duct

Duct Length	$L = 3.54 \text{ (m)}$
Duct Cross-section	$L_y = 0.4 \text{ (m)} / L_x = 0.4 \text{ (m)}$
Density of air	$\rho_0 = 1.20 \text{ (kg/m}^3\text{)}$
Speed of sound (in air)	$c_0 = 341 \text{ (m/s)}$
Electrical resistance of voice coil disturbance	$R_{coil} = 6 \text{ (\Omega)}$
Magnetic voice coil motor disturbance	$Bl = 5.6 \text{ (N/A)}$
Effective cross section of disturbance speaker	$A_D = 0.024 \text{ (m}^2\text{)}$
Effective cross section of panel	$A = 0.16 \text{ (m}^2\text{)}$

### 7.2.3 Control Boundary Model

The thin panel considered as a boundary element couples its dynamics via the impedance function  $Z_L$ , which is an inverse relation to its mobility function. Specifically, the impedance function is given by the following relation:

$$Z_L(x, y, j\omega) = \frac{1}{w(x, y, j\omega)} \quad (7.9)$$

The next step is to evaluate the general mobility formula ( $w(x, y, j\omega)$ ). A vital aspect of the mathematical modelling is what type of boundary conditions can be applied to a rectangular thin plate, figure 7.3. For acoustic problems two types of support commonly found are:

- Simply supported edges.
- Clamped edges.

The difference between the two boundary conditions is that the simply supported case allows rotational motion in contrast to the clamped case. In practice it has been shown with experimental work that even a clamped panel will exhibit some rotational motion at the

boundaries [Wang et al., 1991] and therefore a simply supported panel will be assumed for the modelling. The transverse velocity of a simply supported thin rectangular panel is [Fuller et al., 1997]:

$$w(x, y, j\omega) = j\omega \sum_{m=1}^{\infty} \sum_{n=1}^{\infty} \frac{F_{mn}(j\omega)\psi_{mn}(x, y)}{\rho h_p L_x L_y (\omega_{mn}^2 - \omega^2 + 2\zeta_n j\omega\omega_{mn})} \quad (7.10)$$

The motion of a thin flat panel due to external excitation (in our case point force and incident acoustic wave) is superposition of a infinite number of patterns of motion named modes. That is why the resulting formula of the transverse velocity is a infinite sum equation (7.10). Each mode has a distinctive shape and natural frequency. The terms  $\psi_{mn}$  and  $\omega_{mn}$  are, respectively, the  $nm - th$  mode shape and natural frequency of the panel. Similarly, each individual external excitation (point force, incident acoustic wave) can be broken down to an infinite sum of forces, with each element of this sum relating to a single mode shape. The term  $F_{mn}$  found in equation (7.10) is the modal force associated with the type of vibration or acoustic excitation of the panel. A detail mathematical description of these quantities can be found in Appendix A. It can be assumed that the velocity of the panel will match the particle velocity of the fluid (in our case air) inside the duct and therefore a boundary value problem can be formulated.

Because the model used for the acoustic pressure inside the duct is one-dimensional, equation (7.9) is evaluated at the centre of the controlled panel. Hence, the function used to couple the controlled boundary dynamics to the overall model is  $Z_L \left( \frac{L_x}{2}, \frac{L_y}{2}, j\omega \right) = \frac{1}{w \left( \frac{L_x}{2}, \frac{L_y}{2}, j\omega \right)}$ . The specifications of the plate considered for simulation are grouped in table 7.2.

### Ideal Inertial Actuator / Ideal Velocity sensor

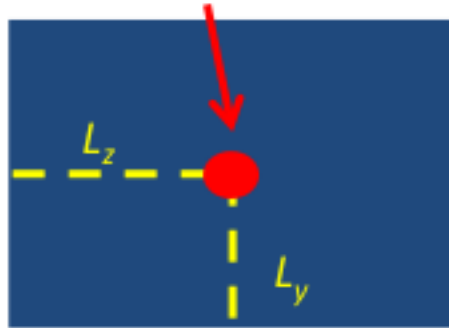


Figure 7.3: Simply supported thin rectangular panel with dimensions  $L_x$ ,  $L_y$ , thickness  $h_p$ . The excitation of the panel is due to the incident sound wave and the control force (inertia actuator illustrated with yellow) positioned in the centre of the panel.

Table 7.2: Reflecting panel specifications

Panel dimensions	$L_y = 0.4(m)/L_x = 0.4(m)$
Thickness of reflecting panel	$h_p = 0.001 (m)$
Density of panel	$\rho_p = 2700 (kg/m^3)$
Young's Modulus	$E_p = 7 * 10^{10} (N/m^2)$
Poisson's ratio	$\nu_p = 0.334$
Damping ratio	$\zeta_n = 0.05$

#### 7.2.4 Disturbance Boundary Model

A quick reminder of the boundary at the disturbance end is given in this part. In order to have a high precision model of the loudspeaker, the full electro-mechanical model must be considered when adding to the disturbance end of the overall model of the acoustic duct [Zimmer et al., 2003]. Therefore if a mechanically analogous system is used to describe the impedance of the speaker, the following impedance equation can be derived [Guicking and Karcher, 1984; Guicking, 1992]:

$$Z_0(s) = \frac{\pi r^2}{A_D s} (m_D s^2 + c_D s + k_D) \quad (7.11)$$

The coefficients of equation (7.11) are related to the disturbance loudspeaker, specifically  $A_D$  is the disturbance speaker's effective cross section,  $m_D$  is the disturbance speaker's cone effective mass,  $c_D$  is the disturbance speaker's damping coefficient and  $k_D$  is disturbance speaker's cone suspension stiffness. Throughout this chapter, the values used for the coefficients of disturbance loudspeaker are detailed in table 7.3.

Table 7.3: Values of coefficients used for the simulated loudspeaker

$m_D$	0.015 ( <i>Kg</i> )
$k_D$	810.87 ( <i>N/m</i> )
$c_D$	5.23 ( <i>N/s</i> )
$r_D$	0.087 ( <i>m</i> )
$A_D$	0.024 ( <i>m</i> <sup>2</sup> )

### 7.2.5 Coupled MIMO Model

The process is grouped into a two input two output system that is labelled as  $P$ . Specifically the two inputs are the voltage fed to the disturbance loudspeaker  $E_{dis}$  and the transmitted force of the controlled smart panel's actuator  $F_{con}$ , the two outputs are the total reflecting sound wave  $P_{ref}$  and the velocity of the smart panel  $w_{panel}$ . The matrix formula of the generalised system is:

$$\begin{bmatrix} P_{ref} \\ w_{panel} \end{bmatrix} = \begin{bmatrix} P_{11} & P_{12} \\ P_{21} & P_{22} \end{bmatrix} \begin{bmatrix} q_{dis} \\ F_{con} \end{bmatrix} \quad (7.12)$$

Because equation (7.3) and equation (7.7) describe the total acoustic pressure (incident and reflecting sound wave) due to the disturbance and control source the separation formula used in the previous chapter is required in order to acquire the reflecting sound wave, hence:

$$\left. \begin{aligned} P_{11} &= G_{dist}(z_2, s)e^{-s\tau} - G_{dist}(z_1, s) \\ P_{12} &= G_{con}(z_2, s)e^{-s\tau} - G_{con}(z_1, s) \\ P_{21} &= w_{pi} \\ P_{22} &= w_{point} \end{aligned} \right\} \quad (7.13)$$

where,  $\tau$  is the time required for a sound wave to travel from one measurement point to the other ( $\tau = c_0 * \Delta x$ ),  $w_{pi}$  is the velocity of the panel due to the acoustic wave generated by the disturbance source and  $w_{point}$  is the velocity of the panel due to the transmitted point force of the control actuator (Appendix A for more details).

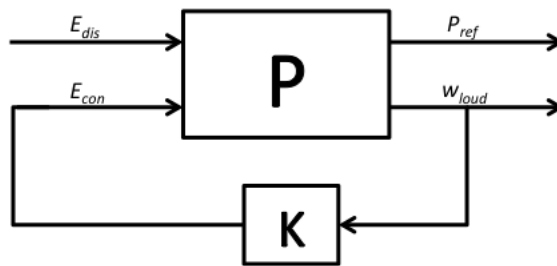


Figure 7.4: Inputs of the generalised process are the disturbance pressure wave and the control force, furthermore the outputs are the undesired reflecting sound wave to be minimised and the velocity of the reflecting panel.

## 7.3 Control Design

In this section a brief description of the two control designs chosen to minimise the undesired reflecting sound is presented. Specifically the  $H_2$  Feedback Control and the Remote Geometric Control design will be examined as proposed control designs.

### 7.3.1 Continuous Time Domain $H_2$ Control

The  $H_2$  design has been previously presented (chapter 4). Because the simulations and designs are conducted in the continuous time domain the design is reintroduced with the

required alterations for successful control design.

The goal is to minimise the performance measurement, which for the case considered here is the reflected sound wave in the duct ( $P_{ref}$ ). In particular the controller is to be designed to minimise the  $H_2$  norm of the closed loop transfer function between the disturbance input ( $E_{dis}$ ) and the performance output ( $P_{ref}$ ). For reasons of consistency with the control literature a discrete state space representation of the system is adopted. Specifically,  $x(t) \in \mathbb{R}^n$  is the state vector,  $d(t)$  is the disturbance input (disturbance voltage  $E_{dis}$ ),  $z(t)$  is the performance or error output (reflecting sound wave  $P_{ref}$ ) and  $y(t)$  is the measurement output (velocity of control panel  $w_{loud}$ ) [Skogestad and Postlethwaite, 2007]:

$$\left. \begin{aligned} \dot{x}(t) &= Ax(t) + B_1d(t) + B_2u(t) \\ z(t) &= C_1x(t) + D_{11}d(t) + D_{12}u(t) \\ y(t) &= C_2x(t) + D_{21}d(t) + D_{22}u(t) \end{aligned} \right\} \quad (7.14)$$

The equivalent compact matrix representation is given by:

$$P = \left[ \begin{array}{c|cc} A & B_1 & B_2 \\ \hline C_1 & D_{11} & D_{12} \\ C_2 & D_{21} & D_{22} \end{array} \right] \quad (7.15)$$

Let  $z = F_l(P, K)$  where  $F_l(P, K) = P_{11} + P_{12}K(I - P_{22}K)^{-1}P_{21}$ .

The design of the optimal feedback controller is based on the popular two Riccati function method [Doyle et al. [1989]]. In order to generate the controller the general  $H_2$  algorithm requires the following assumptions to be valid [Skogestad and Postlethwaite, 2007]:

1.  $(A, B_2, C_2)$  is stabilisable and detectable
2.  $D_{12}$  and  $D_{21}$  have full rank.
3.  $\begin{bmatrix} A - j\omega I & B_2 \\ C_1 & D_{21} \end{bmatrix}$  has full column rank for  $\omega$ .
4.  $\begin{bmatrix} A - j\omega I & B_1 \\ C_2 & D_{21} \end{bmatrix}$  has full column rank for  $\omega$ .

5.  $D_{11}$  and  $D_{22}$  are zero.

6.  $D_{12} = \begin{bmatrix} 0 \\ I \end{bmatrix}$  and  $D_{21} = \begin{bmatrix} 0 & I \end{bmatrix}$ .

7.  $D_{12}^T C_1 = 0$  and  $B_1 D_{21}^T = 0$ .

8.  $(A, B_1)$  is stabilisable and  $(A, C_1)$  is detectable.

Given the assumptions are satisfied, a stabilising controller  $K_{opt}(j\omega)$  exists if and only if:

1.  $X_1 \geq 0$  is a solution to the algebraic Riccati equation:

$$A^T X_1 + X_1 A + C_1^T C_1 + X_1 (-B_2 B_2^T) X_1 = 0$$

2.  $Y_1 \geq 0$  is a solution to the algebraic Riccati equation:

$$A Y_1 + Y_1 A^T + B_1 B_1^T + Y_1 (-C_1^T C_1) Y_1 = 0$$

And in conclusion, the optimal controller is then given by the following formula:

$$K_{opt}(j\omega) = \left[ \begin{array}{c|c} \hat{A}_2 & -L_2 \\ \hline F_2 & 0 \end{array} \right] \quad (7.16)$$

Where  $\hat{A}_2 = A + B_2 F_2 + L_2 C_2$ ,  $L_2 = -Y_1 C_2^T$  and  $F_2 = -B_2^T X_1$ .

It must be added, that in the case where assumptions 5,6 and 7 are not met, an appropriate transformation of the state space problem is possible and will allow the designer to form a optimal controller [Green and Limebeer, 2012].

### 7.3.2 Implementation of $H_2$ Design

Due to the high complexity of the plant's dynamics (figure 7.5 and figure 7.6) in order to design a stable  $H_2$  controller a low order transfer function model is fitted to the frequency bandwidth desired to be controlled. Via simulations it was found that a 8 – th order transfer function is adequate for the designing of the feedback controller. Furthermore, trial control designs revealed that for significant reduction of the reflected sound wave, up to three resonant peaks could be included in the feedback controller's range. Hence, the model is fitted at the

first 100 Hz and will include the first three dominant observed resonances. In contrast to the implementation procedure described for the  $H_2$  controller on the experimental rig (Chapter 4), the  $H_2$  controller for the simulated environment modelled in section §7.2 is implemented in the continuous time domain.

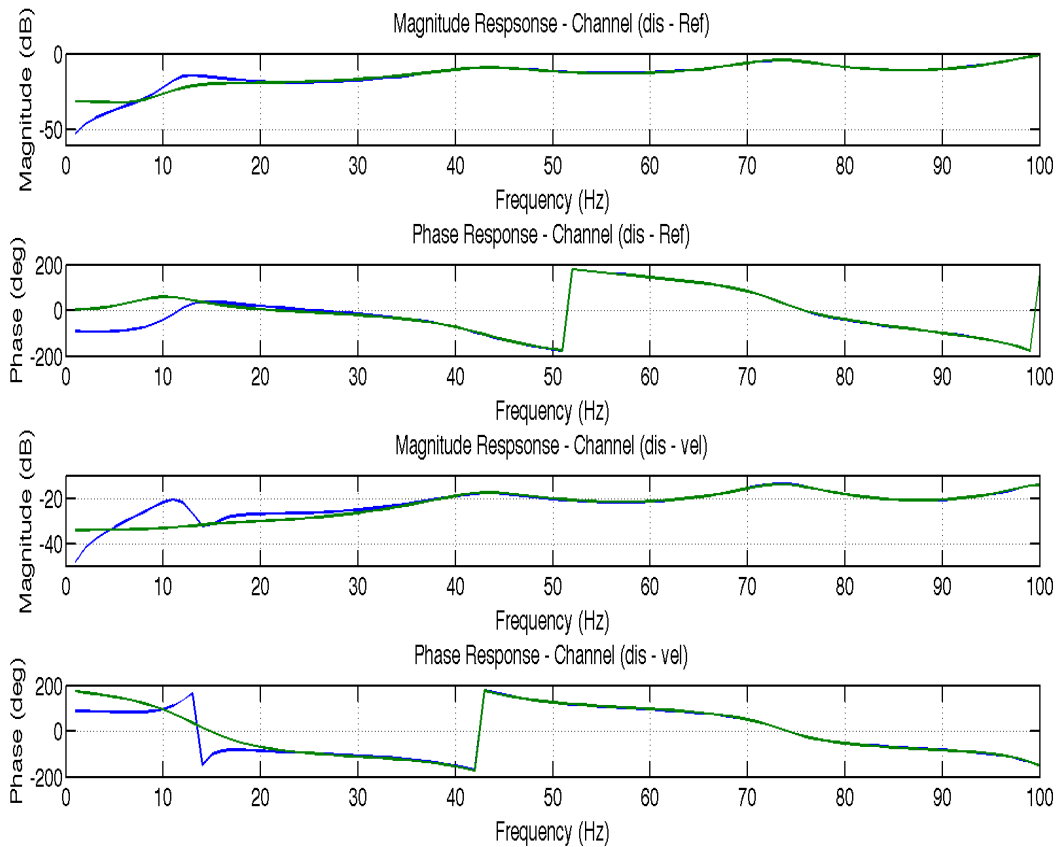


Figure 7.5: Original model for the disturbance path of coupled acoustic duct-loudspeaker-panel setup (blue) Low order ( $8 - th$ ) transfer function model fitted to the original model (green)

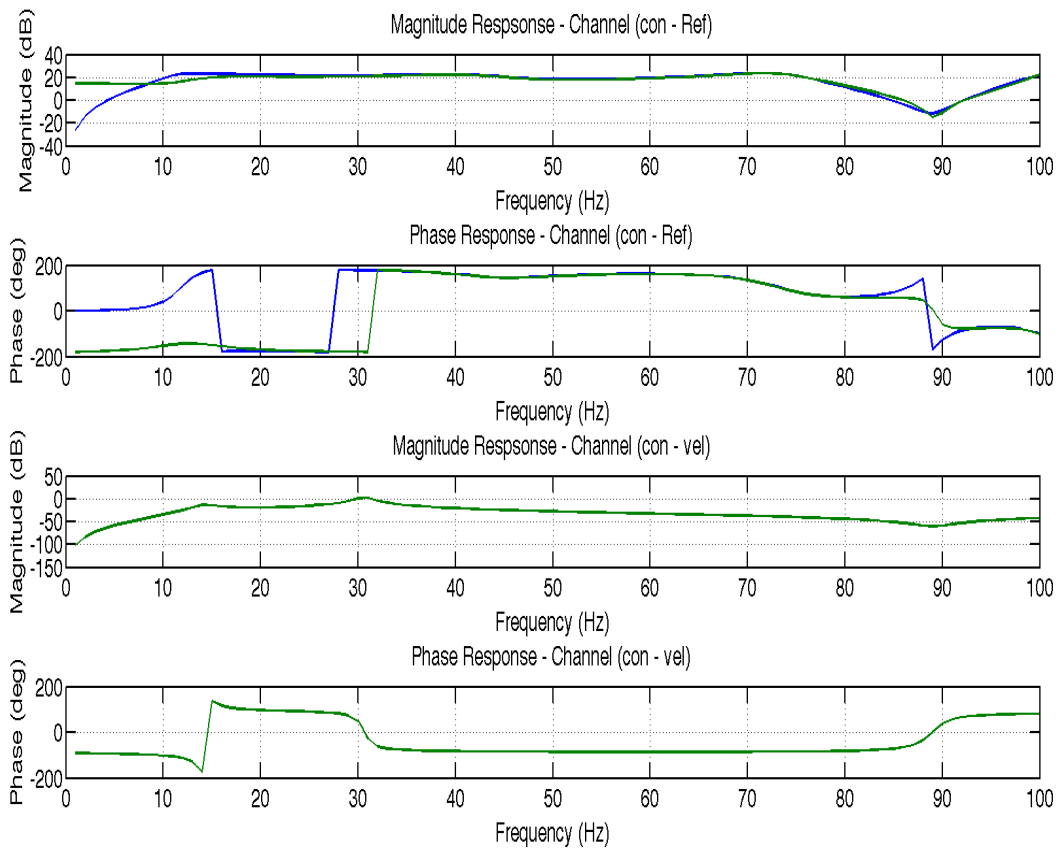


Figure 7.6: Original model for the control path of coupled acoustic duct-loudspeaker-panel setup (blue) Low order (8 – th) transfer function model fitted to the original model (green)

The overall procedure of calculating the velocity  $H_2$  feedback controller offline is presented in a schematic form in figure 7.7.

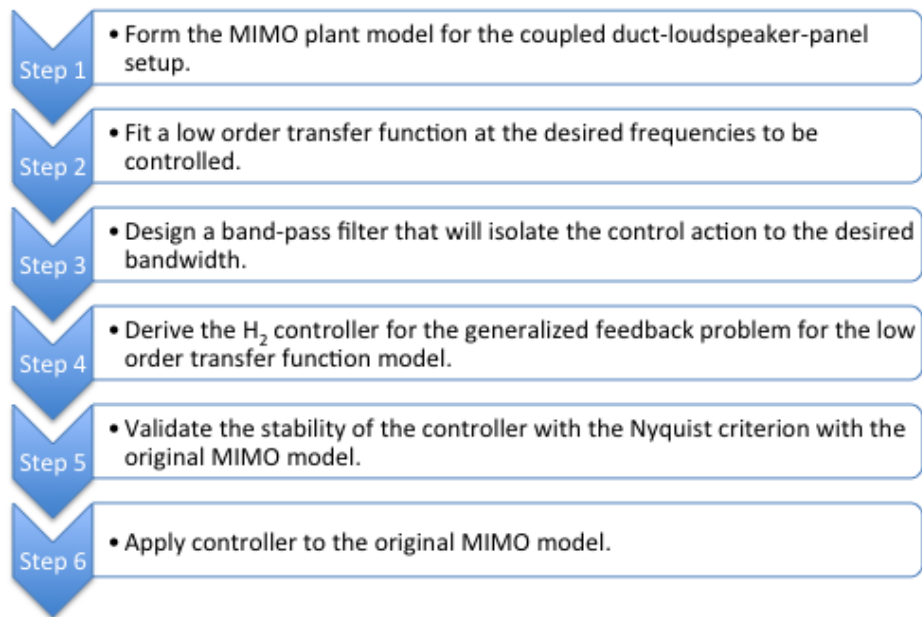


Figure 7.7: Offline  $H_2$  control design for reduction of reflecting noise inside simulated coupled acoustic duct-loudspeaker-panel setup.

### 7.3.3 Remote Geometric Control

The Geometric Design has been previously presented and analysed in depth. Therefore, the reader is referred for further details with regards to the design to Chapter 5.

### 7.3.4 Implementation of Remote Geometric Design

The Remote Geometric design requires a transfer function model of the control path ( $P_{22}$ ), hence an 8–*th* order transfer function is be fitted to the simulated response data (figure 7.8). The order of the model is based on trial simulations, it was noticed that by increasing the order of the model beyond the 8 had insignificant impact on the concluding controller and therefore the transfer function was kept at a low order. Due to RHP zeros a minimum phase transfer function is designed,  $g_{MP}$ , in order to guarantee stability of the controller. Through trial and error it was found that to reduce the magnitude at the acoustic resonances, 8  $\gamma$ –*points* is sufficient to provide a stable and robust controller. The position of which are distributed around the resonant acoustic peaks. This large number of  $\gamma$ –*points* in

comparison to the single pair used for the experimental loudspeaker setup is expected as the mechanical resonance of the control device have now increased, due to the plate's dynamics.  $M$  and  $\sigma$  are found with fine tuning. Finally, because the controller is intended to focus its action in the lower frequency band a low pass filter ( $f_{LP}(j\omega)$ ) with a cut-off frequency at 100 Hz is designed and utilised for the final form of the controller. The design procedure takes place in the continuous time domain.

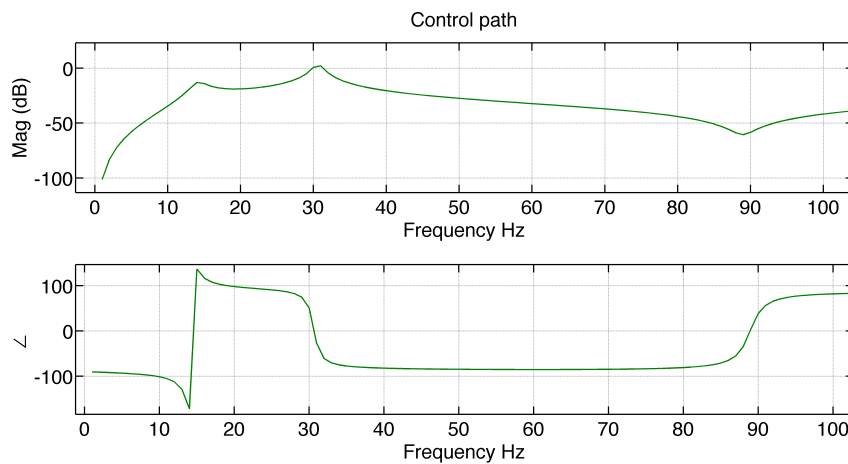


Figure 7.8: Bode plot of the simulated data for the control path to velocity (blue) and bode plot of low order ( $8 - th$ ) transfer function fitted to the simulated data (green).

Now that the overall implementation procedure for the design has been fully described, it is considered convenient to group the steps in a list (figure 7.9) just as it was done for the  $H_2$  design.

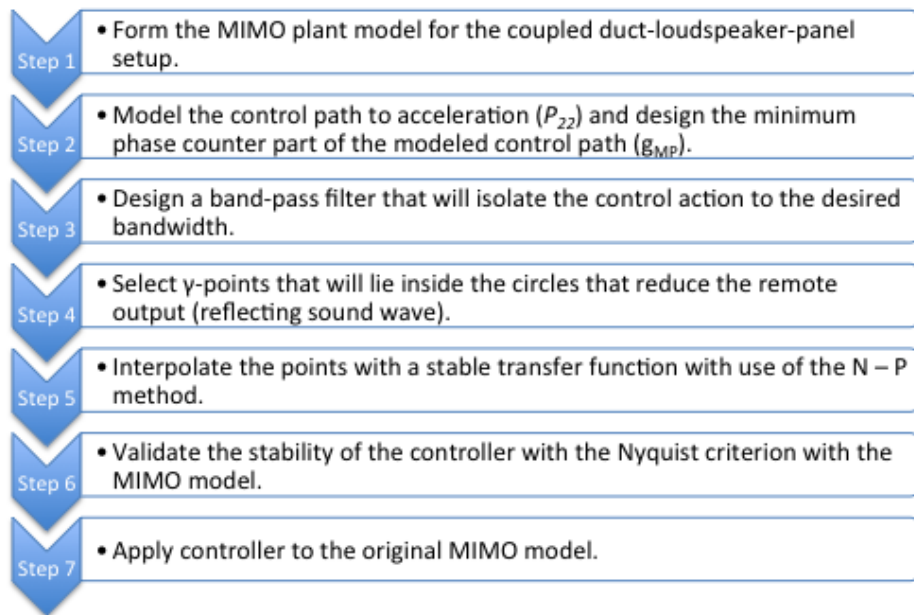


Figure 7.9: Remote geometric control design for reduction of reflecting noise inside simulated coupled acoustic duct-loudspeaker-panel setup.

## 7.4 Results and Analysis

In this section, simulations of the two designs are performed in order to quantify the performance of each strategy. Additionally, a comparison of the  $H_2$  and Geometric design is presented.

### 7.4.1 $H_2$ Control Design

The stability of the design is verified by plotting the Nyquist diagram of the open loop system with the use of experimental data, figure 7.10. It is clearly observed from the Nyquist plot that the controller is stable, due to no encirclement of the critical  $(-1, 0j)$  point.

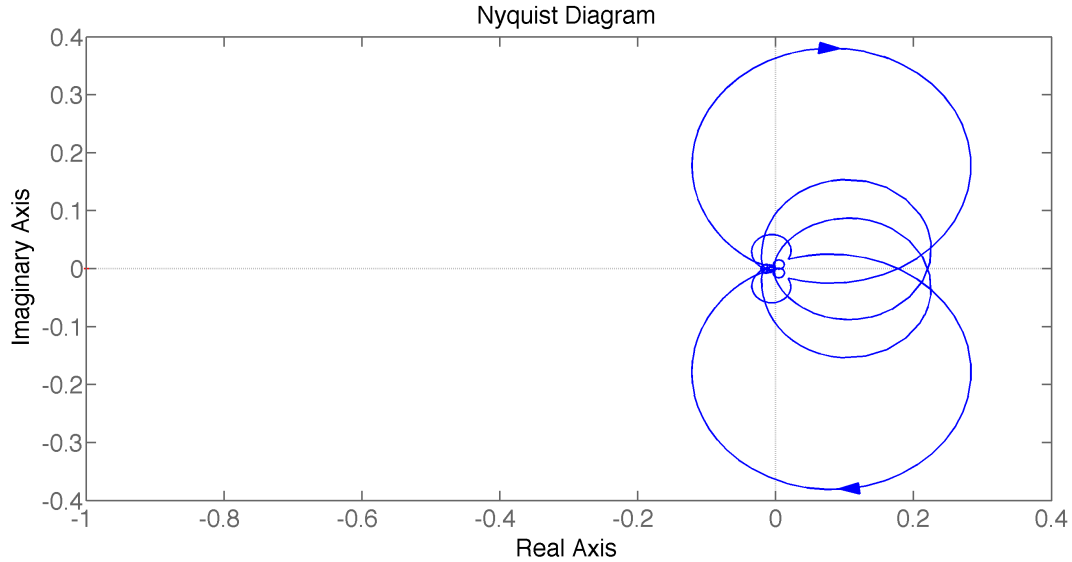


Figure 7.10: Nyquist plot of open-loop system with  $H_2$  controller

The performance of the  $H_2$  control design is demonstrated with the magnitude response of the plant figure 7.11. Because the controller is designed based on a reduced order model for a frequency band between 0-100 Hz the beneficial effect of the  $H_2$  feedback controller is clearly observed with a 20 dB reduction at the second and third resonance peaks ( $f_2 = 43Hz$  and  $f_3 = 73Hz$ ). Additionally, the fourth resonant peak ( $f_4 = 100Hz$ ) is reduced by 10 dB. Finally, the  $H_2$  controller enhances the resonant frequency ( $f_1 = 12Hz$ ) by 10 dB. The resonant frequency located at  $12Hz$  is due to the panels dynamics which can be viewed in figure 7.8.

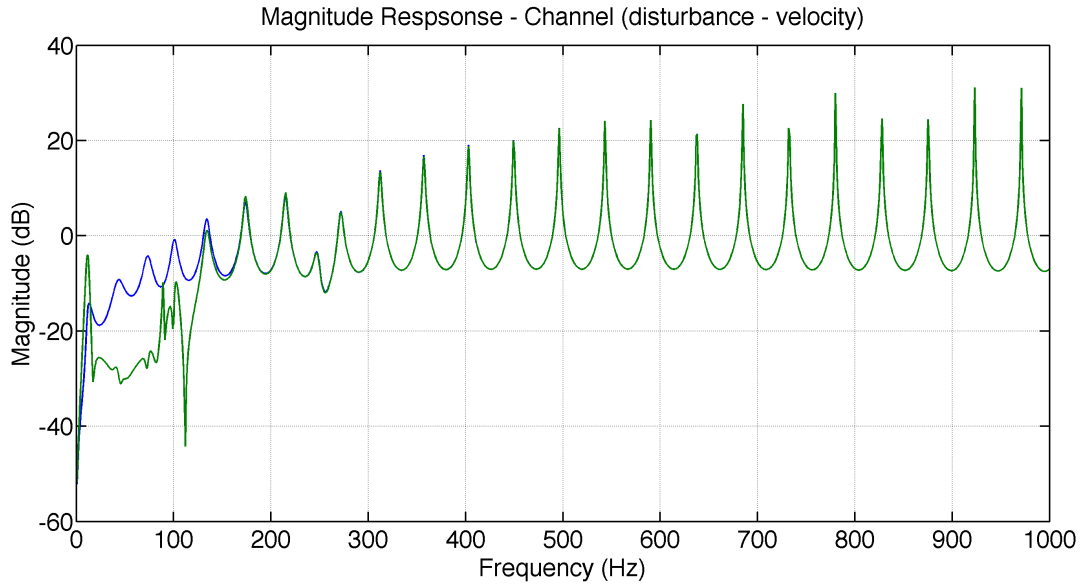


Figure 7.11: Bode plot of reflecting sound wave without control (blue), Bode plot of reflecting sound wave with  $H_2$  velocity feedback control applied (green).

### 7.4.2 Remote Geometric Design

The stability of the design is verified by plotting the Nyquist diagram of the open loop system, figure 7.10. It is clearly observed from the Nyquist plot that the controller is stable, due to no encirclement of the critical  $(-1, 0j)$  point.

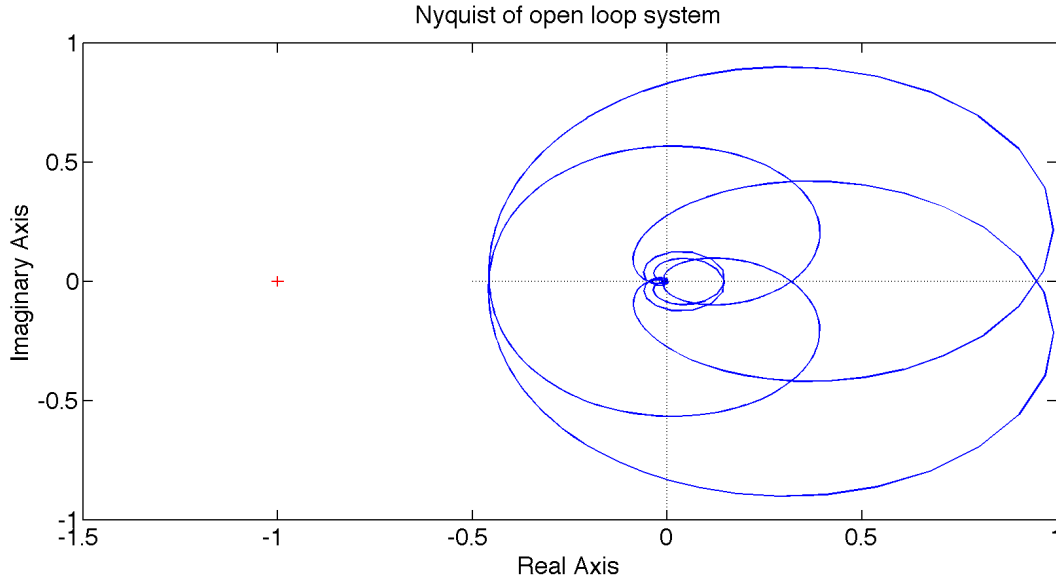


Figure 7.12: Nyquist plot of open-loop system with geometric controller.

The performance of the Geometric control design is demonstrated with the magnitude response of the plant figure 7.13. Just as in the case of the  $H_2$  design the Geometric controller is designed based on a reduced order model for a frequency band between 0-100 Hz the beneficial effect of the design is clearly observed with a 150 dB reduction at the second third and fourth resonance peaks ( $f_2 = 43Hz$ ,  $f_3 = 73Hz$  and  $f_4 = 100Hz$ ). The reason such reduction is achieved is due to the selection of  $\gamma$  - *points* at these frequencies. The noticeable problem from the magnitude response for the Geometric design is the fact that the very large reduction can only be kept for a relatively small bandwidth around each  $\gamma$  - *point*, therefore if the interpolating points were increased the bandwidth of large dB reduction would be greater. In this simulated example 8  $\gamma$  - *points* were used, this number happens to be the maximum value of  $\gamma$  - *points* the interpolation method (Nevanlinna - Pick ) can solve and not lead to an ill posed problem. Finally, the Geometric controller enhances the resonant frequencies  $f_1 = 12Hz$  and  $f_5 = 133Hz$  by 20 dB and 7dB, respectively.

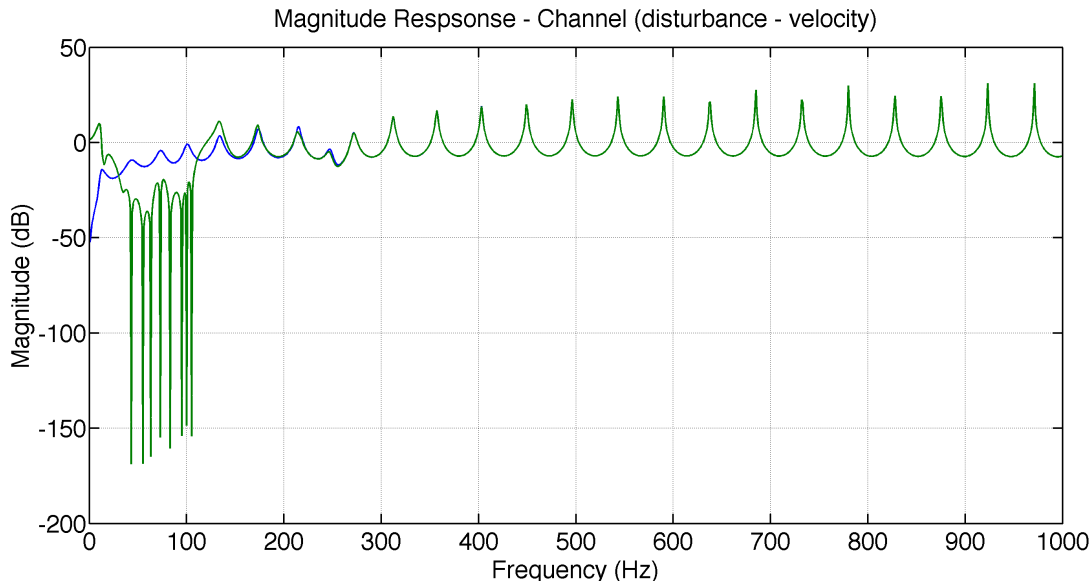


Figure 7.13: Bode plot of reflecting sound wave without control (blue), Bode plot of reflecting sound wave with Remote Geometric feedback control applied (green).

### 7.4.3 Comparison

Now that the two feedback controllers have successfully been implemented the final step is to compare the two designs. In order to compare the performance of the two designs, the magnitude responses are plotted on the same figure. From figure 7.14 it can be viewed that the the Remote Geometric design excites the first resonant frequency ( $f_1 = 12Hz$ ) by 15 dB more when compared to the  $H_2$  controlled response. In addition the Geometric design enhances the acoustic resonance located at  $f_5 = 134Hz$  by 10 dB. With regards to the frequencies between the first ( $f_1 = 12Hz$ ) and fifth ( $f_1 = 134Hz$ ) resonance the remote geometric control is able to achieve significant reduction of the reflecting acoustic wave at short frequency bandwidths near the  $\gamma$  - *points* selected for designing the controller. Hence, in terms of performance the geometric controller delivers slightly better results. Therefore, in terms of performance the Geometric approach is a more favourable choice.

The results in this chapter are derived for a simulated environment, hence a comparison with the designs considering a experimental loudspeaker is not advisable. However, some general remarks can be made. The results given from both feedback designs when using a

flat panel are promising with regards to the achievable reduction of the reflecting sound wave (figure 7.14). When considering a flat panel to reduce the reflecting sound wave, the first mechanical resonance is excited (figure 7.14), this does not occur when using a loudspeaker. The flat panel's dynamics are more complex as additional mechanical resonances are added, hence a more demanding noise reduction problem is formed. The adjustable size of the panel enables this electroacoustic device to be more practical for real life problems in comparison to the loudspeaker.

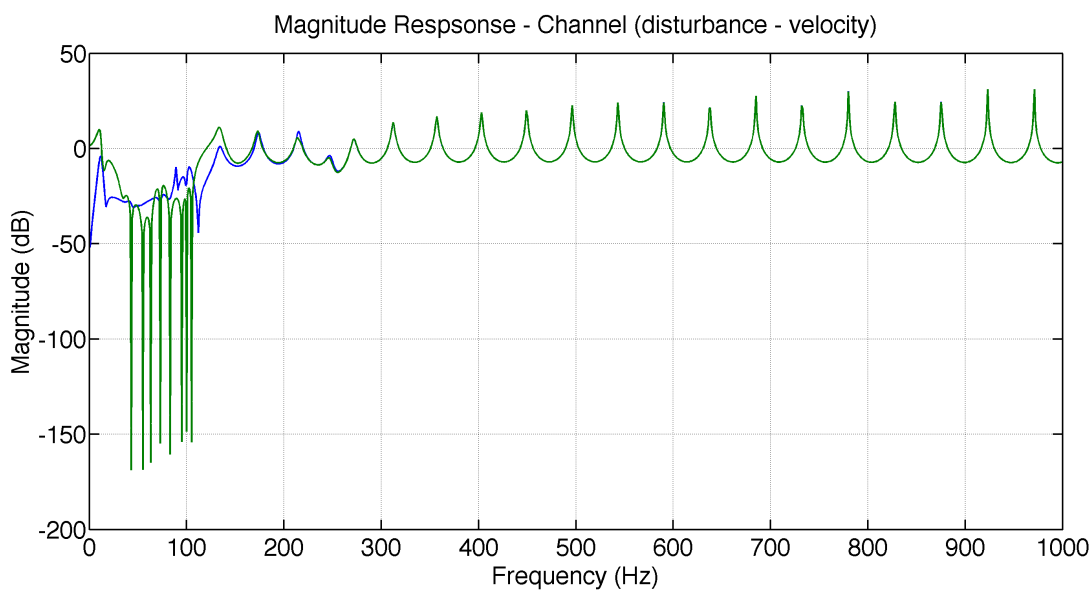


Figure 7.14: Bode plot of reflecting sound wave with  $H_2$  velocity feedback control applied (blue), Bode plot of reflecting sound wave with Remote Geometric feedback control applied (green).

## 7.5 Conclusions

In this chapter, two novel control applications in the field of ANC were developed in order to achieve reduction of the reflecting sound waves in a numerical simulation of a one-dimensional acoustic duct problem, figure 7.1. In contrast to the previous solutions which used a loudspeaker as means of delivering the control output, this investigation considers a flat panel sensor actuator setup [figure 7.3]. Such an approach is of more practical use for real life

problems as the installation of the electroacoustic device is much simpler in comparison to the loudspeaker and the freedom of selecting the panel's dimensions allows it to be more adaptable to the dimensions of a larger number of ANC problems.

The two control strategies utilised only local velocity measurements of the boundary reflecting surface in order to produce the control signal and do not therefore require any remote measurements, such as microphones placed in the fluid (in this chapter air). With regards to performance, the geometric design is able to achieve significant reduction of the reflecting sound wave near the  $\gamma$  – *points* selected to form the feedback controller but away from them is unable to retain the same dB reduction of the undesired sound wave. The  $H_2$  feedback design does not reach the same levels of reduction at the  $\gamma$  – *points* but has comparable performance to the Geometric approach at the rest of the frequencies of the targeted control bandwidth.

In the next chapter a summary of the PhD project's achievements is presented and future work advancements related to the proposed solutions.

# Chapter 8

## Summary and Future Work

### 8.1 Summary of Achievements

With the completion of this PhD project, advances in active noise control designs that attenuate the reflecting sound waves that occur inside closed 1 dimensional environments (acoustic ducts) were achieved. The proposed designs were successfully implemented in a simulated environment and then validated in an experimental environment. Previously proposed solutions, require difficult to acquire remote measurements (pressure microphones) [] or complex models of the feedforward disturbance path of the plant []. The intent of all proposed solutions is focused on how an active control setup for acoustic problems can be implemented in a simpler manner. With respect to the complexity (required plant models) and cost efficiency (actuators, sensors) a feedback approach is by far superior than existent designs (FxLMS). Furthermore, the critical importance of this work is the local nature of the proposed designs. Specifically, only the velocity or acceleration measurements are required to implement the controllers.

Following, is a brief overview of what has been accomplished:

- An experimental pulse tube setup, was reconfigured and used to approximate a one-dimensional wave guide duct arrangement in order to have a apparatus to validate experimentally all the proposed solutions. The feedback architecture adopted throughout this thesis allowed me to consider a novel Geometric design that has never before been implemented in the field of ANC. Specifically, a Remote Geometric design that

has been successfully applied in the field of AVC [Ubaid et al., 2011] was introduced and implemented on the experimental test rig. In terms of achievable performance (reduction of the undesired reflecting sound wave), at the controlled bandwidth between 150 Hz and 300 Hz, the geometric controller delivers a significant dB reduction of the reflecting sound wave. Specifically, the geometric controller achieves a 7 dB reduction at the acoustic resonances located at  $f = 185Hz$  and  $f = 262Hz$ . On the other hand, the Remote Geometric controller excites acoustic resonances beyond the control bandwidth. This negative result is due to the bandpass filter required to avoid control and observer overspill for the formulation of the Remote Geometric feedback controller. Most importantly, the Geometric approach besides the achieved dB reduction, provides a visual inspection of the maximum feasible reduction of any feedback controller, regardless the controller that is chosen. This insight is important as it provides the designer a tool to compare any feedback controller to the optimal achievable performance.

- The previously mentioned Remote Geometric design requires a restrictive interpolation procedure (Nevanlinna - Pick) in order to form the stable and robust feedback controller. This step has a result to limit the number of the controlled acoustic resonances. Furthermore, due to the bandpass filter required to avoid the control and observer overspill, exciting of uncontrolled acoustic resonants was noticed. In an attempt to simplify the interpolation step, a novel alteration of the original Geometric design was considered. Specifically, the proposed design constructs two Remote Geometric feedback controllers that operate in parallel connection (Selective Resonance Geometric Control) and deal individually with each controlled acoustic resonance. By doing this, the overall interpolation procedure is far less computationally demanding. This approach, was successfully implemented on the apparatus. The performance (reduction of reflecting sound wave) of the designs are almost identical at the resonant peaks intended for control. The significant difference is that the standard remote geometric design is exciting a uncontrolled resonant peak at  $f = 262Hz$  (8 dB increase) whereas the selective resonance approach does not enhance this resonant peak. This is due to the presence of two bandpass filters (one for each controller) to avoid the overspill control and observer effect.

- Additionally to the Geometric designs, a well established in the scientific community  $H_2$  optimal feedback controller was designed and successfully implemented on the apparatus [Pelegrinis et al. [2013]]. Furthermore, a FxLMS controller was also successfully implemented and compared to the suggested local feedback controller. The beneficial effect of the  $H_2$  feedback controller is most clearly observed with a significant 10 dB reduction at the acoustic resonance at  $f = 185\text{Hz}$ . Since this is the only significant acoustic resonance within the desired control bandwidth, the higher order modes remain unaffected. In terms of performance (reduction of reflecting sound wave), the FxLMS design is able to reduce the undesired reflecting sound wave significantly more than the  $H_2$  controller and in greater bandwidths. However, the critical importance of this work is the local nature of the proposed feedback design. Specifically, only the acceleration of the controlled loudspeaker's cone is required to implement the  $H_2$  controller making this design a more favourable solution for real life applications.
- A novel application of a PID Frequency Loop Shaping (FLS) local velocity feedback control design was developed to cancel the undesired reflecting sound wave in a one-dimensional setup. An analytical model of the adopted setup was derived and utilised for simulations. The proposed design matched the reflecting boundary element's acoustic impedance to the acoustic impedance of air. Due to the matching of the controlled end, the coupled duct system approximated the dynamics of a semi-infinite acoustic duct, which resulted to a significant reduction of the reflecting sound wave. In order to appreciate the novelty of the application an in depth investigation of the feedback and feedforward control designs applied in solving ANC problems was included with emphasis on the FxLMS. A numerical example of the FLS PID and the FxLMS designs was carried out. Through the investigation of the example it was possible to assess the performance of the proposed novel solution [Pelegrinis et al., 2012]. The FLS PID controller was able to reduce the undesired reflected sound waves within a frequency bandwidth that reached the limits of the cut-off frequency (0 - 1000 Hz) and achieved comparable dB reduction of the reflecting sound wave to the FxLMS method. The novelty of the FLS PID controller lies in the local nature of the design in combination with the automatic tuning procedure utilised to form the feedback controller.

- The local feedback designs that were validated experimentally made use of a loudspeaker in order to deliver the control. A loudspeaker is a rather restrictive electroacoustic device for real life applications, as its dimensions are predetermined and therefore limit the range of applications. Hence, an investigation of the benefits and trade offs of applying local feedback control designs on thin flat panels is considered. This work considers flat panels with an embedded collocated actuator/sensor pair. This electroacoustic device in contrast to the loudspeaker can be fitted to the desired problem regardless the dimension restrictions. Interest is focused on the reduction of reflecting sound waves for of plane wave propagation problem with use of these actively controlled panels. A one-dimensional acoustic duct was considered. The proposed feedback controllers were the  $H_2$  and Remote Geometric design and made use of a theoretical model developed for the purpose of simulations. The two proposed feedback designs ( $H_2$  and Remote Geometric) were successfully implemented and simulated. With regards to performance (reduction of the reflecting sound wave) from figure 7.14 it can be viewed that the the Geometric design excites the first resonant frequency ( $f_1 = 12Hz$ ) by 15 dB more when compared to the  $H_2$  controlled response. In addition the Geometric design enhances the acoustic resonance located at  $f_5 = 134Hz$  by 10dB. With regards to the frequencies between the first ( $f_1 = 12Hz$ ) and fifth ( $f_5 = 134Hz$ ) resonance the remote geometric control is able to achieve significant reduction of the reflecting acoustic wave at short frequency bandwidths. Therefore, in terms of performance the Geometric approach is a more favourable choice. In addition the modelling included actuator dynamics, making the investigated solutions more viable for future experimental validation.

## 8.2 Future Work

The primary objective of this thesis was focused on implementing active feedback control designs that rely on local measurements in order to reduce reflecting sound wave. This aim had as a result the investigation and implementation of the FLS PID controller and its successful application in a simulated environment. The FLS tuning method allows the

designer to make optimal use of the plant's well defined desired response (acoustic impedance of air). The problem with the proposed design was the poor experimental results that led to insignificant reduction of the reflecting sound wave. One proposition that could possibly solve this problem is instead of implementing a PID controller consider a higher order feedback controller and tune it with the FLS algorithm. By doing so, the increased dynamics of the experimental plant can be compensated by the additional poles and zeros the higher order controller. Such an endeavour would require initially a thorough investigation of the stability analysis as the optimisation problem has changed. Additionally, due to the increased number of control coefficients needed to be calculated the use of powerful convex optimisation algorithms would have to be considered.

The work presented in Chapter 7 investigated the implementation of two feedback designs (Remote Geometric and  $H_2$  control) on a smart panel arrangement (ideal sensor/actuator embedded on a thin plate) in order to reduce the reflecting sound waves. This solution showed promising results in the simulated environment as both designs were able to provide good performance (reduction of the reflecting sound wave). The next step should be the experimental validation of the flat panel arrangement.

Given the smart panel is able to achieve satisfactory reduction of the reflecting sound wave, such a device would be a solution for the higher dimensional ANC problem of reducing reflections and scattering sound waves. The reason is the panel's adjustable size to meet the problem's dimensions requirements. It must be noted that for the needs of the three dimensional problem, multiple sensors and actuators would be consider for controlling the panel's response and therefore a MIMO local control feedback design would be investigated.

# References

- R. Alkhatib and M. F. Golnaraghi. Active structural vibration control: a review. *Shock and Vibration Digest*, 35(5):367, 2003.
- M. Alster. Improved calculation of resonant frequencies of helmholtz resonators. *Journal of Sound and Vibration*, 24(1):63–85, 1972.
- D. K. Anthony and S. J. Elliott. Comparison of the effectiveness of minimizing cost function parameters for active control of vibrational energy transmission in a lightly damped structure. *Journal of sound and vibration*, 237(2):223–244, 2000.
- O. Bardou, P. Gardonio, S. J. Elliott, and R. J. Pinnington. Active power minimization and power absorption in a plate with force and moment excitation. *Journal of Sound and Vibration*, 208(1):111–151, 1997.
- W. T. Baumann, F. Ho, and H. H. Robertshaw. Active structural acoustic control of broadband disturbances. *The Journal of the Acoustical Society of America*, 92:1998, 1992.
- L. Benassi, S. J. Elliott, and P. Gardonio. Active vibration isolation using an inertial actuator with local force feedback control. *Journal of Sound and Vibration*, 276(1):157–179, 2004.
- L. L. Beranek. *Acoustics, American Institute of Physics*. 1986.
- L. L. Beranek, L. L. Beranek, and L. L. Beranek. *Acoustics*, volume 6. McGraw-Hill New York, 1954.
- P. Bhattacharya, H. Suhail, and P. K. Sinha. Finite element analysis and distributed control of laminated composite shells using lqr/imsc approach. *Aerospace science and technology*, 6(4):273–281, 2002.

- C. Birdsong and C. R. Radcliffe. A compensated acoustic actuator for systems with strong dynamic pressure coupling. *ASME J. Vibr. Acoust.*, 121:89–94, 1999.
- I. U. Borchers, U. Emborg, A. Sollo, E. H. Waterman, J. Paillard, P. N. Larsen, G. Venet, P. Goeransson, and V. Martin. Advanced study for active noise control in aircraft (asanca). In *Fourth Aircraft Interior Noise Workshop*, volume 1, pages 129–141, 1992.
- C. C. Boucher, S. J. Elliott, and P. A. Nelson. Effect of errors in the plant model on the performance of algorithms for adaptive feedforward control. In *IEE Proceedings F (Radar and Signal Processing)*, volume 138, pages 313–319. IET, 1991.
- J. C. Burgess. Active adaptive sound control in a duct: A computer simulation. *The Journal of the Acoustical Society of America*, 70:715, 1981.
- P. Cominos and N. Munro. *PID* controllers: recent tuning methods and design to specification. In *Control Theory and Applications, IEE Proceedings*, volume 149, pages 46–53. IET, 2002.
- A. Cummings. The effects of a resonator array on the sound field in a cavity. *Journal of Sound and Vibration*, 154(1):25–44, 1992.
- S. Daley and J. Wang. A geometric approach to the design of remotely located vibration control systems. *Journal of Sound and Vibration*, 318(4):702–714, 2008.
- S. Daley and I. Zazas. A recursive least squares based control algorithm for the suppression of tonal disturbances. *Journal of Sound and Vibration*, 2:1270–1290, 2012.
- P. h. Delsarte, Y. Genin, and Y. Kamp. The nevanlinna-pick problem for matrix-valued functions. *SIAM Journal on Applied Mathematics*, 36(1):47–61, 1979.
- A. Doria. Control of acoustic vibrations of an enclosure by means of multiple resonators. *Journal of sound and vibration*, 181(4):673–685, 1995.
- J. C. Doyle, K. Glover, P. P. Khargonekar, and B. A. Francis. State-space solutions to standard  $H_2$  and  $H_\infty$  control problems. *Automatic Control, IEEE Transactions on*, 34(8): 831–847, 1989.

- S. J. Elliot, P. A. Nelson, I. M. Stothers, and C. C. Boucher. In-flight experiments on the active control of propeller-induced cabin noise. *Journal of Sound and Vibration*, 140(2): 219–238, 1990.
- S. J. Elliott. *Signal processing for active control*. Academic press, 2000.
- S. J. Elliott and P. A. Nelson. Multiple-point equalization in a room using adaptive digital filters. *Journal of the Audio Engineering Society*, 37(11):899–907, 1989.
- S. J. Elliott, I. Stothers, and P. A. Nelson. A multiple error lms algorithm and its application to the active control of sound and vibration. *Acoustics, Speech and Signal Processing, IEEE Transactions on*, 35(10):1423–1434, 1987.
- L. Eriksson, M. Allie, and R. Greiner. The selection and application of an iir adaptive filter for use in active sound attenuation. *Acoustics, Speech and Signal Processing, IEEE Transactions on*, 35(4):433–437, 1987.
- F. J. Fahy and C. Schofield. A note on the interaction between a Helmholtz resonator and an acoustic mode of an enclosure. *Journal of Sound and Vibration*, 72(3):365–378, 1980.
- G. Ferreres and G. Puyou. Feasibility of h-infinity design specifications: an interpolation method. *International Journal of Control*, 78(12):927–936, 2005.
- M. Fu. Interpolation approach to h-infinity estimation and its interconnection to loop transfer recovery. *Systems & control letters*, 17(1):29–36, 1991.
- C. R. Fuller and A. H. Von Flotow. Active control of sound and vibration. *Control Systems, IEEE*, 15(6):9–19, 1995.
- C. R. Fuller, S. J. Elliott, and P. A. Nelson. *Active Control of Vibration*. Academic Pr, 1997.
- P. Gardonio. Review of active techniques for aerospace vibro-acoustic control. *Journal of Aircraft*, 39(2):206–214, 2002.
- W. A. Gontijo, O. J. Tobias, R. Seara, and E. M. Lopes. Fxlms algorithm with variable step size and variable leakage factor for active vibration control. In *Telecommunications Symposium, 2006 International*, pages 572–575. IEEE, 2006.

- E. Grassi, K. S. Tsakalis, S. Dash, S. V. Gaikwad, W. MacArthur, and G. Stein. Integrated system identification and PID controller tuning by frequency loop-shaping. *Control Systems Technology, IEEE Transactions on*, 9(2):285–294, 2001. ISSN 1063-6536.
- M. Green and D. J. N. Limebeer. *Linear robust control*. Dover Publications, Inc., Mineola, New York, 2012.
- Y. Gu and C. R. Fuller. Active control of sound radiation from a fluid-loaded rectangular uniform plate. *The Journal of the Acoustical Society of America*, 93:337, 1993.
- D. Guicking. Recent advances in active noise control. In *Recent Developments in Air-and Structure-Borne Sound and Vibration*, volume 1, pages 313–320, 1992.
- D. Guicking and K. Karcher. Active impedance control for one-dimensional sound. *Journal of vibration, acoustics, stress, and reliability in design*, 106(3):393–396, 1984.
- L. Hakansson. The filtered-x lms algorithm. *University of Karlskrona/Ronneby*, 2004.
- C. Hansen. *Active control of noise and vibration*. Taylor & Francis, 1996.
- M. S. Howe. On the Helmholtz resonator. *Journal of Sound and Vibration*, 45(3):427–440, 1976.
- J. S. Hu. Active sound attenuation in finite-length ducts using closeform transfer function models. *ASME J. Dyn. Syst., Meas., Control*, 117:143–154, 1995.
- A. J. Hull and C. J. Radcliffe. An eigenvalue based acoustic impedance measurement. *Journal of Vibrations and Acoustics*, 113:250–254, 1991.
- A. J. Hull, C. J. Radcliffe, and C. R. MacCluer. State estimation of the nonself-adjoint acoustic duct system. *Journal of Dynamic Systems, Measurements, and Control*, 113, 1991.
- T. Inoue, A. Takahashi, H. Sano, M. Onishi, and Y. Nakamura. Nv countermeasure technology for a cylinder-on-demand engine-development of active booming noise control system applying adaptive notch filter. *SAE Technical Paper*, pages 01–0411, 2004.

- J. Jiang and D. Li. Decentralized guaranteed cost static output feedback vibration control for piezoelectric smart structures. *Smart Materials and Structures*, 19(1):015018, 2009.
- S. Johansson, T. Lagö, S. Nordebo, and I. Claesson. Control approaches for active noise control of propeller-induced cabin noise evaluated from data from a dornier 328 aircraft. In *Proceedings of International Congress on Sound and Vibration*, pages 1611–1618, 1999.
- I. Kim, H. Na, K. Kim, and Y. Park. Constraint filtered-x and filtered-u least-mean-square algorithms for the active control of noise in ducts. *The Journal of the Acoustical Society of America*, 95:3379, 1994.
- L. E. Kinsler, A. R. Frey, A. B. Coppens, and J. V. Sanders. Fundamentals of acoustics. *Fundamentals of Acoustics, 4th Edition, by Lawrence E. Kinsler, Austin R. Frey, Alan B. Coppens, James V. Sanders, pp. 560. ISBN 0-471-84789-5. Wiley-VCH, December 1999.*, 1, 1999.
- S. M. Kuo and D. Morgan. *Active noise control systems: algorithms and DSP implementations*. John Wiley & Sons, Inc. New York, NY, USA, 1995.
- S. A. Lane and R. L. Clark. Improving loudspeaker performance for active noise control applications. *Journal of the Audio Engineering Society*, 46(6):508–519, 1998.
- D. J. Lee, J. Lee, J. J. Jeon, Y. S. Seo, and W. Ohm. Dynamic impedance matching for active noise control in a cylindrical waveguide. *The Journal of the Acoustical Society of America*, 132(3):1955–1955, 2012.
- Y. Lee, P. Gardonio, and S. J. Elliott. Volume velocity vibration control of a smart panel using a uniform force actuator and an accelerometer array. *Smart materials and structures*, 11(6):863, 2002.
- H. Levine and J. Schwinger. On the radiation of sound from an unflanged circular pipe. *Physical Review*, 73(4):383–406, 1948.
- H. Lissek, R. Boulandet, and R. Fleury. Electroacoustic absorbers: bridging the gap between shunt loudspeakers and active sound absorption. *The Journal of the Acoustical Society of America*, 129:2968, 2011.

- T. Meurers and S. M. Veres. Online iterative design for periodic vibration attenuation. 2000.
- T. Meurers, S. M. Veres, and S. J. Elliot. Frequency selective feedback for active noise control. *Control Systems, IEEE*, 22(4):32–41, 2002.
- D. R. Morgan. An analysis of multiple correlation cancellation loops with a filter in the auxiliary path. *Acoustics, Speech and Signal Processing, IEEE Transactions on*, 28(4):454–467, 1980.
- P. M. Morse and H. Feshbach. *Methods of Theoretical Physics McGraw-Hill*, volume 2. 1953.
- P. A. Nelson, S. J. Elliott, and J. E. F. Williams. *Active control of sound*. Academic Press Inc, 1993.
- A. N. Norris and G. Wickham. Elastic helmholtz resonators. *The Journal of the Acoustical Society of America*, 93(2):617–630, 1993.
- K. Ogata and Y. Yang. Modern control engineering. 1970.
- R. L. Panton and J. M. Miller. Resonant frequencies of cylindrical helmholtz resonators. *The Journal of the Acoustical Society of America*, 57(6):1533–1535, 1975.
- M. T. Pelegrinis, S. A. Pope, and S. Daley. Acoustic impedance matching using loop shaping pid controller design. In *Advances in PID Control*, volume 2, pages 323–328, 2012.
- M. T. Pelegrinis, S. A. Pope, I. Zazas, and S. Daley. Noise suppression using local acceleration feedback control of an active absorber. 2013.
- D. M. Photiadis. The effect of wall elasticity on the properties of a helmholtz resonator. *The Journal of the Acoustical Society of America*, 90(2):1188–1190, 1991.
- J. T. Post and R. J. Silcox. Active control of the forced response of a finite beam. In *Inter-Noise 90; Proceedings of the International Conference on Noise Control Engineering, Volume 1*, volume 1, pages 197–202, 1990.
- H. R. Pota and A. G. Kelkar. Modeling and control of acoustic ducts. *Journal of Vibration and Acoustics*, 123:2, 2001.

- A. Preumont and K. Seto. *Active Control of Structures*. Wiley Online Library, 2008.
- L. A. Roussos. Noise transmission loss of a rectangular plate in an infinite baffle. In *Presented at the 107th Meeting of the Acoustical Society of America, Norfolk, Va., 7-10 May 1984*, volume 1, pages 7–10, 1985.
- S. Skogestad and I. Postlethwaite. *Multivariable feedback control: analysis and design*, volume 2. Wiley, 2007.
- M. Tahir Akhtar and W. Mitsuhashi. Improving performance of  $FxLMS$  algorithm for active noise control of impulsive noise. *Journal of Sound and Vibration*, 327(3):647–656, 2009.
- U. Ubaid, S. Daley, and S. Pope. Broadband design of remotely located vibration control systems: A stable solution for non-minimum phase dynamics. In *INTER-NOISE and NOISE-CON Congress and Conference Proceedings*, volume 2011, pages 835–840. Institute of Noise Control Engineering, 2011.
- U. Ubaid, S. Daley, S. Pope, and I. Zazas. Experimental validation of a geometric method for the design of stable and broadband vibration controllers using a propeller blade test rig. In *Control (CONTROL), 2012 UKACC International Conference on*, pages 369–374. IEEE, 2012.
- B. T. Wang, C. R. Fuller, and E. K. Dimitriadis. Active control of noise transmission through rectangular plates using multiple piezoelectric or point force actuators. *The Journal of the Acoustical Society of America*, 90:2820, 1991.
- J. Wang and S. Daley. Broad band controller design for remote vibration using a geometric approach. *Journal of Sound and Vibration*, 329(19):3888–3897, 2010.
- B. Widrow and S. D. Stearns. Adaptive signal processing. *Englewood Cliffs, NJ, Prentice-Hall, Inc., 1985, 491 p., 1*, 1985.
- X. Yu, H. Zhu, R. Rajamani, and K. A. Stelson. Acoustic transmission control using active panels: an experimental study of its limitations and possibilities. *Smart Materials and Structures*, 16(6):2006, 2007.

- H. Zhu, R. Rajamani, and K. A. Stelson. Active control of acoustic reflection, absorption, and transmission using thin panel speakers. *The Journal of the Acoustical Society of America*, 113:852, 2003.
- J. G. Ziegler and N. B. Nichols. Optimum settings for automatic controllers. *trans. ASME*, 64(11), 1942.
- M. Zilletti, S. J. Elliott, and E. Rustighi. Optimisation of dynamic vibration absorbers to minimise kinetic energy and maximise internal power dissipation. *Journal of Sound and Vibration*, 2012.
- B. J. Zimmer, S. P. Lipshitz, K. A. Morris, J. Vanderkooy, and E. E. Obasi. An improved acoustic model for active noise control in a duct. *Journal of Dynamic Systems, Measurement, and Control*, 125(382), 2003.

# Appendix A

## A.1 Boundary Value Problem for Coupled Loudspeakers Acoustic Duct

In this section a description of the steps required to solve the boundary value problem presented in Chapter 3 for calculating the total acoustic pressure wave inside the acoustic duct coupled with the disturbance and control loudspeaker. Due to the symmetry of the acoustic duct setup, the solutions for the disturbance path and the control path transfer function are identical. Therefore the solution of the disturbance path is given in detail.

The linear boundary value problem solved to provide the transfer function formula is reintroduced:

$$\left. \begin{aligned} p_{xx}(s, x) - \left(\frac{s}{c_0}\right)^2 p(s, x) &= f(x) \\ p_x(s, L) &= \frac{-A_C p_0}{Z_L(s)} p(L) \\ p_x(s, 0) &= p_0 s \left(\frac{A_D p(s, 0) - g(s)}{Z_0(s)}\right) \end{aligned} \right\} \quad (\text{A.1})$$

where  $f(s, x) = \left(-\frac{p_0 s}{\pi a^2}\right) V(s, x)$ ,  $g(s) = \left(\frac{Bl}{R_{coil}}\right) E_D(s)$ . In order to solve this problem the Green's function method is adopted. Hence the following differential equation is assumed:

$$F_{\zeta\zeta}(\zeta, x) - k^2 F(\zeta, x) = \delta(\zeta - x) \quad (\text{A.2})$$

where  $k = \frac{s}{c_0}$ . Let  $F$  be the generalised solution to the following differential equation:

$$F(\zeta, x) = \begin{cases} A_1 e^{k\zeta} + A_3 e^{-k\zeta} & 0 \leq \zeta \leq x \\ A_2 e^{k\zeta} + A_4 e^{-k\zeta} & x \leq \zeta \leq L \end{cases} \quad (\text{A.3})$$

The selection of the coefficients  $A_1, A_2, A_3, A_4$  is dictated by use of the boundary conditions defined in our problem, so that pressure  $p(x)$  can be calculated from  $F(\zeta, x)$ . Therefore, lets examine the following integral equation:

$$\int_0^L f(\zeta) F(\zeta, x) d\zeta = \int_0^L F(\zeta, x) (p_{\zeta\zeta}(\zeta) - k^2 p(\zeta)) d\zeta \quad (\text{A.4})$$

If the right hand side is integrated by parts, the resulting equation is:

$$\begin{aligned} F(L, x)p_x(L) - F_\zeta(L, x)p(L) - F(0, x)p_x(0) + \\ + F_\zeta(0, x)p(0) + \int_0^L p(\zeta) [F_{\zeta\zeta}(\zeta, x) - k^2 F(\zeta, x)] d\zeta \end{aligned} \quad (\text{A.5})$$

if the boundary conditions from equation (A.1) and the differential equation the Green function satisfies (equation (A.2)) are substituted we obtain:

$$\begin{aligned} \int_0^L p(\zeta) F(\zeta, x) d\zeta = \left[ F(L, x) \left( \frac{-A_C p_0 s}{Z_L(s)} \right) - F_\zeta(L, x) \right] p(L) + \\ + \left[ F(0, x) \left( \frac{-A_D p_0 s}{Z_0(s)} \right) + F_\zeta(0, x) \right] p(0) + \frac{F(0, x) p_0 s}{Z_0(s)} g(s) + p(x) \end{aligned} \quad (\text{A.6})$$

where  $Z_0$  is the impedance of the disturbance loudspeaker,  $Z_L$  is the impedance of the control loudspeaker and  $g(s)$  is the driving force of the loudspeaker.

In order to remove the first two terms on the right hand side of equation (A.6) the appropriate conditions on  $F$  should be chosen as:

$$F(L, x) \frac{A_C p_0 s}{Z_L(s)} + F_\zeta(L, x) = 0 \quad (\text{A.7})$$

$$F(0, x) \frac{A_D p_0 s}{Z_0(s)} + F_\zeta(L, x) = 0 \quad (\text{A.8})$$

Now, let us consider the differential equation:

$$F_{\zeta\zeta}(\zeta, x) - k^2 F(\zeta, x) = \delta(\zeta - x) \quad (\text{A.9})$$

from which we have:

$$F_\zeta(\zeta, x)|_{x_-}^{x_+} - k^2 \int_{x_-}^{x_+} F(\zeta, x) d\zeta = 1 \quad (\text{A.10})$$

when integrated from  $\zeta = x_-$  to  $x_+$ .

Because  $F$  is assumed to be a continuous function at  $\zeta = x$ , the second term on the left hand side is equal to zero, hence we get the following equation:

$$F_\zeta(\zeta, x)|_{x_-}^{x_+} = 1 \quad (\text{A.11})$$

Conditions given by equation (A.7), equation (A.8) and equation (A.11) result in:

$$-(A_1 + A_2) \frac{p_0 s A_D}{Z_0(s)} + k(A_1 - A_2) = 0 \quad (\text{A.12})$$

$$(A_3 e^{kL} + A_4 e^{-kL}) \frac{p_0 s A_C}{Z_L(s)} + k(A_3 e^{kL} - A_4 e^{-kL}) = 0 \quad (\text{A.13})$$

$$A_3 e^{kL} - A_4 e^{-kL} - A_1 k e^{kL} + A_2 k e^{-kL} = 1 \quad (\text{A.14})$$

Furthermore, the continuity of  $F$  at  $\zeta = x$  implies:

$$A_1 e^{kL} + A_2 e^{-kL} = A_3 e^{kL} + A_4 e^{-kL} \quad (\text{A.15})$$

From equation (A.12) and equation (A.13) we obtain:

$$A_2 = a_0(s) A_1 \quad (\text{A.16})$$

$$A_3 = a_L(s)e^{-2Lk} A_4 \quad (\text{A.17})$$

where  $a_0(s) = \frac{Z_0(s) - p_0 c_0 A_D}{Z_0(s) + p_0 c_0 A_D}$  and  $a_L(s) = \frac{Z_L(s) - p_0 c_0 A_C}{Z_L(s) + p_0 c_0 A_C}$ .

From equation (A.14) and equation (A.15) we obtain:

$$(A_3 - A_1) = \frac{1}{2k} e^{-kx} \quad (\text{A.18})$$

and

$$(A_2 - A_4) = \frac{1}{2k} e^{kx} \quad (\text{A.19})$$

By considering all the above equations we can solve the boundary problem and obtain the coefficient values:

$$A_1 = \frac{a_L(s)e^{-2Lk} e^{kx} + e^{-kx}}{2k(a_0(s)a_L(s)e^{-2Lk} - 1)}$$

$$A_2 = \frac{a_0(s) (a_L(s)e^{-2Lk} e^{kx} + e^{-kx})}{2k(a_0(s)a_L(s)e^{-2Lk} - 1)}$$

$$A_3 = \frac{a_L(s)e^{-2Lk} (e^{kx} + a_0(s)e^{-kx})}{2k(a_0(s)a_L(s)e^{-2Lk} - 1)}$$

$$A_4 = \frac{e^{kx} + a_0(s)e^{-kx}}{2k(a_0(s)a_L(s)e^{-2Lk} - 1)}$$

Hence,

$$F(\zeta, x) = \frac{1}{2k(a_0(s)a_L(s)e^{-2Lk} - 1)} \begin{cases} (a_L(s)e^{-2Lk} e^{kx} + e^{-kx}) (e^{kx} + a_0(s)e^{-kx}) & 0 \leq \zeta \leq x \\ (a_L(s)e^{-2Lk} e^{k\zeta} + e^{-k\zeta}) (e^{kx} + a_0(s)e^{-kx}) & x \leq \zeta \leq L \end{cases} \quad (\text{A.20})$$

If we reconsider equation (A.6) based on the assumptions of  $F$  we have:

$$p(x) = -\frac{F(0, x)p_0s}{Z_0(s)}g(s) + \int_0^L f(\zeta)F(\zeta, x)d\zeta \quad (\text{A.21})$$

The transfer function that links the acoustic sound pressure at any point  $x$  inside the acoustic tube to the voltage that drives the disturbance loudspeaker is given by:

$$F_d(s, x) = \frac{p_0c_0}{Z_0(s)} \frac{Bl}{R_{coil}} \frac{(1 + a_0(s)) (a_L(s)e^{-2Lk}e^{kx} + e^{-kx})}{2(1 - a_0(s)a_L(s)e^{-2Lk})} \quad (\text{A.22})$$

Due to the symmetry of the plant the transfer function for the control path is identical and therefore if we assume the same boundary problem with the disturbance source as an external input and the control source as the primary source we end up with:

$$F_c(s, x) = \frac{p_0c_0}{Z_L(s)} \frac{Bl}{R_{coil}} \frac{(1 + a_L(s)) (a_0(s)e^{-2Lk}e^{kx} + e^{-kx})}{2(1 - a_0(s)a_L(s)e^{-2Lk})} \quad (\text{A.23})$$

## A.2 Plate Formulas

In this section a thorough description of the panel's velocity due to a point force or a incident acoustic wave is given. The formula for the resonant frequencies is given by [Fuller et al., 1997]:

$$\omega_{mn} = \sqrt{\frac{D_p}{\rho_p h_p}} (k_m^2 + k_n^2) \quad (\text{A.24})$$

where the eigenvalues  $k_m$  and  $k_n$  are:

$$\left. \begin{aligned} k_m &= \frac{m\pi}{L_x} \\ k_n &= \frac{n\pi}{L_y} \end{aligned} \right\} \quad (\text{A.25})$$

In the previous equations  $\rho_p$  is the density of the plate and  $h_p$  is the thickness,  $L_x$  and  $L_y$  are the dimensions of the plate and finally  $D_p$  is the bending stiffness given by:

$$D_p = \frac{E_p h_p^3}{12(1 - \nu_p^2)} \quad (\text{A.26})$$

where  $E_p$  and  $\nu_p$  are the Young's modulus of the elasticity and Poisson's ratio. It must be

noted that the modal force,  $F_{mn}$ , which is a result to the disturbance can be heavily influenced by an external load. Researchers have investigated the impact of such loads on has to the model force [Gu and Fuller, 1993]. Because the thesis considers only airborne problems we will not consider such situations. An very comprehensive analysis of the model forces for different scenarios of input disturbances is given by Wang et al., 1991.

The first type of input considered is a obliquely incident plane wave. Such an input can be viewed in figure 8.1. The mathematical formula that describes such a wave is given by:

$$p_i(x, y, t) = P_i e^{j\omega t - jk \sin \theta_i \cos \phi_i - jk \sin \theta_i \sin \phi_i} \quad (\text{A.27})$$

The angles  $\theta_i$  and  $\phi_i$  can be viewed in Fig. 5. Because we are only considering airborne problems the load from the fluid is insignificant the input pressure at the plate surface is equal to the plate's blocked pressure. This means that there is perfect reflection and therefore the total pressure in front of the plate is equal to twice the incident pressure wave. By considering this assumption, it was possible by [Roussos, 1985; Wang et al., 1991] to calculate the modal force as:

$$F_{mn}^d = 4P_i I_m I_n \quad (\text{A.28})$$

where the coupling constants are given by:

$$I_n = \frac{n\pi \left\{ 1 - (-1)^n \exp \left[ -\sin \theta_i \sin \phi_i \left( \frac{j\omega L_x}{c_0} \right) \right] \right\}}{(n\pi)^2 + \left[ \sin \theta_i \sin \phi_i \left( \frac{j\omega L_x}{c_0} \right) \right]^2} \quad (\text{A.29})$$

or

$$I_n = -\frac{j}{2} \text{sgn}(\sin \theta_i \sin \phi_i) \quad (\text{A.30})$$

$$\text{if } (n\pi)^2 = - \left[ \sin \theta_i \sin \phi_i \left( \frac{j\omega L_x}{c_0} \right) \right]^2$$

$$I_m = \frac{m\pi \left\{ 1 - (-1)^m \exp \left[ -\cos \theta_i \cos \phi_i \left( \frac{j\omega L_y}{c_0} \right) \right] \right\}}{(n\pi)^2 + \left[ \sin \theta_i \cos \phi_i \left( \frac{j\omega L_y}{c_0} \right) \right]^2} \quad (\text{A.31})$$

or

$$I_m = -\frac{j}{2} \text{sgn}(\sin \theta_i \cos \phi_i) \quad (\text{A.32})$$

$$\text{if } (m\pi)^2 = - \left[ \sin \theta_i \cos \phi_i \left( \frac{j\omega L_y}{c_0} \right) \right]^2$$

Point force due to inertia actuator. When considering a harmonic in nature force of amplitude  $F$  at position  $(x_f, y_f)$ , the modal force formula is given by the following equation:

$$F_{mn}^c = \frac{4F}{L_x L_y} \sin k_m x_f \sin k_n y_f \quad (\text{A.33})$$

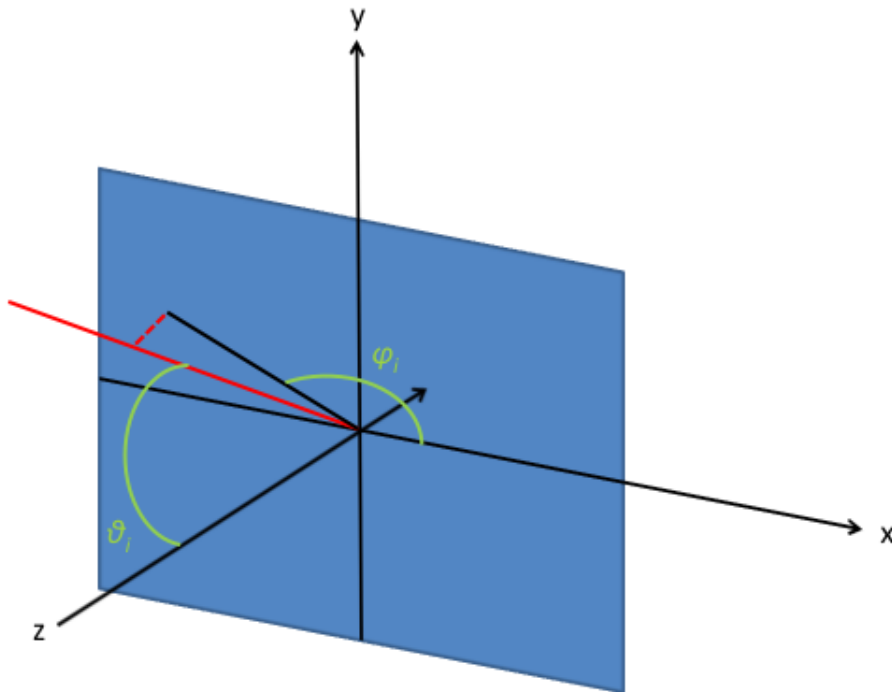


Figure 8.1: Rectangular panel with incident acoustic wave labelled with red. The angles  $\vartheta_i$  and  $\varphi_i$  represent the incident wave's direction.

### A.3 Boundary Value Problem for Coupled Rectangular Thin Plate Acoustic Duct

Compared to the previous boundary problem the only alterations that affect the resulting solution are:

- The rectangular shape of the duct alters the cross section, hence  $A = L_x L_y$
- The reflecting panel element that alters the boundary impedance  $Z_L$  and the driving force formula ( $g(s)$ ) for the control boundary required to couple the dynamics of the reflecting boundary.

Therefore, the disturbance path transfer function identical with the previous function:

$$G_d(s, x) = \frac{p_0 c_0}{Z_0(s)} \frac{Bl}{R_{coil}} \frac{(1 + a_0(s)) (a'_L(s) e^{-2Lk} e^{kx} + e^{-kx})}{2(1 - a_0(s) a'_L(s) e^{-2Lk})} \quad (\text{A.34})$$

where  $a'_L(s) = \frac{Z'_L(s) - p_0 c_0 L_x L_y}{Z'_L(s) + p_0 c_0 L_x L_y}$  and  $Z_L(s)$  is the mechanical impedance of the panel at the centre.

With regards to the control path, the formula is:

$$G_c(s, x) = \frac{p_0 c_0 F_{con}(s) (1 + a_0(s)) (a'_L(s) e^{-2Lk} e^{kx} + e^{-kx})}{Z'_L(s) 2(1 - a_0(s) a'_L(s) e^{-2Lk})} \quad (\text{A.35})$$

where  $F_{con}(s)$  is the transmitted force due to the inertia actuator placed in the centre of the panel (formula is given further down).

## A.4 Panel Velocity for Coupled Acoustic Duct Plant

The generalised plant assumed in Chapter 7 requires also the velocity of the controlled panel. Hence the transfer function of for the different types of excitation (control point force, incident acoustic wave). The general formula for thin plates is given by:

$$w(x, y, j\omega) = j\omega \sum_{m=1}^{\infty} \sum_{n=1}^{\infty} \frac{F_{mn}(j\omega) \psi_{mn}(x, y)}{\rho h_p L_x L_y (\omega_{mn}^2 - \omega^2 + 2\zeta_n j\omega \omega_{mn})} \quad (\text{A.36})$$

It is possible to derive transfer functions relating the velocity of the panel to different types of excitations. Specifically, velocity of a duct due to the intensity of source is given by combing equation (A.36) and equation (A.28):

$$W_{pi} = j\omega \sum_{m=1}^{\infty} \sum_{n=1}^{\infty} \frac{4P_i I_m I_n \psi_{mn} \left( \frac{L_y}{2}, \frac{L_x}{2} \right)}{\rho h_p L_x L_y (\omega_{mn}^2 - \omega^2 + 2\zeta_n j\omega \omega_{mn})} \quad (\text{A.37})$$

In the incident plane wave is given by the two microphone separation formula used to calculate the reflecting sound wave. Specifically:

$$P_{inc} = G_d(z_1, s) e^{-s\tau} - G_d(z_2, s) \quad (\text{A.38})$$

In similar fashion the velocity due to a point force is given by combining equation (A.36) and equation (A.33):

$$W_{point} = j\omega \sum_{m=1}^{\infty} \sum_{n=1}^{\infty} \frac{4F_{con}\psi_{mn}^2\left(\frac{L_y}{2}, \frac{L_x}{2}\right)}{\rho h_p L_x L_y (\omega_{mn}^2 - \omega^2 + 2\zeta_n j\omega\omega_{mn})} \quad (\text{A.39})$$

The transmitted control force  $F_{con}$  due to an inertia actuator is [Benassi et al., 2004]:

$$F_{con} = \frac{T_a}{1 + Z_a Y_c} \quad (\text{A.40})$$

where  $T_a$  is the blocked response of the actuator,  $Z_a$  is the mechanical impedance of the inertia actuator and  $Y_c$  is the mobility function of the panel [Benassi et al., 2004]:

$$T_a = \frac{s^2 m_a}{s^2 m_a + s c_a + k_a} \quad (\text{A.41})$$

$$Z_a = \frac{s^2 m_a c_a + s m_a k_a}{s^2 m_a + s c_a + k_a} \quad (\text{A.42})$$

Hence, the velocity of the panel due to a control point force with the addition of the actuator dynamics is given by:

$$W_{point} = j\omega \sum_{m=1}^{\infty} \sum_{n=1}^{\infty} \frac{4T_a\psi_{mn}^2\left(\frac{L_y}{2}, \frac{L_x}{2}\right)}{\rho h_p (L_x L_y)^2 (1 + Z_a Y_c) (\omega_{mn}^2 - \omega^2 + 2\zeta_n j\omega\omega_{mn})} \quad (\text{A.43})$$

# Appendix B

This paper has been contributed and presented during the IFAC PID'12 conference in Brescia, Italy, 28 - 30 March, 2012.

**Title:** *Acoustic Impedance Matching using Loop Shaping PID Controller Design*

**Authors:** Michail T. Pelegrinis, Dr. Simon A. Pope and Professor Steve Daley.

**Abstract:** For several decades Proportional-Integral-Derivative control (PID) has been successfully used for a wide variety of industrial processes and remains the most used method. Recent work concerning the tuning of PID control coefficients has been proven to provide both robust and near-optimal performance using a Frequency Loop Shaping (FLS) procedure. The FLS tuning method minimizes the difference between the actual and the desired target loop transfer function. Such a control design procedure is ideal for problems in which the desired closed loop frequency response is predetermined over a specific frequency band. This paper explores the possibilities and trade-offs of applying the FLS control strategy in Active Noise Control (ANC) problems. The use of the FLS design is ideal for the problem of noise suppression in ducts, because the required acoustic impedance for the elimination of reflecting sound waves in the one-dimensional case is well defined. Hence, by controlling locally the reflecting boundary structure, a global cancelation of the undesired noise can be accomplished

This paper has been contributed and presented during the ICSV20 conference in Bangkok, Thailand, 7 - 11 July, 2013.

**Title:** *Noise Suppression Using Local Acceleration Feedback Control Of An Active Absorber*

**Authors:** Michail T. Pelegrinis, Dr. Simon A. Pope, Dr. Ilias Zazas and Professor Steve Daley.

**Abstract:** A popular approach for Active Noise Control (ANC) problems has been the use of the adaptive Filtered-X Least Mean Squares (FXLMS) algorithm. A fundamental problem with feedforward design is that it requires both reference and error sensors. In order to reduce the size, cost and physical complexity of the control system a feedback controller can be utilised. In contrast with FXLMS a feedback controller utilises local velocity measurements of a sound-absorbing surface instead of global pressure measurements. Most control problems, including ANC, can be formulated in the General Control Configuration (GCC) architecture. This type of architecture allows for the systematic representation of the process and simplifies the design of a vast number of controllers that include H-infinity and  $H_2$  sub optimal controllers. Such controllers are considered ideal candidates for ANC problems as they can combine near optimal performance with good robustness characteristics. This paper investigates the problem of reflected noise suppression in acoustic ducts and the possibilities and trade-offs of applying H2 control strategies. Hence, by controlling locally the reflecting boundary structure, a global cancelation of the undesired noise can be accomplished. In the paper the H2 local feedback control strategy and performance are investigated using an experimental pulse tube facility.

A draft journal paper containing experimental results with the benefits and trade offs of applying local feedback control for reduction of reflecting sound waves has been written and submitted at IEEE Transactions on Ultrasonics, Ferroelectrics and Frequency Control. Additionally, a journal paper containing the smart panel consideration (chapter 7) is being written.